Brunel University London

Department of Mechanical and Aerospace Engineering

PhD Thesis

Title:

Design of passive compliant end-effectors for robotic and autonomous train fluid servicing

Submission date 31/05/2023

Candidate: Mr Kourosh Eshraghi

Principal supervisor: Dr Cristinel Mares

Second supervisor: Dr Mingfeng Wang

ABSTRACT

Due to the ongoing increase in UK rail traffic, train maintenance automation is becoming essential in meeting the future demands of the industry. The issue is that current industrial robotics are not readily suited for train maintenance in outdoor/unstructured applications. To perform useful work, the robot must interact with the train parts, this can include various tasks such as insertion, latching, griping etc. There will always be some misalignment in the autonomous mating of these parts, using a completely rigid robot will cause failures, especially in tight clearance scenarios. The robot or workpiece must be flexible to facilitate smooth interaction with relaxed contact forces and robot payload, reducing overall cost and safety requirements. Compliant mechanisms and end-effectors are inherently flexible and cheap however, existing literature and solutions are only suitable for robotic tasks with small misalignments (<2mm) and basic mating geometry. Our application of train fluid servicing includes more complicated tasks and geometries with misalignment upto 15 mm and 5 deg. The existing literature uses simplified analytical modelling and trial-and-error design approaches which are outdated and in our case impractical. This thesis uses more modern and practical techniques to structure the design of compliant mechanisms in passive compliance applications with large misalignments and applications of train fluid servicing. We hypothesise that such a design problem is always distinguished by some kind of uncertainty (i.e. misalignments) which manifests itself into loads and displacement. In this manner, Robust Engineering Design (RED) methodologies are formulated to solve the general design issue. The approach includes Pseudo Rigid Body Modelling (PRBM) and Finite Element Analysis (FEA) for large deformation and contact modelling. This was accurate in payload prediction between 5-12% of the physical results. We were successful in enabling a range of largely misaligned automated fluid coupling while significantly reducing robot payload for cam and groove type (CET) fluid couplings. A special mechanism was developed to aid the gripping of fluid port caps with standard grippers. Performance charts were produced to convey design insight. Contributions of this thesis are:

1. A unique outlook and new higher-level framework for passive compliance design with RED methodologies
2. Developing and evaluating design and modelling tools necessary for large misalignment and complex contact scenarios in train fluid servicing tasks
3. Design and parametric insight of new compliant end effectors for train fluid servicing

PUBLICATIONS

Journals and conferences

- Eshraghi, K., Wang, M. and Mares, C. (2023) 'Towards robust and effective passive compliance design of end-effectors for robotic train fluid servicing', *MDPI Machines*, 11(11), p. 997. doi:10.3390/machines11110997.

- Eshraghi, K. *et al.* (2022) 'Preliminary study of end-effector compliance for reducing insertion force in automated fluid coupling for trains', *Journal of Integrated Design and Process Science*, 24(3–4), pp. 139–161. doi:10.3233/jid200017.

- Eshraghi, K., *et al.* (2020). 'Preliminary study on end-effector compliance in automated fluid coupling for trains' *Proceedings of TMCE 2020, (pp. 205-216)*. Dublin.

- Presented with posters and stands at 5x industrial conferences including UKRRIN in Birmingham, EURM in London, RIA in Huddersfield, RIA at Dudley between 2019-2023.

Awards

- Brunel University vice-chancellor travel prize and cited in the newsletter (2020)

- Mingfeng Wang and Kourosh Eshraghi, "Field-trial of novel compliant end-effectors for train fluid servicing", EPSRC Impact Acceleration Account - Brunel University (EP/X525510/1), £25,427.9, 04/2023-12/2023.

ACKNOWLEDGEMENT

CONTENTS

LIST OF FIGURES

LIST OF TABLES

1. INTRODUCTION

Overview

In this chapter, we discuss the issue of robotic and autonomous train servicing and how it's the motivation of this thesis. We make remarks on previous work and recent developments in the rail industry and research to justify the industrial need for autonomous train servicing. Followingly the lack of existing solutions is highlighted, to demonstrate the need for further research in the field of passive compliant end-effectors. The hypothesis and approaches of the thesis are briefly discussed in this chapter.

1.1 Important background information

Pre-covid estimates had UK rail traffic to surge significantly by 2047, requiring a commensurate increase in the national passenger fleet between 5,500 and 12,000 vehicles. that's almost a 100% increase (Rail Delivery Group, 2018). Recent post-covid numbers by the Department of Transport (DoT) are showing passenger rail traffic has fully returned to pre-covid levels (Duckworth, 2023). Therefore, continued growth and pre-covid estimates are no longer looking farfetched. Conversely, new ways of working such as 'hybrid' and 'work from home' schemes, may reduce peak time commutes.

Despite the uncertainties, the rail industry seeks to maintain its competitive edge against other modes of transport. With recent developments in Robotic and Autonomous Systems (RAS), and improved sensing and data technologies, it seems that our infamous rail industry is falling behind. Active measures are encouraging innovation throughout the industry, for example by DoT, Innovate UK, Rail Safety and Standards Boards (RSSB) and Network Rail initiatives. As a result rail research and innovation have gained significant momentum recently. We have witnessed the development of the UK Rail Research and Innovation Network (UKRRIN) which includes many UK universities and sectors of excellence for rail research. This includes the Birmingham Centre for Railway Research and Education (BCRRE). Huddersfield University Institute Railway Research (IRR) which now includes the Smart Rolling Stock Maintenance Research Facility (SRSMRF). Other centres such as the Very Light Rail National Innovation Centre (VLRNIC), Global Centre of Rail Excellence (GCRE) and the national Catapult services also facilitate innovation in rail.

The increase in the number of passenger trains with today's economic, social and environmental requirements, poses a new challenge for all rail sectors such as train manufacturing, signalling, operations and maintenance. This will produce a comparative challenge for train maintenance depots in terms of increasing service capacity and ensuring higher train availability measures. There will also be increasing demand for accurate service data and asset condition monitoring, vital for modernising maintenance. New ways of working will be required to respond to these challenges, and this will provide, but opportunities to assist humans in tasks that may be considered dangerous, difficult, dirty or dull, in order to improve working conditions, safety and job satisfaction.

Autonomous servicing and maintenance is a challenge in many industries which are rapidly working on developing new solutions. This includes autonomous refuelling of domestic cars or servicing and refuelling of satellites in orbit. Only recently we have seen the development of robotic solutions for train maintenance. For example, Colleagues at Cranfield University are investigating the robotic cleaning of trains (Tomiyama et al., 2017). The study identifies design requirements to conceptualise two 6 Degree of Freedom (DoF) robots for cleaning the train nose front. The current manual method requires the workforce to handle water around high voltage systems (25000V). A robotic solution should increase the safety and throughput of the process. Subsequent work has discussed the force-control and trajectory algorithms for the cleaning end-effector (Moura et al., 2018). Autonomous cleaning motions are achieved on unknown curved surfaces thus, applicable to different train designs. Fellow researchers demonstrated the technical feasibility of this system on a tabletop prototype.

It is generally accepted that autonomous systems will have positive contributions to meeting future rail demands. This is supported by, for example, an economic and technical feasibility study of a robotic system for train-fluid servicing (Atherton et al., 2020). Our research group at Brunel University (Hill et al., 2017) conducted a requirements and feasibility study for train fluid servicing robots and proposed two design concepts. The "Cartesian" design can be more cost-effective than other proposed designs with articulated robots (Atherton et al., 2020). This design has fewer DoFs and fluid pumps which results in a reduced number of motors and drives. We then built an almost full-scale proof-of-concepts robot called CyberFluids. This system was initially introduced by the author of this thesis in two publications (Eshraghi et al., 2020b, 2020a). As discussed in these papers, the key unaddressed issue in previous work of our colleagues is how the proposed autonomous systems will achieve effective mechanical connections between the robot (end-effector) and the train. The technical motivation of this thesis is a deeper investigation of this issue and the development of resolutions.

One of the major issues in train servicing i.e. fluids is that train parts must be gripped, inserted, removed, replaced, latched, unlatched, etc. It is often the case that clearances between mating parts are relatively small, thus even small inherent robot positional inaccuracies (misalignments) can disrupt the operation. Given the robot and train parts are rigid, small misalignments can develop very large forces leading to equipment failure and damage to assets. Previous literature has shown that incorporating flexibility (mechanical compliance) in the

robot will resolve such issues (Wang et al., 1998). Previous efforts of researchers saw even a 0.5mm misalignment may cause significant assembly/manipulation failure. Solving this issue turned out to be very challenging and invoked a large body of research commonly associated with the keywords "Peg-in-Hole" and "robot compliance". Train fluid coupling which includes peg-like objects (i.e., fluid coupler) and hole-like objects (i.e. fluid port) is a similar problem. However, much higher misalignments are to be expected. Unlike manufacturing plants, the train maintenance environment is difficult to control. The train itself is exposed to an uncontrollable terrain which results in process variations in autonomous servicing operation. Thus the train fluid servicing system must be robust and capable of outdoor operation (Hill et al., 2017).

In the last few years, we saw the development of robotic refuelling systems for cars, such as FuelMatic, RoboFuel and AutoFuel. At first glance, these products seem to rely heavily on active and vision systems to autonomously refuel cars. There are two distinctions here, firstly vision systems are well known for their lack of reliability where lighting, surface texture and other environmental variables are uncontrollable. Second, a car fuel nozzle and car fuel port have a large radial clearance of >5mm with no seal or lock. It may be possible to achieve this insertion task without even encountering external parts (no need for compliance). Train fluid ports have a relatively low radial clearance of 0.4 mm with a cam and grooves latch system which forms mechanical connections to a secure high-flow and prolonged refuelling. The RoboFuel system designed for truck refuelling seems to have a more relatable fluid coupling operation. The prototype seems to work fine but we have no knowledge or track record of the systems used. Generally, there is no public literature regarding the design or performance of these products. Even though there is a wild consensus that state-of-the-art vision systems are highly capable of autonomous robotic operations, they are not very reliable and accurate in positioning (and "vision-based servoing") of robots. Furthermore, we found no relevant solutions distinctly capable of reliable operation with varying environmental parameters such as lighting, debris and dirt that are prevalent in the train maintenance environment.

Work conducted in this thesis is based on an ideology that a simple and high-speed automated system with mechanically intelligent compliant end-effectors, is the most viable and economical solution to train fluid servicing. The aim is to pave the way for the design and technical feasibility of compliant end-effectors and contribute to existing public knowledge. Accordingly, engineers i.e., those concerned with train maintenance systems, can make more

informed technical and financial trade-offs with the potential for UK rail to make substantial cost savings in the mass deployment of these systems.

1.2 Problem outline

Rolling stock maintenance includes dirty, heavy, and demanding tasks taking place out-of-hours, and in outdoor environments. Today this creates an undesirable working condition for both humans and machines. Robotics available industrially are not as capable in such unstructured, semi-structured and outdoor environments. These settings induce more errors in autonomous robot positioning. Uncontrollable factors such as weather, lighting, dirt, debris, fluids, part wear and texture conditions make it difficult for robots to sense, identify, locate and contact objects (Akpınar, 2021; De Cubber et al., 2004; Martin, 2007). The latest humanoid robots or autonomous vehicles still account for severely large uncertainties in measured data in order to ensure safe operations. This deficiency does not hinder the automation of ordinary human activity such as bringing a vehicle to a stop, making a sandwich or picking a strawberry. However, it cripples engineering tasks that must meet the high speed, precision, cost, and intricacy demands of relevant industries.

In maintenance, the robot physically contacts external workpieces to manipulate it. If for example robot positioning data is not correct (misalignment exists), undesirable forces will quickly result in physical damage to assets. In such conditions, robot compliance has been used to accommodate and guide robot motions while interfacing with an external object. This is commonly in the form of a spring-like stiffness. In more technical terms, the relationship between the motion and forces generated by a robot manipulator and an external part at their point of contact (e.g., end-effector) is called, robot compliance. This can be categorised into active and passive compliance. Active compliance is achieved by controlling robot actuators and servo-motions to imitate flexibility (Xu et al., 2019). Passive compliance is defined as intrinsic structural deflections such as flexibility of the robot base, limbs, joint transmissions, and compliant end-effector. Active compliance reduces reliance on physical elements and corresponding complexity and also aims at ensuring safety for humans. However, it also presents disadvantages such as potential power losses, relatively slow dynamic responses and reliance on sensors and control systems. Passive compliance is an inherent mechanical capability which can be considered more reliable, faster in operation and cheaper to

manufacture (Wang et al., 1998). The key disadvantages are the lack of adaptability to different tasks and increased design difficulty due to inherent mechanical complexities of structural deformations, nonlinear contact, and uncertainties. The economy i.e., initial cost, running costs, throughput capacity and reliability of the compliance solution are key for an industrial RAS which continuously repeats the same tasks.

Any new application of RAS will try to levy on existing technology which is commercially sold as industrial robots. These systems are typically stiff articulated arms, cartesian gantry, and cylindrical or delta-type systems. For assembly applications that require some compliance, often SCARA robots are used for the insertion operation. Their redundant actuator design can deliver compliance in the X-Y plane (Shariatee et al., 2014). However, their configuration is not versatile for other tasks. Cobots are articulated arms designed to operate alongside humans (Robla-Gomez et al., 2017). They incorporate active control systems and are more versatile but they have little payload and are very expensive. Due to the inherent benefits of compliant end-effectors, they have been much more popular for insertion tasks and manufacturing assembly (Wang et al., 1998). A robot may perform many different tasks by automatically changing its end-effector during operation. A stiff, industrial robot can switch end-effectors to meet different requirements and specific compliances for each task. This is the key feature of incorporating compliance within the end-effector. It results in a faster operation and costs little to make, especially if recent developments in compliant mechanism design and manufacturing are used. For example monolithic structures and one-hit manufacturing operations (Howell et al., 2013). Thus, in this work, we focus on passive-compliant end-effectors for train servicing tasks.

As shown by (Hill et al., 2017), fluid servicing robots should operate outdoors of maintenance depots, to save space and keep the current scheduling architecture. Relative to the manufacturing assembly environments that are highly controlled, the train maintenance environments can be considered unstructured with a high degree of uncertainty regarding the position of fluid ports (ie. misalignments) and the nature of the contact (friction coefficients, geometry of contact) between robot and train. However, existing end-effector solutions and corresponding design/modelling theory do not consider these issues and only operate with a small misalignment range of <2mm, <2deg. Furthermore, they consider very simple mating parts which are in the form of cylindrical shafts (pegs) and bearings (holes) (Cannon et al., 2005; Daniel E. Whitney, 2004; Haskiya et al., 1998; Jiang et al., 2017; Kamnik et al., 2001;

Southern and Lyons, 2002; Usubamatov and Leong, 2011; Whitney, 1982; Whitney and Rourke, 1986; Xia et al., 2006).

A major part of engineering design is being able to model the problem so that various tests and optimisation processes are conducted to ensure performance (Ulrich and Eppinger, 2015). A model may be a physical prototype, computational simulation or some analytical mathematics. Of course, virtual and fast models are highly preferred as they undercut the costs of physical testing. But this is often at the cost of introducing more assumptions, simplifications and errors. Simplifications are required to fit the real physical system to existing mathematical and physical laws used for modelling. For example in structural design, engineers always assume that cantilever beam deformations in the axial direction are negligible given relatively small deformations of the beam (below 5% of the length), hence they can employ simple beam theory. They also restrict the design of their beam to commonly simple geometries such as I-sections. Compliant mechanisms are effectively structures that undergo useful motions. In the field of passive-compliant end effectors, the assumptions of simple geometry and small deformations are overwhelmingly common but these do not match the train maintenance problem.

The train maintenance environment requires end-effectors with larger misalignment capability of >15mm,<5 deg (indicating large motions/deformations), with peg and hole geometries that are vastly different. For example, the Controlled Emission Toilet (CET) ports common across almost all British rail fleets have a cam and grooves latch system which ensures a secure connection. This geometry is not well-modelled by a simple cylinder or square shape. Another issue with previous work is their sole focus on modelling Peg-in-Hole (PiH) insertion force not considering other practical aspects such as meeting misalignments or material fatigue requirements.

Accordingly, we seek to develop a more general design approach through which we and other designers may consider more complex and practical aspects of passive-compliant end-effector design for robotic applications. The author believes the following are distinguished reasons why we have not previously seen a comparable research effort in the field of passive-compliant end-effector design.

1. Previous lack of design and modelling theory for compliant mechanisms. Compliant mechanisms constitute a passive compliance device. At the time when compliant end-effectors became popular (1980-2000) little design theory was available for compliant mechanism design, especially in the large motion range. The author recognises the book (Howell, 2001) as a milestone in compliant mechanism design. Today compliant mechanisms are one of the hottest topics in mechanical engineering.

2. Lack of practical applications
Only recently we have seen the demand and development of technologies for robotic and autonomous systems in unstructured environments. Thus, there is little existing (previous) research in terms of compliant end-effector development in such cases.

These issues have led to a gap in the literature resulting in the following questions:

How do we approach the problem of compliant end-effector design today? What is defined as performance for compliant end-effectors? how do we model it considering large deformations and contact between complicated mating parts?

The general idealogy proposed in this thesis suggests a passive compliance design problem should be distinguished by the existence of some kind of uncertainty which manifests itself through the force-displacement relationship between the end-effector and an external workpiece. In most cases, uncertainties are between mating parts including misalignments, geometrical dimensions, surface finish (friction) etc. Despite the uncertainties, the compliant mechanism must convert resulting loads and displacement to perform a useful task. This is usually regulating forces or providing guiding motions. Accordingly, we approach the passive compliance design problem with a Robust Engineering Design (RED) method (Atherton and Bates, 2004; Montgomery, 2012). This approach aims to optimise the design against uncertainties which results in minimum performance variance with maximum possible average performance. Indicating the effect of uncertainty is minimised and a satisfactory performance level is achieved. Generally, this process requires a series of structured tests around various design configurations and uncertain (noise) conditions. We fulfil this requirement within a Design of Experiments (DoE) framework which also reduces the number of tests required (Montgomery, 2012). Since physical experimentation can be costly during the initial stages of

design, a simulation model is required to facilitate performance evaluations. In this work, we use physical experiments and demonstrate how to use Finite Element Analysis (FEA) and Pseudo Rigid Body Modelling (PRBM) for passive compliance problems (Howell, 2001). Such a modelling approach will work for any range of misalignments, any shape of peg and hole or other contact geometries. The whole process is packaged within a general mechanical design process that is proposed in Chapter 3.

This novel approach to passive compliance design is applied to various train fluid servicing applications demonstrating the successful development of new large misalignment compliant end-effectors for train servicing applications. See for example compliance optimisation of an end effector in Chapter 4, or design and development of an RCC end-effector in Chapter 5. Also, a completely new compliant solution for gripping fluid port dust caps is proposed in Chapter 6.

The designs and solutions in this thesis are retro-fittable however new industry standards and subsequent fulfilment from train manufacturers can significantly reduce the existing difficulties of autonomous train fluid servicing. Design changes to the location of fluid ports and fluid port designs can make them more accessible with features that increase clearances or provide guides for compliant end-effectors. Future work must consider this it can lead to a significant reduction in the complexity of the robotic system and increase its throughput. However, today, proposing design changes to train manufacturers is an unattractive solution for stakeholders.

1.3 Aims and objectives.

To summarise, this thesis aims to develop means of compliant end-effector design for largely misaligned robotic tasks found in train fluid servicing. This can be split into the following:

1. Formulate a general and practical design approach for passive end-effectors design, developing and evaluating modelling and design tools necessary for passive compliance in large misalignment and complex contact scenarios
2. Design and develop new compliant end-effectors enabling fluid coupling and manipulation for train fluid servicing applications.

3. Build a robotic train fluid servicing rig for testing and evaluation of the design approach and end-effector performance.

Objective O1.0. Realised in Chapter 2. Conduct a literature review, in order to discuss and measure existing approaches to passive compliance and compliant mechanism design
1. Identify previous design concepts relevant to passive compliance end-effectors and discuss their limitations in terms of handling misalignments.
2. Assess the feasibility of modern compliant mechanism design theory passive compliance in the large displacement range.

Objective O2.0, Realised in Chapter 3. Demonstrate a general design process with robust engineering methods
1. Illustrate methodology in the form of discussion, flow charts and figures.
2. Suggest and validate modelling of performance with physical experiments.
3. Discuss design performance evaluation with the methodology

Objective O3.0. Realised in Chapter 4. Develop a robotic system to test and benchmark end-effector compliance performance.
1. Build and demonstrate the operation of a train fluid servicing robot
2. Analyse the performance of end-effector compliance on the robot

Objective O4.0. Realised in chapters 5 and 6. Demonstrate the application of the proposed methodology to develop new end-effectors suitable for train fluid servicing
1. Develop new design concepts capable of required misalignments while operating under feasible contact forces.
2. Demonstrate how to model and analyse these concepts to optimise and tune performance for the particular train fluid servicing application
3. Discuss performance and produce selection charts which provide parametric design Insite into performance.

2. LITERATURE AND BACKGROUND WORK

Overview

Here we look at some of the previous work on design and modelling compliant end-effectors. There is a special focus on Peg-in-hole (PiH) problems in manufacturing where a large body of research relates to the train fluid port coupling problem. Then we discuss compliant mechanism design and modelling theory, in particular Topology Optimization (TO) and Pseudo Rigid Body Modelling (PRBM). From this review, we make critical conclusions and recommendations in the last section of the chapter.

2.1 History of passive compliant end-effectors

Passive compliance is an issue in many robotic applications. However, it was initially addressed upon the introduction of robotics in manufacturing systems, especially the assembly of mechanical parts. Thus, the body of literature available revolves around this field of application. This chapter begins with an in-depth review of the issue and solutions proposed.

A large portion of assembly tasks involve the insertion of peg-like components in holes i.e. shafts to bushings, bearings in housing etc. Due to inherent inaccuracies of industrial robots, close-fitting of pegs and holes typically yields 3 failure modes, missing the hole, jamming and wedging. Chamfers on holes provide a funnelling effect; this reduces the chance of missing the hole. To avoid jamming and wedging, certain undesirable forces and geometric conditions resulting from misalignments must be prevented. It is generally accepted that robot compliance can help to compensate for such misalignment. Thus, there have been efforts to develop compliant stages for assembly systems. For example, a Stewart platform design but with encapsulated springs instead of linear actuators (McCallion et al., 1979). Or a passive-compliant wrist design for robot manipulators (Havlík, 1983).

However, in a series of studies, it was shown that a special type of compliant mechanism is required to prevent jamming, and wedging and reduce insertion forces (Whitney, 1982). The studies are regarding vertical and round PiH assembly via a 2-dimensional quasi-static approach. They consider part lateral misalignments but ignore the angular errors and nonlinearities to maintain simple closed-form solutions. The compliant motion of the peg is lumped on a few springs that create a centre of compliance above the peg. This is where a compliant support or end-effector would hold it. Given the stiffness factors of the spring, the insertion force can be found for a misalignment case often described by clearance ratio and friction factor. Initial misalignments are uncertain parameters that are bounded by the accuracy of the robot. Hence the controllable factors are the gripper stiffness factors and moment arm counting from the tip of the peg to where the gripper centre of compliance/motion is. These parameters must be optimized to achieve the desired compliances. Moving the centre of compliance towards the tip of the peg (near or beyond the assembly contact point) i.e. reducing the moment arm, has a pronounced effect on preventing jamming and wedging. When the centre of motion is at the assembly point contact forces pass through the vicinity of this centre thus,

lateral forces at the assembly interface only cause lateral motions and moments only cause rotations. thus, during chamfer crossing no moments are augmenting angular misalignments and when the peg is inside the hole, moments cause a corrective turning effect. The Remote Centre Compliance (RCC) mechanism was proposed as a device that archives that. Essentially the function of this mechanism can be summarised as, A) Allow 5-axis compliant motions. B) Stiff in the insertion direction C) project the centre of motion. Further details of RCCs, varieties of PIH problems ie chamfers insertions with a special passive compliance device, and plots of allowable angular misalignment before two-point contact can be found in the literature (Whitney, 2004). Depending on requirements and specifications, generally coupling performance may be regarded as:

- Insertion forces
- Maximum possible misalignment
- Or the amount of part insertion in units of distance.
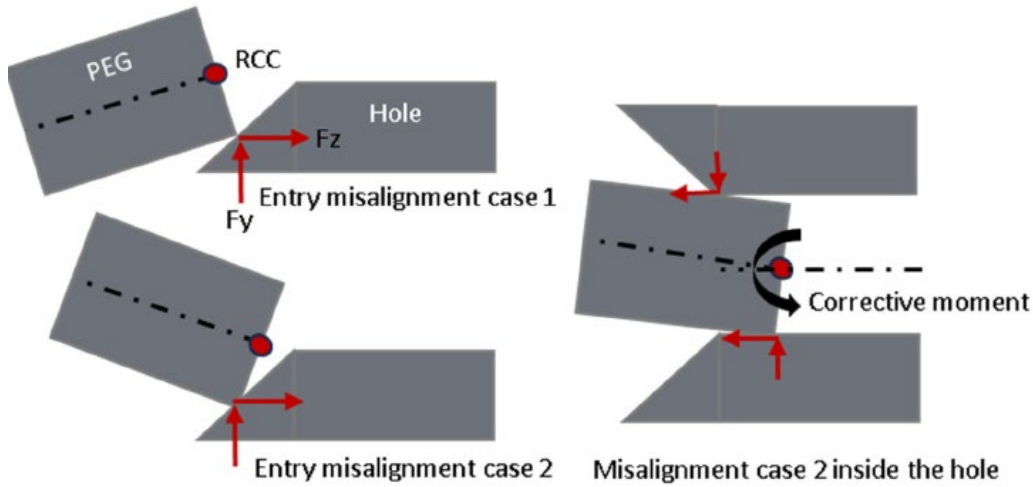
Figure 2.1 The Peg in Hole insertion with RCC

The literature contains other developments in the field of automatic PiH insertions with passive compliance. investigation of high-speed insertions considering the dynamics involved and developed "no bounce" conditions between the peg and hole (Asada and Kakumoto, 1988 Zohoor and Shahinpoor, 1991). Investigation of this problem in 3D the Spatial RCC (SRCC) for polygon-shaped parts (Sturges and Laowattana, 1996). Multiple PiH insertion(Sathirakul and Sturges, 1998), was a concern in the automation of battery lid assembly (Kamnik et al.,

2001). Chamfer-less PiH and a new type of compliance device based on the RCC (CVHRCC) (Haskiya et al., 1998). Consideration of the angle of insertion (often assumed to be parallel to the hole) yielded useful equations for identifying the critical angle of jamming (Usubamatov and Leong, 2011). The problem of contact deformation (Xia et al., 2006). Incorporation of dashpot models for the CVHRCC the effects of damping during insertion (Pitchandi et al., 2017). PiH insertions for large aircraft components under small assembly misalignments and 5-DoF compliant mechanisms (Jiang et al., 2017). The PiH issue for micro-assembly and a five DOF RCC-based end-effector using Pseudo Rigid Body Modelling (PRBM) (Wang et al. 2019).

Given previous work it is still unclear how we develop practical passive compliance designs for large misalignment applications. There are existing commercial assembly compliance devices retailed by manufacturers ATI and RAC. There is no general public knowledge of these devices, other than their specification which only provides basic information. Visually we can confirm that they use elastomer shear pad beams similar to those discussed by Whitney. These devices are capable of fairly large angular misalignments however they still do not match train fluid servicing requirements as shown in Figure 2.2. There is no information about insertion force estimates, which is significantly important in sizing robots.
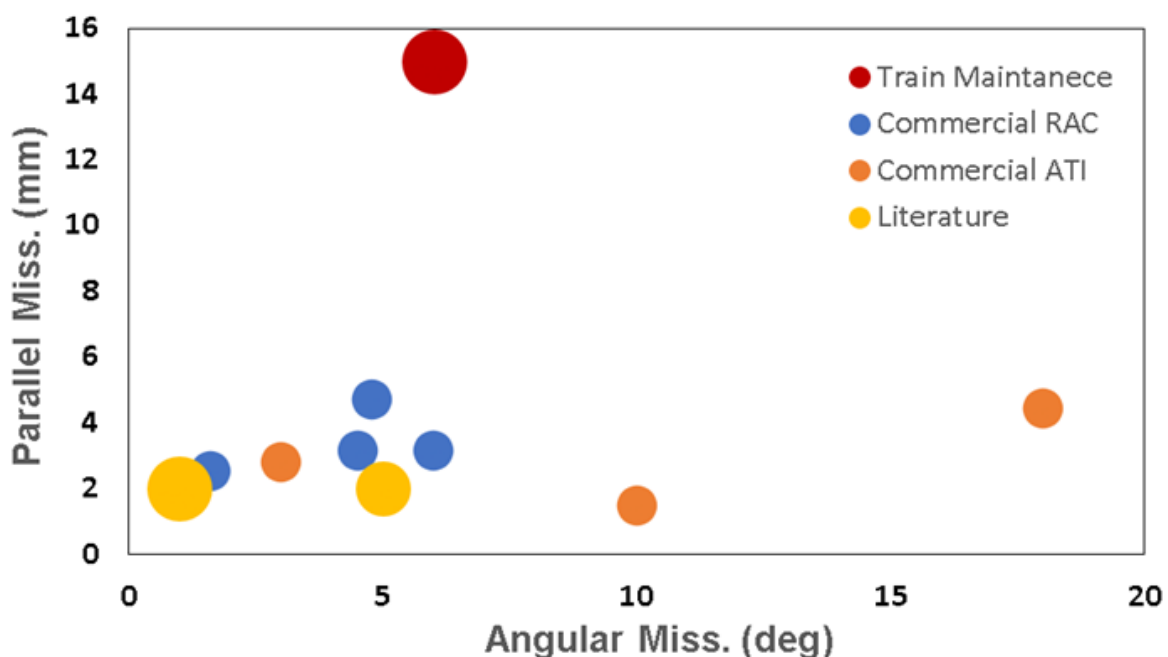
Figure 2.2 Misalignment range of end-effector solutions

Table 2.1 Exiting solutions in the literature and misalignment capabilities

Mechanism	Authors/year	Parallel	Angular	Clearance
Compliant stage	McCallion 1978	1-2mm	1.5-2.5°	0.01-0.02 mm
Flexure RCC	Watson 1982	1 mm	1°	0.01 mm
ESP type RCC	Whitney 1984	2mm	1°	0.01-0.02 mm
CHVRCC	Haskia 2001	0.4 – 2mm	0.5°	<0.375 mm
Train maintenance	-	15mm	5°	0.4-0.6 mm

2.2 The contacting part: geometry and robustness

The working operations of a compliant end-effector may be separated into two interconnected systems. The contacting part is often rigid i.e. the peg and hole, and the flexing part allows for end-effector motion. The design of these two systems can ensure better alignment for example incorporating contact shapes with funnelling effects or compliant mechanisms with stiffness ratios that provide more corrective motions. In this section, we evaluate the contacting part.

A cartesian or track-based robot with fewer DoFs is more desirable in terms of technical and economic feasibility (Atherton et al., 2020). However, such a robot will not be able to handle all the various motions and manipulations required to handle all different types of fluid ports on a train. The ports have different functions, geometry and modes of operation. Their shapes are also not represented by simple cylinders or squares that existing peg-in-hole models employ. The material properties and shape of the ports will have a significant impact on coupling success and insertion forces. Understanding and predicting these metrics will be essential to the compliant end-effectors design process. Previous work suggests the standardisation of fluid ports however today we are not sure of what the "Standard" fluid port will look like on a train. Hence a compliant end effector design approach useful for our applications should be able to handle various independent contact geometry. This renders almost all aforementioned peg-in-hole models obsolete.

Figure 2.3 Various fluid ports and couplers used for train fluid servicing

Various coupling mechanisms and geometries have been used in alignment and latching applications in other industries. Consider for example automated power transmission, couplings and latching components for assembly and fluid transfer, such as air-to-air fuelling (Thomas et al., 2014), docking of spacecraft, and autonomous refuelling/servicing of satellites (Delrobaei and McIsaac, 2008; Feng et al., 2016; Flores-Abad et al., 2014), and coupling of modular robots (Parrott et al., 2014; Saab and Ben-Tzvi, 2016). A general review and classifications of gendered, genderless and other designs for alignment can be found in the literature (Saab et al., 2019) (Yan et al., 2018). Key observations from previous work include:

- Most coupling designs require a peg-like or latch component to inter a larger hole.
- Depending on their face symmetry, couplings can allow connections in multiple orientations. The placement of connecting features around the roll axis of the connector determines the symmetry of the coupling mechanism. An asymmetric coupling mechanism can dock in only one orientation, whereas a two-times axisymmetric mechanism can dock in two orientations at 0° and 180° offsets, and a fully axisymmetric mechanism can dock at any offset angle i.e., a cylindrical peg. In turn, this reduces the roll axis passive compliance required and reduces bounded misalignments
- In a lot of highly misaligned scenarios such as spacecraft dockings. The alignment problem is split into two tasks, soft coupling and hard coupling. in the first stage, a large amount of misalignment is compensated, and the parts remain unlatched. During the latching process, remaining misalignments are compensated and parts are coupled rigidly. As opposed to autonomous servicing, in mechanical amply tasks of PiH there is usually no latching.

The geometry of mating parts plays a critical role in the success of the coupling (Saab et al., 2019). This is also emphasised by other work (Whitney, 2004), which suggests pegs with undercuts such as the groove in the train fluid port can increase coupling performance since two-point contact occurs deeper in the hole, preventing jamming.

2.2.1 Design robustness

The above observations on coupling interface design suggest some design features can improve the robustness of the coupling process under misalignments. Robustness is a very interesting topic of discussion (Collins et al., 2004). In the physical sense, systems can be inherently inclined to produce a certain consistent output. Consider why most systems in nature remain intact given harsh weather and the environment. For example, some trees have leaves that fold under wind to create a more aerodynamic shape which reduces loads on the tree trunk. The design of the leaf has gone through millions of development to produce a self-regulating mechanism which adapts to various wind conditions.

Engineering methods for product and process improvement and robustness such as Kaizen, Poka-yoke, Taguchi and Robust Design Methods (Arvidsson and Gremyr, 2008) are very popular in Japanese lean manufacturing systems. Famously incorporated by Toyota and Sony, these are some of the philosophies which gave a significant edge to Japanese engineering in the 1980s. Designers should always try to incorporate robust design techniques to ensure their products and processes will perform given potentially harsh environments. The contact geometry design should also strive to develop similar systems that make it robust to an environment with misslagliment dirt and debris. As discussed various procedures or design features may help for better fluid port coupling. We may use robust design approaches alongside these, to conduct a series of tests which will optimise contact geometry by minimising the mean and various performance measures say, the insertion force. In chapter 3 we use this approach to design the flexing part of the end-effector. We may also consider using Poka-yoke to minimise potential errors during coupling and mitigate their risks (Estrada et al., 2006). For example, a prevention-based Poka-yoke acts before or during the error occurrence to correct it. This may be regarded as the Control approach. A Detection-based Poka-yoke warns the user of errors to encourage correction. This is regarded as the warning approach. Poka-yoke mechanism may be implemented in 3 ways:

1. Contact method

2. Fixed-Value method

3. Motion-step method.

The contact method is most relatable for passive compliance issues, it detects any deviation in shapes, dimensions, forms, position or other physical characteristics through mechanisms that are kept in direct contact with the part. Contact method can be used in situations with environmental problems such as poor lighting, critical temperature, dust, noise and so on. Errors must be identified and related to design characteristics and requirements. Thus, alongside functional design requirements, new Poka-yoke requirements must be included in the design stage. Poka-yoke requirements for manual assembly are well described (Estrada et al., 2006) Some of these are relevant and useful for fluid coupling interface design.

2.3 The flexing part: Compliant mechanism design

So far in this chapter, we discussed the history of compliant end effectors for Peg-in-hole insertions. We also studied various procedures, shapes and design features which can improve the robustness of insertion. To fully understand the issues of passive compliance we must expand our scope to the general theory of compliant mechanism design. This will constitute the flexing parts of the passive compliant-end effector. The corrective motion generated as a result of peg-in-hole contact is not only governed by the contact geometry but also by motion features and degrees of freedom (compliance) of the end-effector. As opposed to traditional rigid link mechanisms, compliant mechanisms, especially monolithic ones are inherently cheaper to manufacture and maintain and thus useful for our economically aware application.

2.3.1 Conceptualisation

Conceptualisation usually marks the beginning of a design process. the first step should be to investigate existing designs. These may be found in design banks of compliant mechanisms (Howell et al.,2013) and satisfy many design problems. Even rigid mechanisms can inspire and lead us towards their compliant counterpart. The PRBM approach can be used to convert rigid designs into compliant counterparts and vice versa. However, the major downside of this approach is that in most cases 2D planar mechanisms are realized. TO aims to combine conceptualisation, modelling, and optimisation in one, however TO for compliance mechanism

is a relatively new research field and the approach has many practical issues. modelling approaches are further discussed in the following sections.

What is known as constrained-based design significantly aids the conceptualisation process of compliant mechanism design. Various building blocks or compliant elements with known degrees of freedom and constraint can be arranged to achieve the desired motion (Howell et al.,2013). For example, parallelogram-guided beams provide a single translational DoF, folded flexures can be constraint motion in one direction and cross flexures provide rotational DoFs. Morphological charts and tree diagrams can be used to develop concepts using various building blocks(Ulrich and Eppinger, 2015). When designing for large motion it's crucial to make use of elements that incorporate distributed compliance with no focal hinges or small-length flexures. Due to large stress concentrations, these elements do not perfume well in large displacements. In the capitalisation stage designs can be organised in decision matrices and rated against their performance in various specification measures which should include large motion criteria described in the following section.

The design of a compliant mechanism is certainly more challenging than rigid link mechanisms. Since the output motion is achieved with implicit structural deformations of mechanical elements, kinematics alone will not suffice. Thus, structural mechanics must also be incorporated to model the mechanism. This issue gets more complicated if the structural deformations are relatively large (>5% of the characteristic length or strain). This is due to the geometrical nonlinearities that are introduced in physics. Furthermore, in larger motions, stresses and fatigue can build up quickly and render a design obsolete. Large motion hinges aim to increase compactness while maintaining acceptable error in terms of parasitic motion and stress limits. Accordingly, important characteristics of a compliant mechanism or joint can be measured by the following metrics.

1. Range of motion- How much absolute motion can be achieved. A more useful interpretation of a range of motion is compactness which can be described by the range of motion/ characteristic length of the mechanism.
2. Motion axis drift- The amount of movement of the axis of motion, a more useful measure of comparison would be the range of DoF motion/ axis drift.
3. Off-axis stiffness or drift- The amount of movement of the other axis, a more useful measure of comparison would be a range of DoF motion /off-axis drift.

4. Stress concentration- a measure of how well stress is distributed within the mechanism, this may be represented by a ratio of average stress /peak stress. In comparison to large displacement joins max stress/ max DoF motion is also a good indicator of the stress capabilities of the joint/mechanism

5. Force-displacement relationship- constant stiffness or nonlinear behaviour.

Large displacement hinges (building blocks) of compliant mechanisms are well discussed and compared in the literature (Trease et al., 2005). RCC-type joints are often used for revolute motion joints in the micro/nanoscale. The design and accurate modelling of such joints have been discussed in some detail (Lobontiu et al., 2001). In other work, different types of large-motion spherical and translational joints are proposed (Rommers et al., 2021). Interestingly, their spherical joints attain RCC characteristics for a large range of motion. There are many research papers proposing new large displacement compliant joints, useful as building blocks in compliant mechanism design. In order to predict and optimize the performance of compliant mechanisms they must be modelled. For small motions, this can be done through analytical methods (Lobontiu et al., 2001) using beam models, and for larger motions with PRBM or FEA.

2.3.2 Modelling with PRBM

Although the PRBM method has been investigated for many years, the book (Howell, 2001) presents it in the entirety that it is known today. In this method, the compliant mechanism is replaced with an equivalent rigid mechanism which enables the use of classic mechanism synthesis and kinematic modelling such as the vector loop approach. Howell presented PRBM parameters for small-length flexures, fixed-pined, pined-pined and fixed-fixed compliant beams. When using proposed models, the accuracy of PRBM is reduced in dealing with fixed-fixed beams. This inaccuracy is tolerable at around 6% (Lyon and Howell, 2002). Recalling that a large displacement, fully compliant mechanism is often monolithic with slender beams, hence most useful scenarios should include fixed-fixed beams. The literature has more to offer, such as more accurate and useful beam models for PRBM applications (Midha et al., 2015; Su, 2009 Chen, 2011). Usually, these models have more joints and springs to more accurately mimic the compliance. Often the PRBM model is referred to by the number of springs/joints it imposes on a cantilever beam, I.e., 2R,3R etc. A downside of increasing the number of joints, springs and DoFs is the increased complexity of modelling. A more important drawback of the

PRBM is that it usually applies to 2D linkages type design, which restricts the conceptualisation design space.
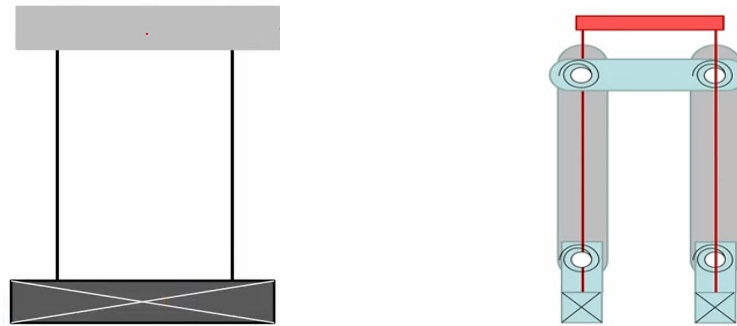
Figure 2.4 Conversion of compliant mechanism to its rigid equivalent

Figure 2.4 shows a compliant parallelogram mechanism with 2 compliant beams and a rigid coupler. the rigid body counterpart of the compliant mechanism is shown on the right side of the figure. Note the addition of shorter rigid links and torsional springs upon every pin joint. The lengths of the links and location of pin joints are found depending on which models have been used. In this case, the fixed guided model is used since the rotational motion of the coupler is negligible. The model provides the stiffness of the springs as:

$$K = 2\gamma K_\theta \frac{EI}{L}$$
<div style="text-align:right">2.1</div>

K_Θ and γ are given by given by for specific applications (Howel et al 2013). From here onwards, typical linkage design analysis can be conducted through methods such as vector loop kinematics and force balance can be used to evaluate force-displacement relationships.

Designing a mechanism for specific tasks or motion requires either optimisation or application of mechanism synthesis methods.

1. Type and number synthesis: where the mechanism type or topology is determined often by determining the number and position of links and joints.
2. Dimensional synthesis: where the size of the links is determined which results in a specific type of motion. There are generally 3 ways to do this:
   i. Function generation: where a desired function/relationship between input and output link is realised through a series of discretised precision points.

ii. Path generation, where a selected point on the mechanisms is required to move on a desired path.

iii. Motion generation, where the motion of a rigid body or technically a line on a plane is realised.

When DoFs of the mechanism increase or the problem includes nonlinear contacts and friction, it becomes very cumbersome if not impossible to use analytical approaches of traditional mechanism design and synthesis. In such cases, numerical rigid body solvers are coupled with optimisation to interactively find suitable design parameters. This approach highly suits our applications and will be discussed in more detail.

2.3.3 Modelling with topology optimisation methods

TO is a material distribution problem in which the algorithm identifies the optimal layout of material within a Finite Element (FE) grid. The method has roots in structural design where most often the objective is to minimise compliance with the least amount of material. Before TO, methods of shape or size optimisation were highly fashionable in the literature on structural optimisation. Consequently, the topology optimisation method introduced by Bendsøe and Kikuchi, 1988, is very relatable to those techniques. In this type of TO, design variables are typically the size of micro-structural voids within each element. This size variable essentially controls the amount of material within that cell and in turn, is used to determine the equivalent mechanical properties of that element via the Homogenisation theory. Eventually, this optimisation problem is solved using an appropriate programming algorithm. Optimality Criteria is a heuristic but well-established solver that is used extensively in structural optimisation and now TO. The method of Moving Asymptotes is also popular, but in general, Gradient-based are often used to solve the optimisation problem.

SIMP is a more direct approach to homogenous TO. There is no need for microstructures to optimise the size of, and hence no need for homogenous theory. However, the optimisation and programming procedure is essentially the same. In the SIMP method, a virtual element density parameter is the design variable. For better physical representation of this virtual variable, it has been reinterpreted as a control factor of the element's Young's modulus (Bendsøe and Sigmund, 2004), taking a value between 0 and 1. These densities are often penalised by a power law to push the result to a more realisable, 0-1 or black-and-white solution. Intermediate densities are difficult to manufacture using conventional techniques. In almost all cases of

topology optimisation a filter and regularisation, technique is required to coverage to optimal, and mesh-independent solutions.

Recently papers discussing the homogenised method are very rare, on the other hand, we can see the application of SIMP methods in commercial CAE packages; SIMP has become much more popular. Considering the Finite Element nature of the problem, the SIMP TO problem is mathematically stated as

$$\textbf{Min: } 0.5 U^T K U \qquad\qquad 2.2$$
$$\textbf{Subject to:}$$
$$V^T \rho \leq V^*$$
$$KU = F$$
$$\rho_{min} \leq \rho \leq 1$$

Where ρ is the vector of design variable virtual density of elements that co-exist in the global stiffness matrix. It can be directly multiplied with the stiffness matrix or alternatively, included in the constitutive matrix where the elastic modulus sits. Note that if external solvers are used, there is typically no need to include the constraint KU=F, this is satisfied when FEA is implemented.

Generally, there are not many mathematical bounds on the theory of evolutionary TO. They are based on the evolution theory that takes place, very slowly, in nature. One of the more sophisticated versions of the method is the soft kill BSEO in which a removed element can get a chance to reinter the mesh. When evolutionary methods are posed well, they will produce similar results to other methods while being easier and more flexible in implementation (Alonso et al., 2014). There is no need for optimisation (programming) algorithms that are more complicated. Nonetheless, this method seems like a yet again more direct but discrete approach to the SIMP method (Sigmund and Maute, 2013). In answer to this criticism, many papers were reviewed to get a sense of the development and applications of evolutionary methods (Munk et al., 2015). These approaches certainly deserve more appreciation from the TO community and their weaknesses are just similar to other methods (e.g. local optimums). Furthermore, the flexibility of the evolutionary method should be prized due to the capability of synergy with other design optimisation methods such as the Design of Experiments and Genetic Algorithms.

There are other approaches such as topological derivatives, and phase field methods. Recently Level-set methods are also trending in the literature. A comprehensive review of various approaches with concluding remarks appoints the top 3 contenders are the SIMP, BESO and level set methods (Sigmund and Maute, 2013). Due to a large number of variables (elements of the mesh), methods such as GA or direct search are computationally inefficient for solving TO. As the gradient/sensitivities are most often analytically obtainable, the problem is often solved using gradient-based methods. Where c is the cost function (minimising compliance) sensitivities/gradients are given as:

$$\frac{\partial c}{\partial \rho_e} = \mathbf{0.5} U^T \frac{\partial K}{\partial \rho_i} U = -U_e^T n \rho_i^{n-1} K_e U_e \qquad 2.3$$

The literature recommends filtering schemes to ensure the existence of solutions and the prevention of checkerboard patterns (Bendsøe and Sigmund, 2004). There are many different filtering schemes, a density filter operates by modifying the value of each design variable based on the weighted value of neighbouring elements (design variables). This is the density filter (Bruns and Tortorelli, 2001) :

$$\rho_i^f = \frac{\sum_{jEN_i} H_{ij} V_i \, \rho_j}{\sum_{jEN_i} H_{ij} V_i} \qquad 2.4$$

Where Ni = {j : dist(i, j) □ R}, Hij = R − dist(i, j)

ρ_i^f, is the filtered density, V_i is the volume of the ith element, H_{ij} is the matrix of weighting factors that are based on the distances neighbouring elements, N_i is the set of elements that neighbour the ith element. 'dist' is the matrix of distances between the ith and jth element, R is the radius that determines neighbourhood and which j elements will modify the ith element.

Due to the filtering, design variables are interrelated. To obtain new sensitives the chain rule must be employed:

$$\frac{\partial c}{\partial \rho_e} = \sum_{i:N_e} \frac{\partial c}{\partial \rho_i^f} * \frac{\partial \rho_i^f}{\partial \rho_i} \qquad 2.5$$

Another filtering method includes the filtering of sensitivities (Sigmund, 1997). Both the density and sensitivity filters produce good results and are still widely applied in various topology optimisation problems.

$$\frac{\partial c}{\partial \rho_i}^f = \frac{\sum_{jEN_i} H_{ij} \frac{\partial c}{\partial \rho_i}}{\max(x_i, \gamma) * \sum_{jEN_i} H_{ij}} \qquad 2.6$$

Where, γ is a small number (e.g., 10-3) to avoid division by zero.

2.3.3.1 Compliant Mechanism TO

Compliant mechanism TO differs from structural formulations since there is an output port which must behave in a certain way, (output load or displacement). See typical formulation below (Frecker et al., 1997).

$$\text{Min:} \frac{\text{Flex}}{\text{Stiff}} = \frac{-U_1}{SE} = -\frac{u_v^T KU}{0.5 U^T KU} \qquad 2.7$$

$$\text{Subject to:}$$

$$V^T \rho = V^*$$

$$KU = F$$

$$Ku_v = f_v$$

$$\rho_{min} \leq \rho \leq$$

For a mechanism, the quotient rule of differentiation is used to derive the sensitivity:

$$\frac{\partial c}{\partial \rho_e} = \frac{u_{v_e}^T n \rho_e^{n-1} K_e U_e}{U_e^T n \rho_e^{n-1} K_e U_e} \qquad 2.8$$

Where $u_v^T KU$ And $Ku_v = f_v$ are new (compared to structural) terms in the formulation. These arise due to the nature of this objective function that requires the displacement at the particular node (and direction) which is to be maximised for the compliant mechanism. $u_v^T KU$ Is this displacement and f_v is the load vector containing a unit load (dummy/virtual load) at this degree of freedom. The only difference between structural problems is that 2 load cases are defined as vectors F and f_v. U and u_v are solved separately using, $Ku_v = f_v \ and \ KU = F$, note K is the

same in both cases. Again constraints $KU = F$ and $Ku_v = f_v$ are being satisfied by FEA implementation.

The five most commonly used objective functions are based on stiffness-flexibility, Mechanical Advantage (MA), Energy efficiency, Geometrical Advantage (GA) and displacement (Deepak et al., 2009). These formulations tend to result in minor differences in topologies. Bigger differences are observed when considering a performance criterion for the mechanism. For example, when using the MA formulation one can attain a value of 2 for a given topology but using the Stiffness-flexibility method one may only converge to a solution that has a MA of 1.5. Hence, selecting the formulation is somewhat case-dependent and it is promising to see typical mechanism specification criteria i.e., GA and MA can be optimised within TO. What is common to all of these approaches is the appearance of one-node and de-facto hinges which result in relatively undesirable lumped compliance topologies.

2.3.3.2   *Large displacements*

Including large displacement in TO is nothing more than performing nonlinear FEA instead of a linear one, or adding constraints to regulate parasitic motion in large displacements. there are large motion performance improvements yet still using nonlinear FEA significantly increases difficulties of convergence and complexity. It is generally argued that linear FEA suffices for the topology optimisation stage of the mechanism since the goal is to find an optimal topology that transfers motion in the desired direction. Thus quantitative performance measures are revisited in a post-processing stage. (Pedersen et al., 2001)

2.3.3.3   *Practical design issues*

We developed a 2D SIMP topology optimisation MATLAB code based on the mutual strain energy objective function (more information in Appendix A1), a few examples of designs are shown in Figure 2.5 and Figure 2.6. Practical issues are observed coinciding with the literature.

One node hinges have no tangible meaning in terms of topology thus a classic solution is to replace them with slender beams or other hinges in a post-processing stage (Pedersen et al., 2001). In this phase, it is also important to consider fatigue and stresses, especially in these hinges. It may be the case that several iterations are required to make a trade-off between performance measures see Figure 2.5. Figure 2.3. The exact method of the postprocessing stage is not quite clear and it is often neglected by academic journalists. With the addition of some

complexity and computational cost, stresses can be included in the algorithm as a constraint or an objective, in which case one node's hinges tend to disappear (De Leon et al., 2015). However, the algorithm still tends to produce lumped compliance designs with de-facto hinges. Since these hinges have physical meaning they are often welcomed and excused by designers that are primarily after meeting specifications. Distributed compliance topologies are achievable, for example by using a weighted sum objective function of output displacement, and compliances at the input/output nodes (Yin and Ananthasuresh, 2003 Zhu et al., 2014).

There remain more subtle issues in TO. Some of these have been experienced by the author in the development of a useful TO approach. Most algorithms rely on a very narrow range of user-defined parameters (i.e., stiffness of the output spring) to provide a solution (Cao et al., 2015, 2013). In a practical example, a designer may face the situation of low resistance from a workpiece and thus defines a small stiffness for the output spring, the algorithm may not provide a viable solution (if one exists) unless:

1. Optimiser parameters such as objective function scale, number of iterations, optimality etc suit
2. Other inputs such as the number of elements, input force and filter radius find their "golden values".

So, the compliant mechanism TO is not as settled and automated as promised but relies on the ongoing contribution of researchers and the inputs of an experienced user. This is not entirely the case for structural TO where the objective function is much simpler and does not require the addition of springs. Furthermore, issues of large displacements and stresses do not appear frequently in structural TO. Minimising compliance (a universally accepted objective function for structural problems) tends to address both of these issues indirectly, making it an overall simpler and more efficient algorithm. There have been recent efforts to solve these issues within the algorithm itself, these are discussed in a great review paper (Zhao 2020).
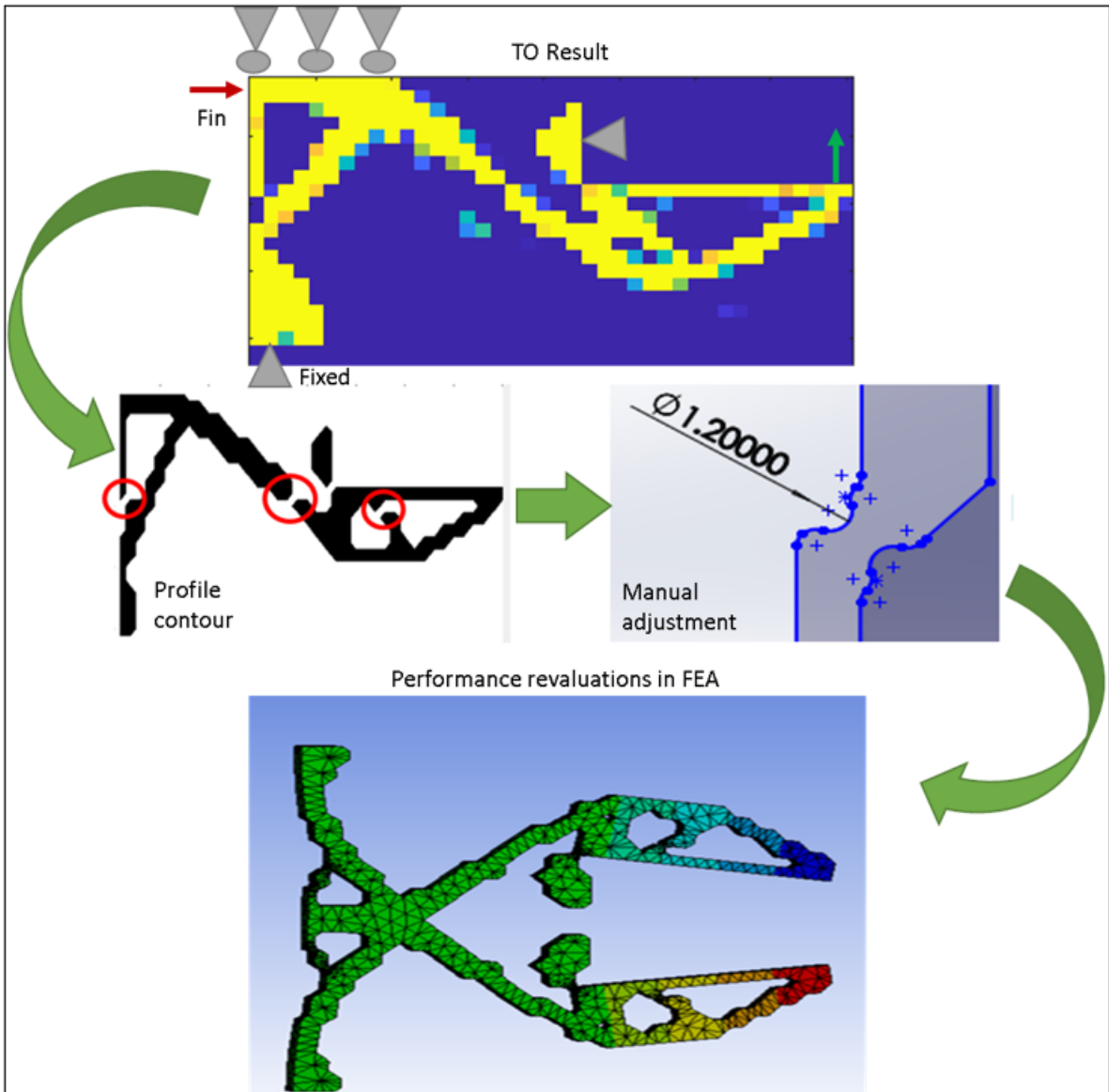
Figure 2.5 Example of post-processing a gripper topology.

2.3.3.4 Robust TO

At present, two main approaches consider uncertainties in topology optimization. RBTO relies on defining one or more failure states that are functions of the uncertain parameters and it is sometimes difficult to immediately define a meaningful failure state. When a failure state is not defined, an alternative approach to RBTO is Robust Topology Optimisation (RTO). This method tends to be more popular with engineering designers since there is a large background of knowledge of robust design techniques such as sensitivity-based optimisations, direct search, Taguchi methods or design of experiments.

Initial efforts in RTO realized what is called the worst-case method. This is where the worst possible objective function is evaluated at each TO iteration and the corresponding load case is set as the objective function to optimise. Thus, the non-deterministic problem is turned into a multiple-load case deterministic TO, see Figure 2.6 (author's work). Since the worst possible case is being optimised, it is argued that results are robust. When the uncertainty interval is relatively large, discretisation of the interval with efficient sampling and approximation of the objective function is essential in avoiding prohibitive computational costs, relating to solving many FE load cases. Within the RTO method, many researchers rather use a probabilistic objective function. Popular choices are to minimize, either, or a combination (often weighted sum) of expected and variance of the objective function. However, most often similar discretisation, and approximation are required.
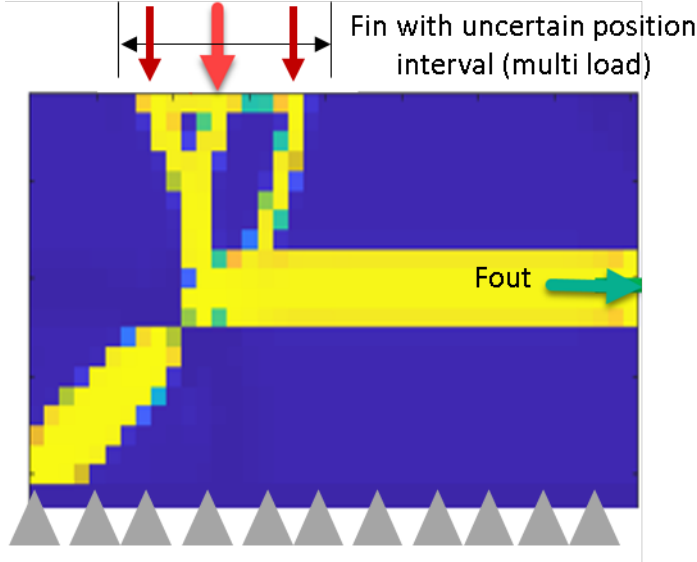
Figure 2.6 Example of load transfer mechanism with the worst-case multi-input approach

Various parameters can affect the robustness and reliability of a structure, including loading, geometry and material properties. We are mostly concerned with loading uncertainties imposed by misalignments. A probabilistic objective function and corresponding first-order gradient-based approximations (only apply to small values of uncertainty) can produce robust designs (Kogiso et al., 2008). Analytical efforts proved that uncertainty in loading magnitude and angle in structural problems can be exactly modelled using 3n+1 load cases, where n is the number of uncertain loads (Dunning et al., 2011). Essentially removing the need for sampling and approximation of the objective function. This method applies only to structural problems with

a probability distribution of the uncertainty and does not consider the uncertainty in load position.

Very few studies are concerned with load position uncertainty. See for example a worst-case approach using some interval arithmetic and Taylor series approximations for structural problems (Wang and Gao, 2019). This study requires expressions for the derivatives of various structural load cases useful in developing those Taylor series approximations which, are used to identify the worst-case load. Unfortunately, the implementation of this method, especially in deriving gradients is quite uncertain due to the lack of information instigated by these journalists. A much clearer but similar approach using Chebyshev approximations (Wu et al., 2016). Then again only considering structural problems with load angle and magnitude uncertainty. There it has been very difficult to find even one study that addresses load position uncertainty for TO of compliant mechanisms, not even for small amounts of uncertainty.

Table 2.2 Comparison of robust topology optimisation papers

Name	Year	type	method	Uncertainty	Form	Large uncertainty
Wang	2019	STRUC	SIMP	Force. P	Approx	NO
Wu	2016	STRUC	SIMP	Force.M+A	Approx	NO
Dunning	2011	STRUC	Level set	Force.M+A	Analytic	YES
Kogsio	2008	MECH	Homoge.	Force.M+A	Approx	NO

2.4 Summary

Previous end-effector solutions and existing literature do not match well with passive compliance problems observed in unstructured environments such as train fluid servicing. Even though some commercial compliance devices provide a fair amount of misalignment compensation, they still do not match our requirements. We cannot model and estimate insertion forces which are crucial to safety, robot sizing and cost. Nonetheless, previous work has made it clear that RCC can significantly reduce insertion forces and prevent jamming and wedging during alignments. Unfortunately, the studies do not consider larger misalignments or propose a design method for end-effector development. Furthermore, most assembly parts in these studies tend to be cylindrical or rarely square.

As discussed there are some design considerations which can significantly improve PiH alignment process. For example conical, convex and generally tapered shapes, or asymmetric connecting faces. Here we can conclude that the problem of alignment may differ from the assembly or coupling of parts. In alignment problems, peg and hole shapes may be a free design parameter along with end-effector compliance. Unfortunately, today, in train fluid servicing, we cannot consider changes to fluid port interfaces.

In modelling, nonlinearities can arise due to material and geometrical issues. Material nonlinearity can be thought of as a nonlinear stiffness such as in the case of hyperelastic material such as rubber. Most engineering materials such as steel or aluminium have linear stiffness until the yield point beyond which plastic deformation occurs. Compliant end-effectors will operate in the elastic region and thus material nonlinearities can be ignored for most engineering materials. Large deformations cause geometrical nonlinearities since they significantly change geometrical behaviour and boundary conditions, such as the position and direction of applied forces. Here we did not discuss analytical models that can be used for simpler problems, often those not including nonlinear contact or large deformations. The beam constraint models can be used for up to 10% strain (Howell et al., 2013). However, the mathematics and derivation involved can quickly become cumbersome and sometimes impossible for slightly complex designs with multiple DoFs and nonlinear contact.

PRBM can approximate large motions by modelling the compliant mechanism with equivalent rigid components. These methods enable the use of classical mechanism (linkage) design theory such as kinematic vector loops and synthesis (function/path generation). Linkages are often planar (2D) which makes their synthesis and design bearable with such numerical methods. 3D designs, nonlinear contacts and large motions can be solved many orders of magnitude faster than nonlinear FEA by coupling PRBM with rigid body solvers (e.g. SolidWorks motion analysis, Ansys rigid body dynamics) which makes this approach very powerful, fast and user friendly. Force and displacement estimates are solved relatively well with PRBM however, due to the significant simplification required to measure stresses, this important parameter is often overlooked and passed on to later stages of the design process.

Topology Optimisation (TO) is another modelling and design method for compliant mechanisms, studies have shown that nonlinear Finite Element Analysis (FEA) can be coupled with TO to account for large motions. However, the method is not mature enough to practically consider uncertainties and implement robust design methods. Furthermore, TO has other limitations which include difficulties in modelling contact, impractical design generation, unreliable, sensitive to user input and time expenses associated with extensive FEA runs. This renders this method useful only for conceptualising simple designs, as opposed to modelling performance in practical applications.

A more general and practical approach is required to design, model and optimise passive compliant end-effector. This should be regardless of the particular shape of the fluid coupling interface or the amount of misalignments. It should consider practical design aspects such as material fatigue so that engineers will find it useful in their analysis.

3. ROBUST DESIGN METHODOLOGY

Overview

Here we discuss what comprises a passive compliance design problem and formulate it as a robust engineering design issue. We discuss how this will be useful in the design process and how various performance measures are formulated to optimise the performance of compliant end-effectors. Finally, two distinct modelling approaches are developed and measured against physical experiments conducted inside the lab.

3.1 Introduction

Currently, the design process of passive-compliant end-effectors is unclear. Generally, a mechanical design procedure follows an orderly process which includes the stages of problem definition, conceptualisation, modelling, and performance evaluation (Ulrich and Eppinger, 2015). For a more comprehensive approach, this process can be implemented iteratively according to Figure 3.1.
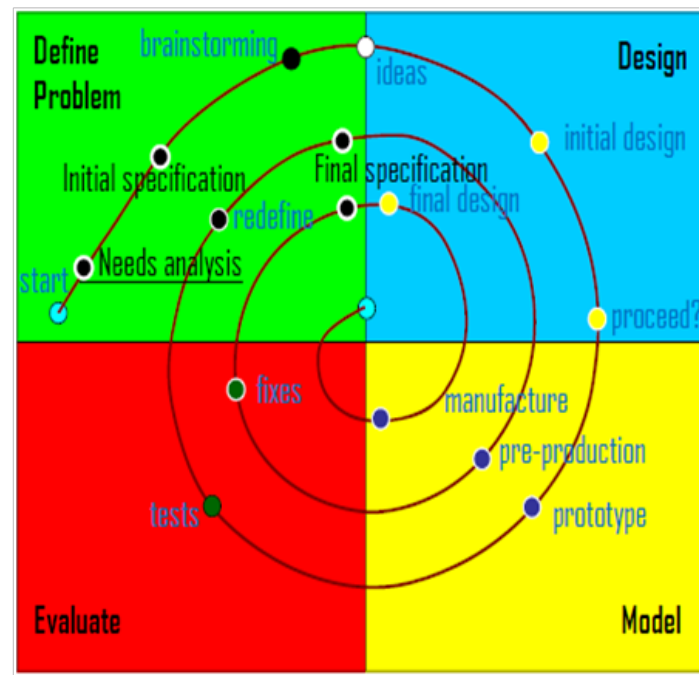
Figure 3.1 Spiral design methodology (M.Atherton, 2020)

Requirements analysis, specifications, and establishing performance measures are conducted in the first block. In the second block, design concepts are realised, compared, and selected. In the third block, concepts are modelled numerically, or prototyped so their performance can be measured and analysed in the final block. The results are compared to a specification which may need updating due to limitations or prospects of the design. The loop continues around and iterates to a successful product. In this work we consider this approach as a standard, however, many questions can be raised regarding how one implements such an approach for compliant end-effectors. The questions that raised the interest of the author are as follows:

1. How can we measure the performance of a compliant end-effector, and which quantities are relevant?

Requirements must be tied to metrics whose quantality illustrates the capability of the design in delivering them. Development of specifications, understanding requirements, benchmarking, and concept comparisons all depend on performance measures.

2. How can we model performance considering general peg and hole shapes, large deformations and nonlinear contacts?

Compliance is associated with contact of two components, modelling contact can be challenging, coupled with large structural deformation of the compliant mechanism, and it can be acknowledged that modelling of such a problem will not be trivial.

3. How can we achieve desired performance metrics and specifications with uncertainties of misalignment?

When operation includes uncertain input parameters such as misalignments the performance may be hindered. A guaranteed level of performance is required.

In this chapter, we construct a methodology to answer these questions.

3.2 A general approach

A compliant end-effector consists of a compliant mechanism which converts contact forces with an external workpiece to useful and accommodating motions. Since it will be impossible to accurately line up the end-effector and workpiece, especially in an unstructured environment, the amount of contact forces and their location are often subject to uncertainty.

The general ideology proposed in this thesis suggests a passive compliance design problem can be distinguished by the existence of some kind of uncertainty, which manifests itself through the force-displacement relationship between the end-effector and an external workpiece.
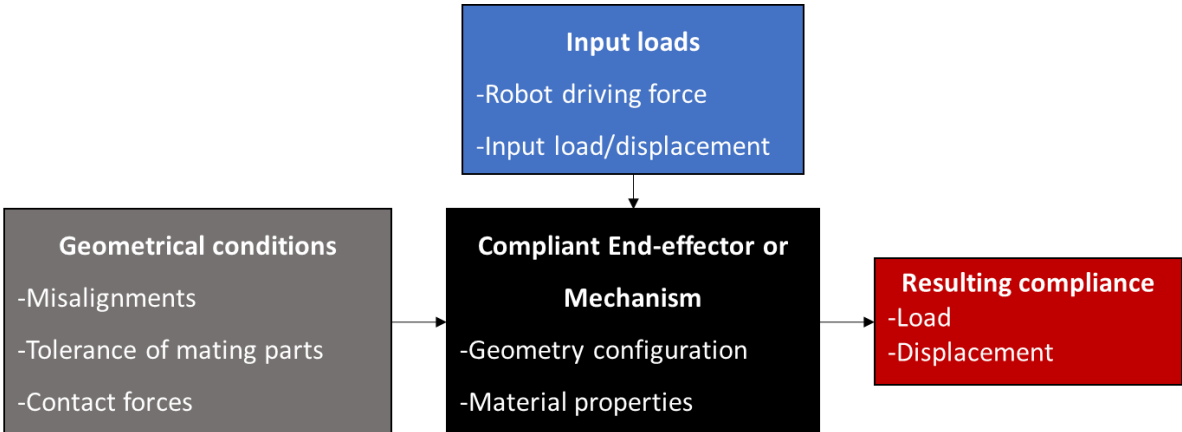
Figure 3.2 The general passive compliance design problem

In most, if not all cases. uncertainties between mating parts include misalignments, geometrical dimensions, surface finish (friction) etc. Hereafter, these uncertainties are referred to as noise factors. The compliant mechanism must convert all inputs into useful output loads and displacement which in turn achieve a task. Usually regulating forces or providing guiding motions. The geometry, dimensions, topology and material properties of the mechanism are design factors related to the compliance (i.e., stiffness, and load-displacement relationship, all loosely referring to the same quantity) of the mechanism. Bounded by the specification, the designer is free to select the value of these design factors. What we will call signal factors, are deterministic but cannot be selected by the designer. They are usually constrained by the application or a user input parameter to the system. For example, a gas pedal input to a car is set by the driver, not the designer.

Mechanical engineers rely on various physical laws, mathematical models, and prototype models to identify suitable values for design factors which achieve the desired performance. However, when noise factors are introduced to the system RED should also be incorporated to ensure feasible performance. See the comparison of Figure 3.2 and Figure 3.3.

The RED approach aims to optimise the design for robustness which results in minimum performance variance (or standard deviation) with maximum performance mean. Indicating that the effect of uncertainty (noise) is minimised on a satisfactory performance level. This process requires a series of structured tests (performance evaluations) to facilitate a search for a feasible design configuration. A trial-and-error approach to this search, for example, Monte Carlo sampling, can result in many performance evaluations before reaching a desirable solution. If changing design configuration and testing performance is a difficult task, for example in physical modelling and experiments, the cost of this approach is very undesirable.
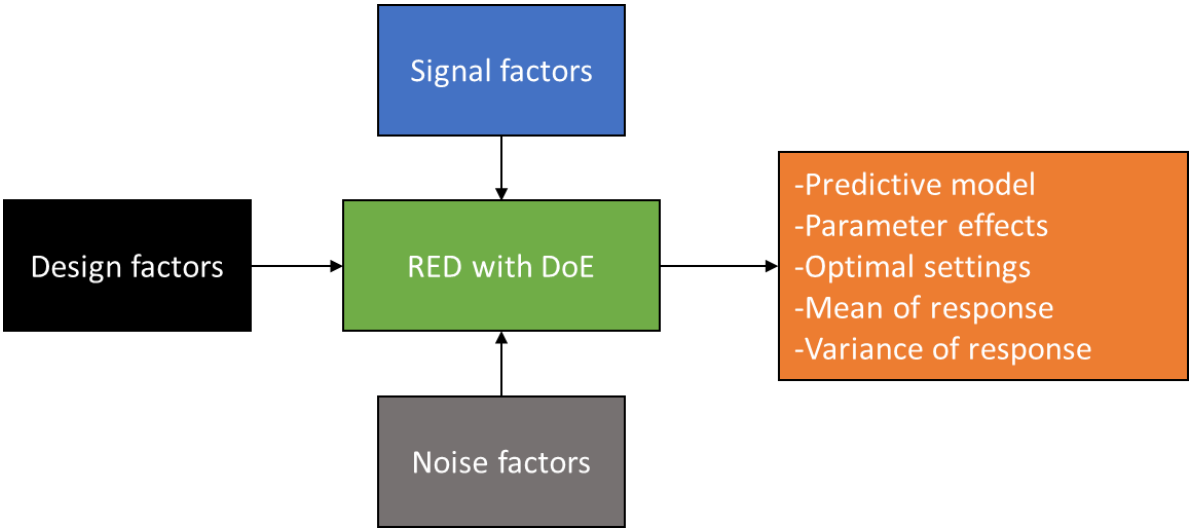
Figure 3.3 The general robust design process with DoE

Given a rigorous mathematical model of the problem which entails the effect of all noise and design factors, it is possible to analytically derive variance and mean with little effort. In most practical cases this luxury isn't available, and many experiments/simulations are required to facilitate the derivation of performance mean and standard deviation.

$$\bar{Y} = \frac{1}{n}\sum_{i=1}^{n} Y_i \qquad\qquad 3.1$$

The standard deviation is given by.

$$Y_{sd} = \sqrt{\frac{\sum_{i=1}^{n}(Y_i - \bar{Y})^2}{n-1}}$$

<div align="right">3.2</div>

Where Y is the response, n is the number of samples.

There are several more efficient approaches to RED, for example, Taguchi methods, Genetic algorithms or other optimisation/search algorithms that incorporate mean and variance in a cost function. Generally, these approaches, require the "explicit" (none analytical) evaluation of performance mean and variance. That is multiple performance evaluations at various noise conditions for each design configuration. However, they still aim to minimise the number of performance evaluations required and accelerate the search procedure.

$$minimise: [-\bar{Y} ; Y_{sd}]$$

<div align="right">3.3</div>

$$Subject\ to:$$
$$x_{min} \leq x \leq x_{max}$$
$$z_{min} \leq z \leq z_{max}$$

Where x are design /signal factors and z are noise factors in vector formats.

Design of Experiments (DoE) is another approach to robust design (Montgomery, 2012). Other than minimising the number of tests, this method isolates and reveals the effect of experimental factors on performance. The Taguchi method can be considered a special case of the DoE, which requires much less statistical effort to implement, this of course has a trade-off which will become apparent in due course. DoE uses a pre-set plan including a particular number of performance evaluations to develop performance-predicting regression models usually similar to Formulation 3.4. These equations are then very easily manipulated, similar to analytical models.

$$Y(x,z) = \beta 0 + \gamma 1 z 1 + \beta 2 x 2 + \beta 3 x 3 + \delta 12 z 1 x 2 + \delta 13 z 1 x 3 + \cdots + \varepsilon$$

<div align="right">3.4</div>

Where y is the response, x are design factors, and z are noise factors, β and γ are the regression coefficient that describes the effect of each term in the model.

DoE methods such as full factorial and fractional factorial design are widely applied with 2-level factors. Despite the advantages of having only 2-level such as reduced experiment, it is inadequate for predicting precise and non-linear behaviour of the system. Response Surface Methodology (RSM) is a branch of DoE concerned with higher-order (typically second-order) regression models.

$$Y = \beta_0 + \sum_{i=1}^{n} \beta_i x_i + \sum_{i=1}^{n} \beta_{ii} x_i^2 + \sum_{i=1}^{n} \sum_{j=2}^{n} \beta_{ij} x_i x_j + \varepsilon \tag{3.5}$$

R represents system response, n stands for the number of factors, x_i stands for each independent factor, β is the coefficient for each independent term and ε is the error term.

Once the structured tests of the DoE are complete, the regression can be fitted. DoE models undergo Analysis Of Variance (ANOVA) and have their validity measured by comparing the significance of regression coefficients, P-values, R-squared values and cross-validation checks with the physical observations. Once approved, the model becomes an 'emulator' of the physical or simulation system. By inputting design/noise/signal configurations, it will predict the performance of the system. A benefit of the RSM approach lies in the reduced number of physical/simulation performance evaluations required to develop such powerful predictors

Since the mathematical model is easy to manipulate it can facilitate many forms of optimisation or robustness analysis. Even though mean and standard variance can be computed numerically ("explicitly"), Montgomery, 2012 presents a more analytical approach to this. Given the general regression model in the form:

$$Y(\boldsymbol{x}, \boldsymbol{z}) = f(\boldsymbol{x}) + h(\boldsymbol{x}, \boldsymbol{z}) + e \tag{3.6}$$

When assuming noise variables have the mean expected value of zero and the covariance between them is zero, then the mean can be evaluated analytically.

$$E\big(Y(\boldsymbol{x}, \boldsymbol{z})\big) = f(\boldsymbol{x}) \tag{3.7}$$

Using the transmission of error approach with Taylor expansion of the response model, the Variance is given by (Myers et al., 2016)

3.8

$$V[Y(\boldsymbol{x},\boldsymbol{z})] = \sum_{j=1}^{y} \left[\frac{dY(\boldsymbol{x},\boldsymbol{z})}{d\boldsymbol{z}}\right]^2 \sigma_z^y + \sigma^y$$

The beauty of the DoE approach is the revealing and illustration of factor effects. We can plot the overlayed contour of the mean and variance versus the design variables of interest. This illustrates the design configuration in which the desired performance can be obtained, see Figure 3.4. By expanding the number of factors or their ranges the charts can be "generalised" showing performance across a range of design configurations. For example, analogues to chain selection charts, or compressor efficiency maps that are used directly for design. With little effort, a fellow designer may use these results to embody a design for their specific applications.
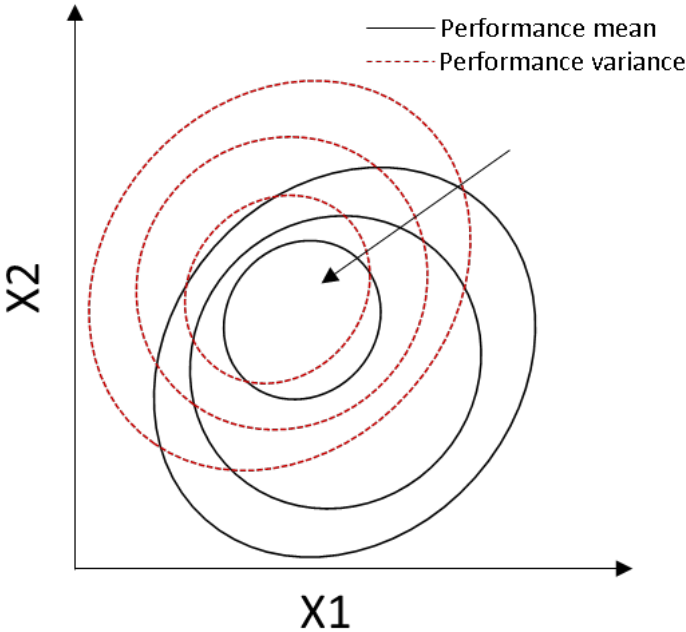
Figure 3.4 Overlaid mean and standard deviation example.

The flowchart of Figure 3.5 summarises the general approach proposed for the design of compliant end-effectors. In summary, the first step is to investigate the requirements of the end-effector to propose and analyse design concepts. For further detail in this regard refer to existing literature (Ulrich and Eppinger, 2015). In this work, we use engineering judgment and knowledge to come up with concepts. We have also introduced topology optimisation methods in the previous section, this is another tool which can significantly guide initial design concepts

and inspirations. In the next stage, key design factors and any uncertain parameters are identified. Followingly a model is developed which can evaluate the performance of the design. The RED plan is then selected where a series of experiments/simulations are conducted. Results are integrated to identify optimal design configuration. In the following, we will further discuss, various DoE/RED plans, performance measures and modelling.
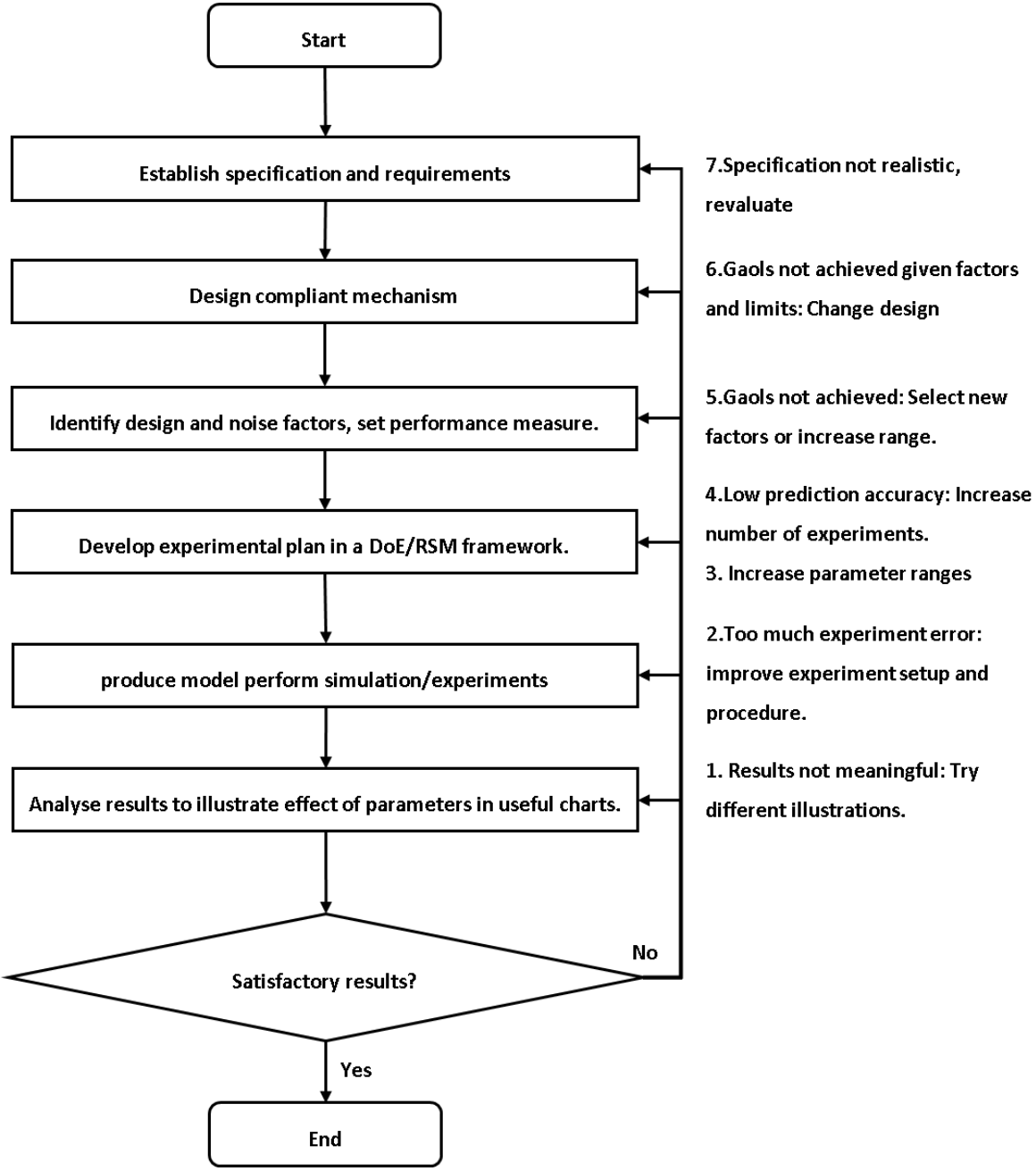
Figure 3.5 General approach: methodology flowchart

3.2.1 Choice of DoE plan

For more general advice regarding DoE the reader is referred to (Montgomery, 2012) the following is a brief discussion of some important aspects

3.2.1.1 Factorial and fractional factorial and Tagguchi methods

These methods are suitable where the only purpose of the analysis is to reach a better design. The resolution of the DoE approach describes its capability in terms of evaluating various effects present in the regression model. For example, a resolution 3 DoE only guarantees the "main" effects, that is the direct effect of design or noise variable. In the regression model that would be the term which only has the factor multiplied by a regression coefficient. A resolution 4 design incorporates 1st order interactions that are the cross-effect of 2 variables. In order to maintain a feasible number of runs, usually, the resolution is reduced for 2-level factorials. In most cases, this is a reasonable assumption since multifactor effects such as 3rd order or 4th order interactions are often little.

Due to the reduced number of levels and experiments, it will be hard to make a definitive analysis of what happens between each level, thus we can only rely on the results we see at the particular configuration. Often linear interpolations are used to interpolate effects between levels, for highly complex systems this will not yield satisfactory results.

3.2.1.2 Response surface methodology

More comprehensive results are obtained by adding levels to the experiment plan to satisfy second-order (or higher) models. In this work, RSM is used to explain the nonlinear effect and relationship of factors.

Take, for example, 2 design factors, 2 "signal factors" and 2 noise factors, that's a total of 6 factors. Crudely, a minimum of 1 run is required per each term in the second-order model. Thus, 6 factors require at least 28 runs. However common practice utilises more runs for better approximation of error terms or prediction confidence intervals. Thus, for example, a CCD will require 90 runs and 5 levels, and a Box Behnken Design (BBD) will require 54 runs and 3 levels. These experiment designs are often considered the most robust due to the consistency of prediction across the design space (Montgomery, 2012). When allocating design points three types of CCD can be applied, namely circumscribed (CCCD), inscribed (ICCD) and faced

(FCCD). CCCD tends to create new extreme limits for factors, indicated by the four axial points outside the design space, this can often lead to physically unrealisable designs. ICCD can be seen as a scaled-down version of CCCD with axial points created inside the design space. For ICCD no combination of factors at extreme levels is investigated, e.g. largest misalignments in X and Y at the same time.

Costs associated with physical experiments make it difficult to test many configurations and various levels (this often improves prediction capability). In most simulations this is very easy hence space-filling designs are often preferred; these include Latin Hyper-cube Sampling (LHS) or Sphere Packing Designs (SPD). Space-filling designs have no repeated designs and covers have a wide range of factors levels beyond the 3 or 5 levels. Another benefit is that the number of experiments can be set by the user and can be used to fit any type of regression model. Generally, increasing the sample size (number of experiments) will tighten confidence intervals of prediction and provide more statistical degrees of freedom for error and lack of model fit predictions. More details regarding this approach are found in the existing literature on DoE and RSM. (Myers et al., 2016).

3.2.2 Performance measures for compliant mechanisms

The aforementioned RED approach requires the rapid evaluation of system performance through various design configurations. A nonphysical model of the system will prove essential to most mechanical design procedures due to the cost associated with physically evaluating many system configurations. For the passive compliance problem, this thesis proposes and demonstrates two distinct modelling approaches which will be discussed in due course. It is more important to first understand what it is we are trying to model. What do we want to measure, what is performance?

In general, the typical application of passive compliance can be categorised as follows.

- Force regulation and accommodation
  Given uncertain input load or displacement a particular force quality (e.g., force in a particular direction) must be controlled. For example, in PiH problems the aim is to reduce insertion forces (F_z) during the task. Hence objective Y (see 3.3) becomes :

$$Y = F_z \qquad \text{3.9}$$

- Load/displacement transfer

  Given an uncertain input, some amount of output displacement or load is required. in such cases, we can look at load transfer efficiency and the geometrical or mechanical advantage of the mechanism.

$$Y = \left[GA = \frac{d_{out}}{d_{in}} ; MA = \frac{F_{out}}{F_{in}} ; \eta = \frac{F_{out} d_{out}}{F_{in} d_{in}} \right] \qquad \text{3.10}$$

- Displacement function, path, or motion generation

  Given a certain load or displacement, the mechanism's output port should move according to a function or path. In this case, displacement error (perhaps a sum of errors) to the path or function would be the performance measure. we have not found an application of these mechanisms in train fluid servicing yet.

$$Y = \sum_{i=1}^{p} \left(d_{out,i} - d_{target,i} \right)^2 \qquad \text{3.11}$$

Where $d_{target,i}$ is the target displacement at precision point i, there are p precision points approximate the desired output function from a given load.

- Stress is often overlooked in compliant mechanism design.

  Performance measures including stress will ensure acceptable fatigue life. Stress can be included in performance measures for example through the below formulation.

$$Y = -\frac{d_{out}}{\max stress} \qquad \text{3.12}$$

Ratio-type formations are great for simplifying multi-objective cases. Alternately performance measures can be combined in a weighted cost or desirability function.

$$Y = 0.5 * d_{out} + 0.5 * maxstress \qquad \text{3.13}$$

An even better approach which, DoE enables, is the derivation of multiple regression equations from the same experiment plan and results. The responses can be overlayed (as in the case of mean and variance for example) or Pareto fronts can be used to select the best configuration best on performances.

$$Y_1 = \beta 0 + \gamma 1 z 1 + \beta 2 x 2 + \cdots$$

$$Y_2 = \beta 1 + \gamma 1 z 1 + \beta 3 x 2 + \cdots$$

3.14

Performance measures should be set according to the specifications and requirements analysis this is the first step of the design process discussed at the beginning of this chapter. There are usually other generic requirements such as reduced mass, reduced material cost etc. Reaching all specifications is often a difficult task. and will require a very iterative. multi-objective and concurrent design process. Let's further discuss this with an example of misaligned PiH insertion shown in Figure 3.6. This is the form often referred to in the literature. Disregarding the fact that this model is of limited use in large misalignment applications, we will only use it for illustration purposes. The peg is held by a lumped compliant support (in real life a gripper or end-effector). The questions we can ask relating to performance are:

- How much force is required for insertion?
- How much force is required to support the peg and hole in other directions?
- Will the peg slide completely into the hole?
- How much does the end-effector weight?
- Will the material in the springs fail due to stresses and fatigue?
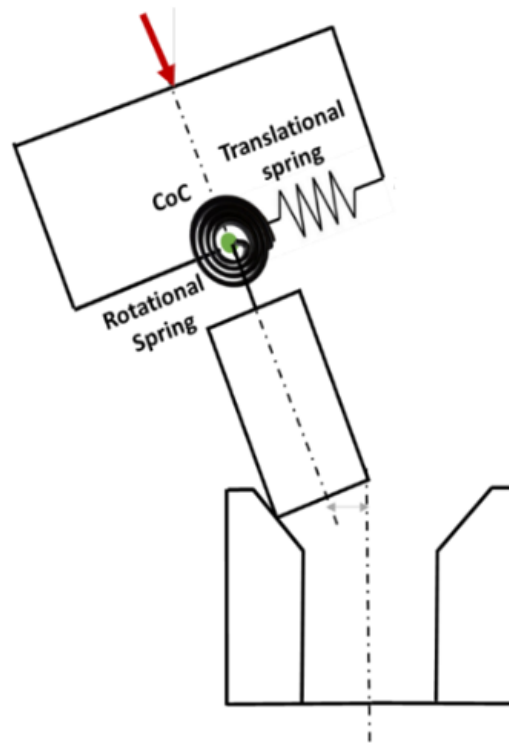
Figure 3.6 Lumped compliance general peg in-hole problem

Depending on what exactly is required from the compliant end-effector, the performance measure will vary. Let us borrow the specification made in Chapter 5 for our discussion here. This is the established target specification for a fluid coupling end-effector used in train maintenance. This end-effector must reduce insertion forces for a larger range of misalignment as compared to the existing design. This in turn reduces robot requirements in terms of payload and degrees of freedom.

Table 3.1 Example specification for passive compliance PiH insertion device

Need	Metric	Importance	Target	Units
R1.2. Reduces forces	M1.2 Max insertion force Fz	1	100	N
R1.3. Large misalignments	M1.3 Max possible misalignment	1	15, 5	mm/°
R1.4. Robust/durable	M1.5. Stress factor	3	1.5	-
R1.5. Lightweight	M1.6 Mass	2	5	Kg
R1.6. Compact	M1.7 Max misalignment/ characteristic length	4	0.1	-

Notice there are 5 performance metrics and requirements which are mapped to each other. It's almost guaranteed that steering design towards one of the metrics will counteract others. This effect is well illustrated in a Quality Functions Development (QFD) or a metric relation matrix (Ulrich and Eppinger, 2015). For example, reducing insertion forces will likely lead to reduced compactness, but it will surely improve insertion forces since the length of the compliant mechanism has a significant effect on reducing its stiffness. Metrics should have an importance rating and the designer should aim to steer the design towards the most important ones and keep updating the specification to ensure other metrics are still within acceptable levels, hence the name target specification. Another useful approach is to select a narrow range for the design factors perhaps based on a preliminary analysis, and then we can expect the metric to be close to the target spec even after steering the design towards a particular metric.

Metrics may be related but not counteracting. Consider the same fluid coupling example of Figure 3.6. The contact forces are energy input to the compliant end-effector, ignoring dynamic effects, energy must persevere as

$$U_{strain} = F_{in}d_{in} + W_{friction} + W_{gravity} \qquad \text{3.15}$$

The total strain energy is stored in the mechanism in the form of:

$$U_{starin} = U_{bending} + U_{shear} + U_{torsion} + U_{axial} \qquad \text{3.16}$$

For most engineering materials operating within the elastic range stress and strain at any point on the compliant mechanisms have a linear relationship described by the elastic modulus, E:

$$E * Strain = Stress \qquad \text{3.17}$$

According to the above formulations, we can reasonably hypothesise that reducing contact forces (insertion forces) will reduce strain and work done due to friction. Generally, reduced strains will result in lower stresses. Thus, steering a design towards minimum insertion force should also reduce stresses. This assumption remains valid under certain conditions. For example, in TO the objective of the algorithm is to minimise total strain energy and maximise motion. This often leads to lumped compliance designs where the motion and strains are

focalised to create highly stressed hinges. Thus, great care must be taken to not include design factors which create hinges or small-length flexures. For large motion applications, the designer should always select a distributed compliance mechanism which does not have localised areas of motion or stress.

The first goal of modelling the coupling process is to ensure it occurs successfully with minimum force on the compliance mechanism. Insertion depth can be used as a continuous parameter which indicates the success of coupling. However, an unsuccessful coupling that leads to jamming and wedging will most certainly result in unreasonable force values which are reflected when evaluating the mean and variances, of the coupling. Hence measuring insertion forces and steering design towards it many other metrics such as stress, and insertion depth will also improve.

3.3 Modelling Methods

Passive compliance end-effectors contact the external workpiece. In each case the shape of the contact area will be different, in peg in hole analysis of manufacturing assembly it is usually a cylindrical shaft and a bearing. In train fluid servicing it's camlock fluid couplers. There will be a bunch more applications where a generalised modelling approach capable of incorporating various shapes of contact and large deformation will be useful.

Two distinct modelling approaches are proposed, depending on the specification and performance measures of interest, each model has benefits and drawbacks. The Pseudo Rigid Body Modelling approach (PRBM) approach is simpler and faster however it does not satisfy stress monitoring. The FEA approach can be more time-consuming, but it usually satisfies all performance measures. These methods can also be used in a hybrid approach in which most of the evaluation is conducted in the PRBM model and a few post-FEA runs can ensure stress limits are respected. In this approach, we capitalise only on the benefits of each model.

We will use the RCC end effector concept from Chapter 5 as the application of the methods discussed here.
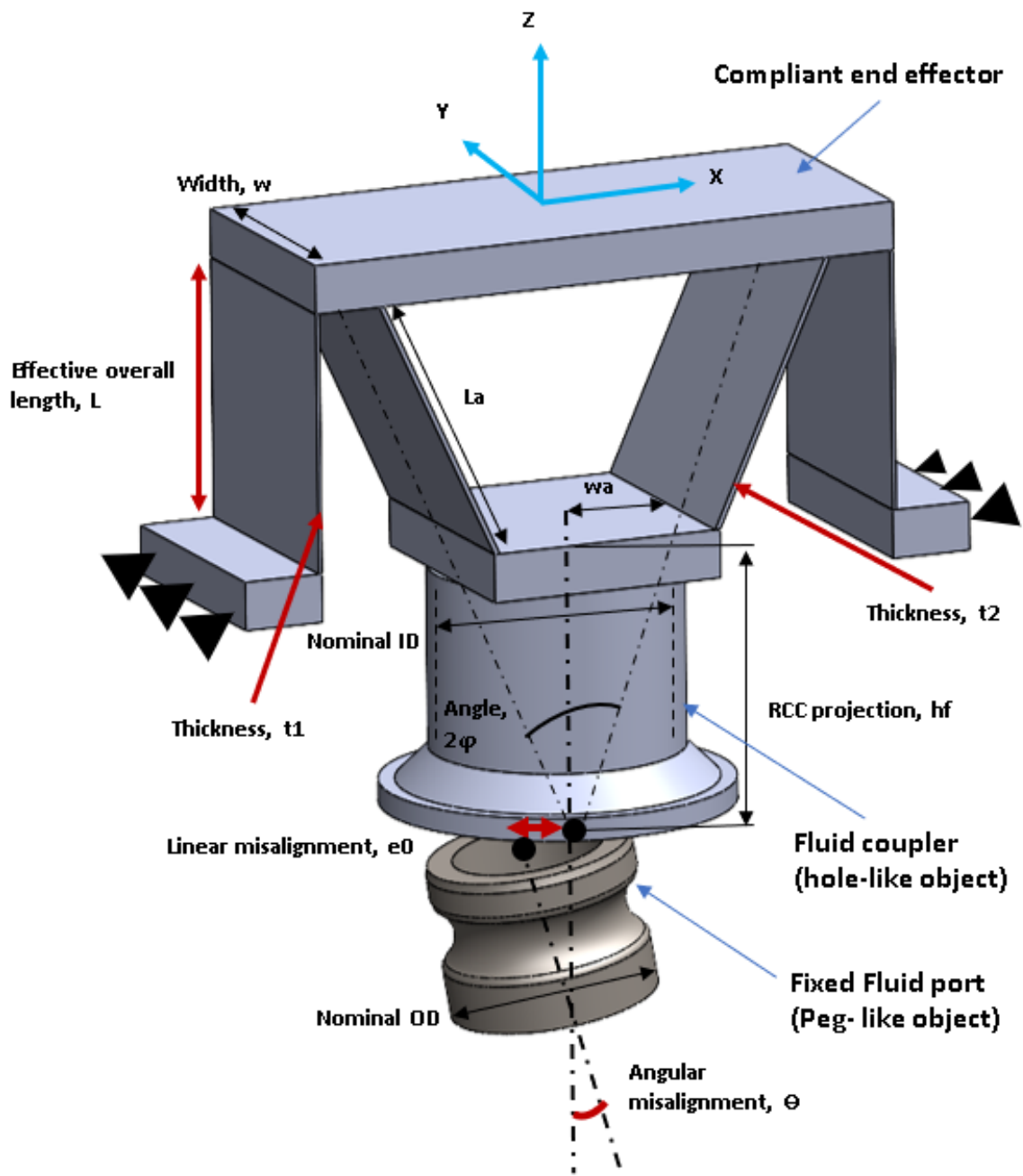
Figure 3.7 Illustration of experimental parameters on one of the end-effector modules (important parameters highlighted with red marking)

3.3.1 PRBM

Compliance models for compliant end-effectors found in the existing literature are mostly based on highly lumped models and small displacement assumptions. Typically, rotational compliances are lumped into torsional springs, and linear ones into translational springs. Highly lumped models often do not perform well in large misalignments, a convenient example is the rotational stage pin joint model in section 3.4.1.2. A PRBM approach is more suitable for larger misalignment. The PRBM modelling approach conducted follows the given order:

1. Convert the design to its rigid body equivalent following the PRBM method.
    This requires the modification of link lengths, the addition of revolute joints and springs
2. Investigate design performance.

Stiffness, force and displacement are analytically found.

3. In more complicated cases: Produce CAD model of the rigid version and simulate fluid port coupling with a rigid body solver.

In order to obtain accurate force and displacement models for complicated scenarios with multiple bodies and contact. the entire system is modelled using a rigid body solver. A CAD file of the new rigid equivalent model is required. In this work, SolidWorks Motion Analysis is the solver of choice. The problem must be set-up properly with suitable numerical parameters representative of the actual coupling process.
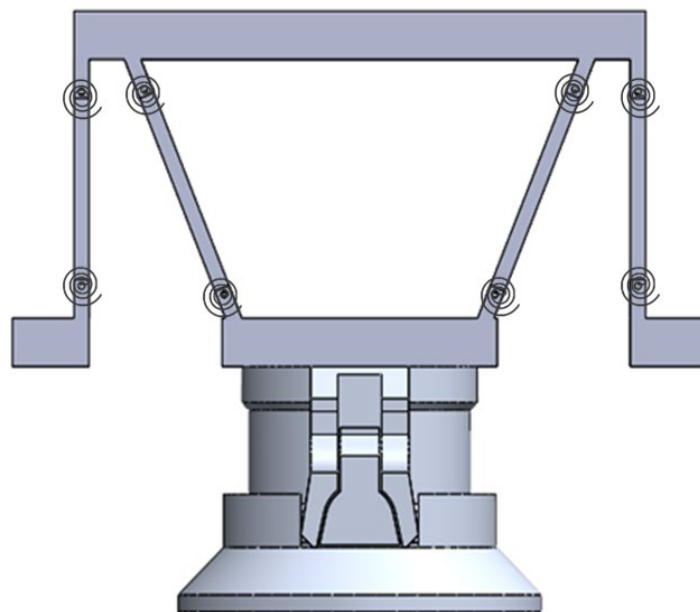
Figure 3.8 PRBM model with 2R springs for angular stage

3.3.1.1 *Rigid equivalent spring rates and link sizes*

The first step is to convert this compliant mechanism to its rigid body equivalent see Figure 3.8 or Figure 3.18. According to the PRBM method (Howell, 2001), the beams comprising the parallel stage can be considered as fixed guided beams since the angle of the motion stage and beam ends do not vary relative to the fixed stage. Since both beams are identical all four springs on the parallel stage will have the same stiffness given by:

$$K_p = 2\gamma K_\emptyset \frac{EI}{l} \qquad\qquad 3.18$$

K_θ and γ are parametric coefficients known as stiffness coefficient and characteristic radius factor (respectively). These parameters depend on loading conditions hence typically updated during the analysis as load conditions change. However, for a large range of loading conditions, these values can be nearly constant. In fluid coupling forces are compressive and lateral, thus these parameters are given:

$$\gamma = 0.852144 - 0.0182867n \; ; \qquad\qquad 3.19$$
$$for - 1.8316 < n < 0.5$$
$$K_\theta = 2.654855 - 0.0509896n + 0.0126749n^2 - 0.00142039n^3 +$$
$$0.00000584525n^4 \; ;$$
$$for - 1 < n < 10$$

n is the load factor which is the proportion of lateral force in the axial direction on the beam. n is positive for compressive loads and zero where there is only a lateral force present. γ also revealed the position of the torsional springs (and revolute joints) along the beam. At this point, the rigid body equivalent of the parallel stage is fully defined.

Generally, most distributed compliance mechanisms would be modelled with fixed-fixed beams. for example, the angular stage in our case should be modelled with fixed-fixed beam equivalents such as the 3R model (Su, 2009; Chen et al., 2011). However, as mentioned by Howell the fixed-guided approach can also be used with a slight comprise in accuracy. However, errors can be very small at lower deformations (Lyon and Howell, 2002). This trade-off in accuracy significantly simplifies the model and avoids additions of many springs and

joints. Since in our case, the total angular motion is relatively smaller (>6deg) compared to the parallel stage, the trade-off in accuracy and complexity of the model can be justified if necessary. Thus, the same approach discussed above is suitable to apply for the angular stage, however, it should be noted that the value of gamma and Kc correspond to a suitable load direction (Howell et al., 2013).

In the case of the 3R model we will follow Chen's approach, the spring the torsional stiffness is given by:

<div align="right">3.20</div>

$$K_i = Kc_i \left(\frac{EI}{L} \right)$$

Kc and gamma which define the location of each bema are given in the table below:

<div align="center">Table 3.2 PRBM parameters for the 3R model</div>

K1	K2	K3	$\gamma 0$	$\gamma 1$	$\gamma 2$	$\gamma 3$
3.25	2.84	2.95	0.125	0.351	0.388	0.136

For highly nonlinear systems, It is very difficult to model the whole process accurately with previous analytical methods. The rigid equivalent of the PiH problem should be modelled using a numerical rigid body solver, in our case SolidWorks Motion analysis. In the upcoming sections, we will compare the performance of models vs physical fluid coupling experiments. in this section, we discuss setting up the model.

3.3.1.2 *Ball parking stiffness and stress with PRBM (preliminary analysis)*

In a lot of cases, upcoming analytical approaches will completely model the problem, this may not be possible in more complicated scenarios. In the latter case, upcoming stiffness models will prove useful for quick calculations which put the design configuration in an approximate operation zone. For example in the case of fluid coupling, simple calculations including maximum misalignment ranges (displacement) and stiffness of stages can give an idea about

the range of expected forces during the insertion. Actual insertion forces will be larger than these approximations. This is due to the force in the insertion direction, contact friction and geometrical conditions. Hence if at this early stage forces observed are not desirable then the design should be reconfigured to fall into a feasible range.

$$F_{lateral} = Max\ linear\ misslaigments * stiffness\ of\ linear\ stage \qquad 3.21$$

$$M = Max\ angular\ misslaigments * stiffness\ of\ angular\ stage \qquad 3.22$$

For a general 4-bar linkage whose fixed link is l1, as in the case of our linear or angular stage, a kinematic vector loop equations yield :
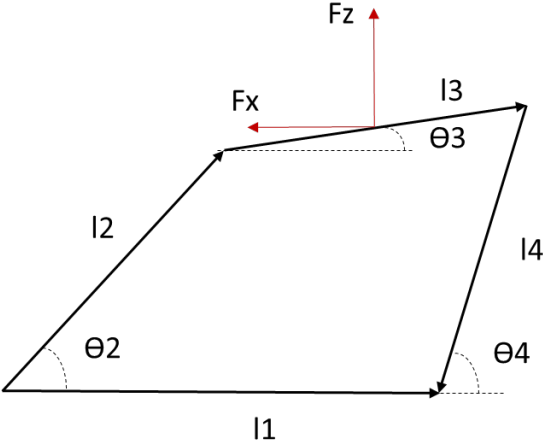
Figure 3.9 General 4 bar linkage vector loop

$$l_2 cos\theta_2 + l_3 cos\theta_3 - l_4 cos\theta_4 = l_1 \qquad 3.23$$

$$l_2 sin\theta_2 + l_3 sin\theta_3 - l_4 sin\theta_4 = 0$$

θ_3 and θ_4 are found based on DoF input θ_2. Applying energy principles in the form of minimum potential energy

$$PE = U_{starin} + W_{potential} \qquad 3.24$$

For equilibrium

$$\frac{dPE}{d\theta_2} = 0 \qquad\qquad 3.25$$

Hence

$$\frac{dPE}{d\theta_2} = \sum_{i=1}^{4} K_{ti} e_i \frac{de_i}{d\theta_2} - P_x \frac{d\Delta P_x}{d\theta_2} - P_y \frac{d\Delta P_y}{d\theta_2} = 0 \qquad\qquad 3.26$$

Where e is the rotation of the springs measured from the initial configuration, K is the spring stiffness and ΔP is the displacement at the force input location

Using this methodology we can analyse various linkage-type mechanisms. With further manipulations and substitutions, the above equations yield a nonlinear relationship between P and θ_i. Of course, solving for P or θ_i will not be a difficult task.

More specific to our case, considering a simple fixed guided beam shown in Figure 3.10, it is reasonable to assume that the stiffness of the parallel stage will be twice that of this beam.
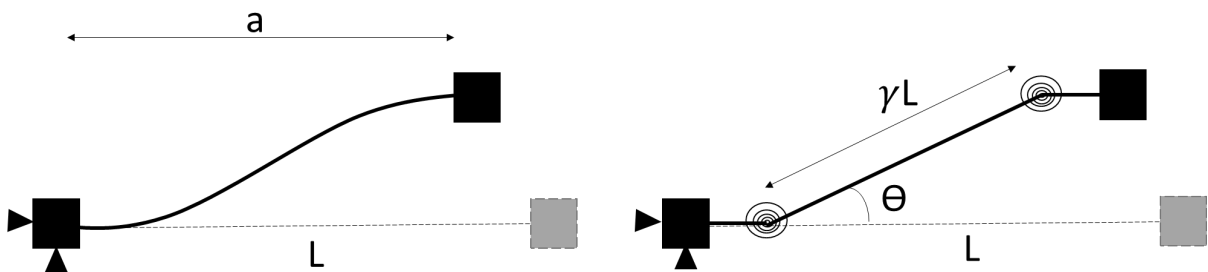
Figure 3.10 Fixed guided beam and its rigid equivalent.

This system has 1 DoF and the displacements of each spring are equal, hence we can write all displacements in terms of the generalised coordinates (DoF) θ, and potential energy is given as

$$PE = \frac{1}{2} K\theta^2 + \frac{1}{2} K\theta^2 - P(\lambda l sin(\theta)) \qquad\qquad 3.27$$

For equilibrium

$$\frac{PE}{d\theta} = 0;$$ 3.28

Hence

$$2K\theta = P(\lambda l cos(\theta))$$ 3.29

K is given for a fixed-guide beam and is substituted here. To consider the stiffness of two identical beams stiffness is multiplied by 2. This yields the system force-displacement relationship

$$F_x = \frac{8K_\emptyset EI\theta}{l^2 cos(\theta)}$$ 3.30

Where

$$I = \frac{hb^3}{12}$$ 3.31

At this stage, a maximum displacement of the linear stage can be prescribed, and the calculated load is compared with weight specifications. EI, or displacement due to gravity is adjusted until preliminary performance is satisfactory. Similarly, this equation can also estimate maximum lateral force due to maximum linear misalignment.

The maximum stress due to bending occurs at both ends of a fixed guided beam given by (Howell, 2001)

$$\sigma = \frac{F_x ac}{2l}$$ 3.32

c is the distance from the neutral axis to the surface of the beam. Due to the parallelogram configuration, we can assume the load is the same on the two beams. a is the length of the beam after deformation, given (Howell, 2001)

$$a = l\left(1 - \gamma\left(1 - \cos(\boldsymbol{\theta})\right)\right) \qquad 3.33$$

The angular stage can be simplified to a pin joint and link (similar to a counter-leaver beam) as shown in Figure 3.11. This simplified model has little error for relatively smaller motions(Xu et al., 2008). Since angular displacements are relatively small in train fluid coupling <10deg this model is used instead of the more complete 4 bar linkage.
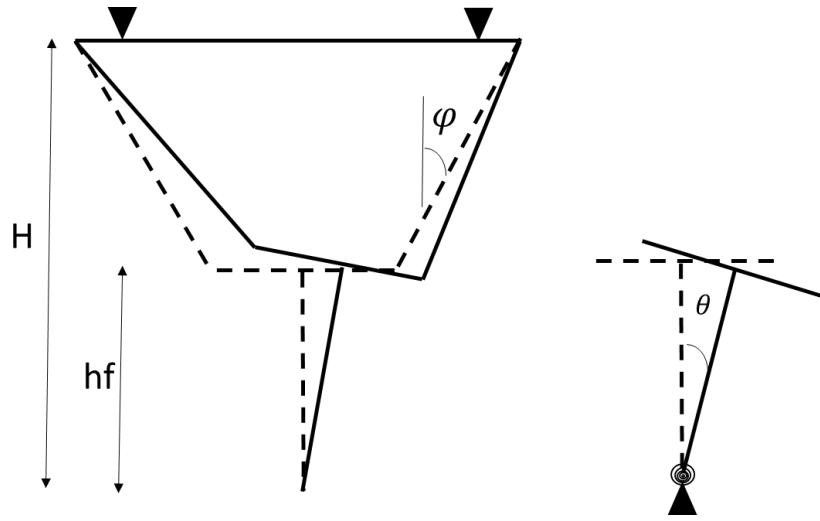
Figure 3.11 Pin-joint model of the RCC mechanism.

$$M = \left(\frac{8EI\left(H^2 + Hh_f + h_f^2\right)cos(\varphi)}{\left(H - h_f\right)^3} \cos\left(\frac{h + 8h_f}{8\left(H - h_f\right)}\theta\right)\right)\theta \qquad 3.34$$

If angles are not severely large and hf/H is less than 7/16, so that.

$$\frac{h + 8h_f}{8(H - h_f)} \leq 1 \qquad 3.35$$

The moment equation can be further simplified to:

$$M = \left(\frac{8EI\left(H^2 + Hh_f + h_f^2\right)cos(\varphi)}{\left(H - h_f\right)^3}\right)\theta \qquad 3.36$$

3.3.2 FEA approach

3.3.2.1 Static FEA: rigid body motion and nonlinear contact

Static FEA often referred to as structural FEA, is a very powerful tool for passive compliance design. If PRBM stiffness calculations are to be avoided, static FEA is the next best thing if applicable. The PRBM calculations are analytical and very simple, they provide direct insight into the effect of each design parameter. If the design does not take the form of linkages or is just not modellable with PRBM methods, then Static FEA should be considered. Even with nonlinear (large deformation) simulation, which regularly updates the stiffness matrix, K to account for changes in boundary conditions and geometric nonlinearities, simulation times often take less than an hour. Where static FEA is suitable, it will outperform PRBM modelling since strain and stress are also measured. However there will be no parametric insight, and a series of tests must be conducted to see the effect of various design parameters.

$$F = Ku \qquad\qquad 3.37$$

Static formulation: F is the nodal forces, K is the stiffness matrix and u is the displacement.

Static FEA should be considered where no pure rigid body motion is possible in the simulations. This is where a body is allowed to kinematically move regardless of any structural deformation in the system. There will be many passive compliance problems where this is the case. Where rigid body motions may be present and uncertain impact positions create large gaps between contact elements, static FEA is of little use. Even with large-deformation considerations (stiffness matrix and boundary conditions updates), achieving convergence will be very difficult and sometimes impossible. To tackle large contact areas and multiple contact points, it is possible to model such a problem in a quasi-static format with many load steps and discretised contact areas. Successful implementation of this approach will require prior knowledge of impact positions, which may not be available. Even in such an approach, rigid body motions could prevail.

Most FEA contact formulations use a penalty-based algorithm which generates anti-penetration forces to regulate contact force and position. This force may couple with contact friction forces to create a bouncing effect during contact, if one of the contact pairs is a rigid body (for example in a PiH coupling) this will result in very small, but problematic, rigid body motions. Numerical

stabilisation methods such as contact stiffness adjustment or contact damping stabilisation may treat this, but they introduce errors. Contact stiffness can be numerically reduced to reduce anti-penetration forces. However, this leads to high penetrations which for tight clearance problems such as PiH could lead to very inaccurate results. Contact damping stabilisation relies on the addition of dampers or stiffness elements to rigid movers. This numerical approach may introduce a slight error by changing the compliance nature of the system.

3.3.2.2 Dynamic FEA

A dynamic approach is more suitable since rigid body motions are solved with the equations of motion. Furthermore, velocities and dynamics effects can be observed. From the equation below, we can see the quantities that are solved. This approach usually has a longer run time and can be difficult to set up. Also considering the consequences of the nonlinear numerical approach, it is not a surprise that large models can take days to run. Hence a hybrid approach, to modelling will prove very useful. For example, most performance evaluation and optimisation can be done with PRBM solvers, and a few dynamic FEA runs can ensure all other specifications metrics are met.

$$Mu''(t) + Cu'(t) + Ku(t) = F(t) \qquad\qquad 3.38$$

Dynamic formulation: M is the mass matrix, C is the damping matrix, t is time.

Implicit dynamic FEA formulations require convergence of internal and external forces/displacements. If the contact nature of each simulation is different i.e. the case of a misaligned PiH, one may find implicit approaches often unreliable in achieving convergence. Requiring, mesh adjustments and stabilisation that add to the burden of simulation time.

We have found the explicit approach more reliable as there are no nonlinear iterations for the convergence of time steps. The caveat is in meshing difficulties and controlling time steps for feasible run times. Geometry must be meshed such that there are no relatively smaller elements, generally, a more uniform mesh is desirable. This is due to the timestep calculations that are based on the critical Courant number. This condition ensures that stress wave propagation through the elements is captured in the simulation. Time steps beyond that, cause instabilities and invalid results. Usually, in cases with very small elements and high speeds, total simulation

time is limited to a couple of seconds. Scaling of elemental mass and load rates to manipulate critical timestep and simulation time is common practice for explicit dynamic modellers. If conducted responsibly, this kind of numerical tuning will reduce simulation run times and still produce valid results.

$$t_{crit} = \frac{fL}{C}$$

<div align="right">3.39</div>

f is a numerical safety/scale factor and takes the value of 0-1, L is the characteristic length of the smallest flexible element and C is the speed of sound through the flexible material

There is no stress wave through an ideally rigid body (the peg and hole can be considered ideally rigid relative to the compliance of the end-effector). Thus, since timesteps are regardless of rigid body meshes, mesh refinement can be allocated to these important contact regions with little added time expense.

It is also highly desirable to model thin components often found in compliant mechanisms such as beams or flexures with shell elements. Due to the characteristic length of these elements, larger critical time steps can be attained. If there is a need for a reduction in the number of elements it is also possible to model relatively rigid portions as surfaces with shell elements. Typically, deformations and stresses are negligible in these areas so there is no need for accurate prediction across these elements. Depending on the software, a more uniform mesh can be achieved if a unibody is split into multiple bodies respecting a cartesian coordinate system.

In explicit dynamics, one key aspect to keep in mind is the energy conservation of the system. Even though there are no iterations for solving motion equations (no convergence problems), the explicit approach relies on an energy balance of the system. For accurate results, ensure energy errors must not be significant (>5%). Few more tips regarding energy conservation, which are employed in this work:

- Ensure hourglass energies are less than 5 % of total energy.
  Hourglass energy is a form of non-physical phenomena which measures element deformations that mathematically provide no stress or strain due to the geometrical

nature of the element deformation. This does not happen in real life. A more appropriate mesh often resolves high hourglass energies.

- For near static cases (very slow speeds) ensure kinetic energies are close to zero. Kinetic energies must be orders of magnitude lower than internal energies for static scenarios. Reducing speeds and introducing artificial damping such as Ryleigh's damping can also regulate dynamic effects.

3.4 Physical comparison of models

A physical system is set up within the CyberFluids rig to experiment with misaligned fluid port insertions, see Figure 3.12 to Figure 3.15. A linear guided actuator carries the arm and end-effector. An additional support rail and carriage are mounted 90 degrees to the driving carriage. This ensures the stiffness of the insertion arm structure. The linear guide is fixed to a rigid aluminium frame that is fixed parallel to the train side fluid port with a tolerance of +/- 0.3 deg.

A 5-axis non-back driveable motion stage is used to misalign the fluid port relative to the linear guide and end-effector. Misalignments are measured using vernier callipers and combination square sets. The resolution of the linear misalignment measurement is +/- 0.05mm and the angle measurement is +/-0.3 degree.

The compliant mechanisms of the end-effector are made of 3D printed PLA with elastic modulus, E=3Gpa and Poisson's ratio,v=0.33.

The material of the funnel and coupler is 6082 aluminium, and the fixed fluid port is stainless steel as provided with the Dixon EZ link Cam and groove range. all contacting surfaces have been machined and finished.

3 verification tests are performed at various misalignment conditions. Results are compared with the numerical models. Before conducting experiments and comparing results between various models, it is important to establish the value of some uncertain parameters. These include the PiH friction coefficient. To make a fair comparison, these parameters should be consistent between physical and nonphysical models.
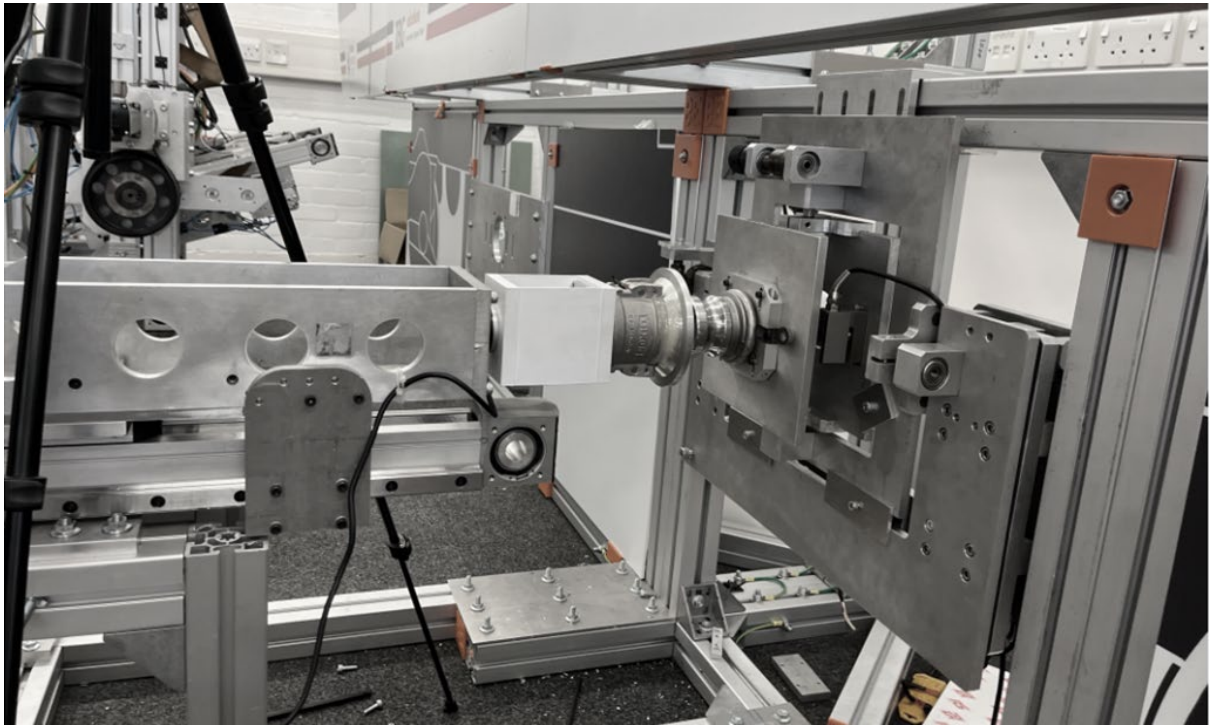
Figure 3.12 Physical setup used for model comparisons.
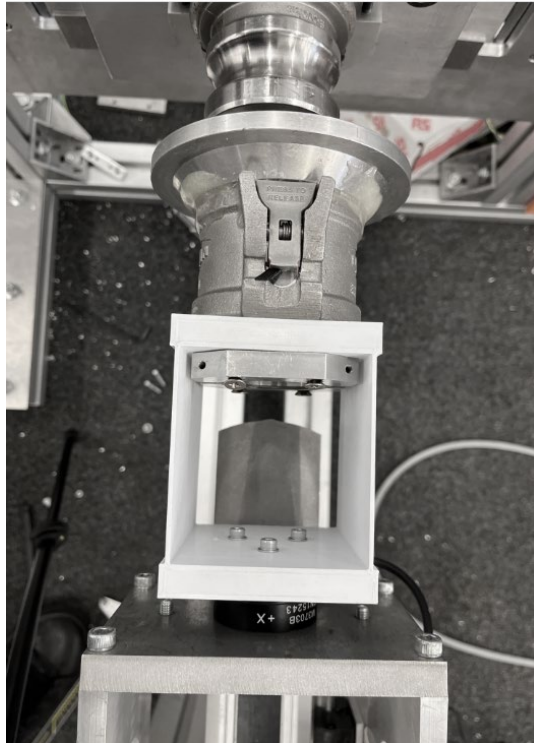
Figure 3.13 Single DoF parallel stage end-effector with 6Axis force/torque sensor
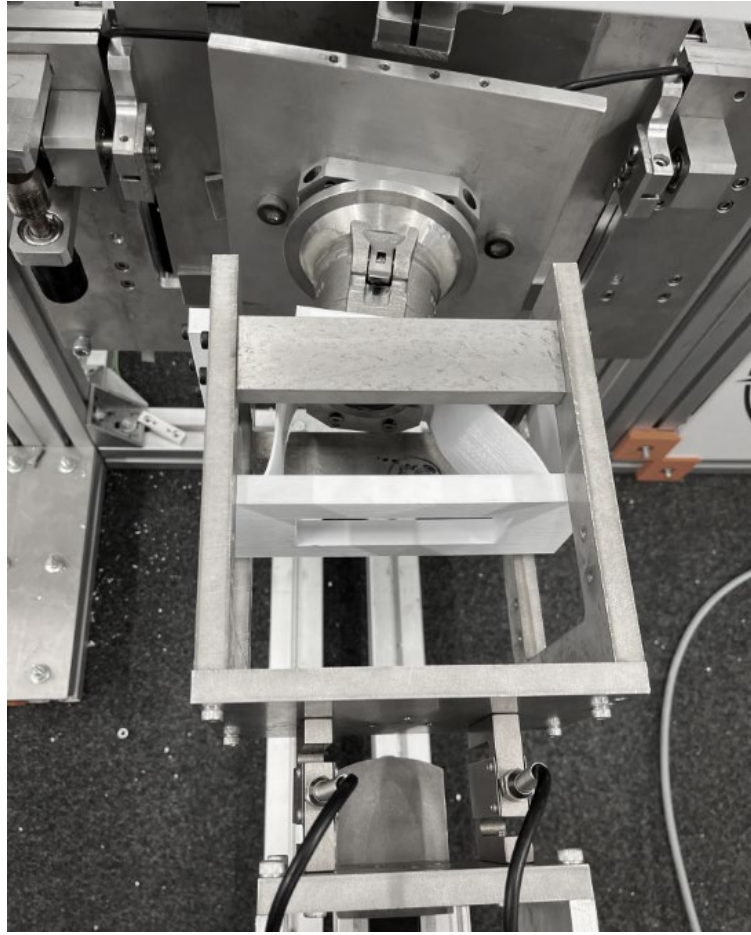
Figure 3.14 Two DoF end-effector
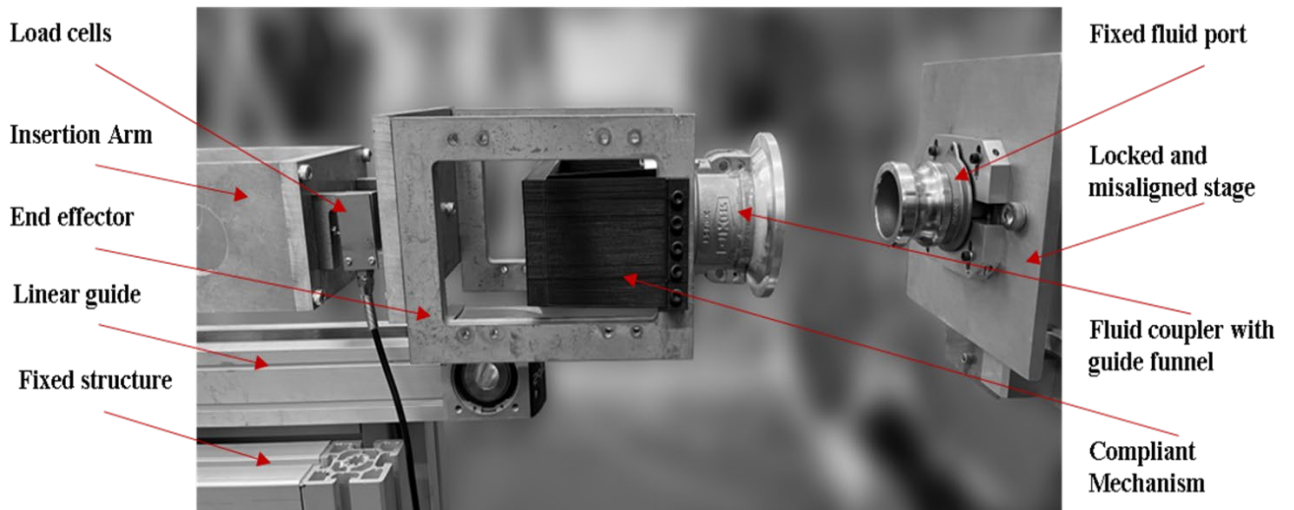
Figure 3.15 Components of the experiment set up

3.4.1 Friction and force sensing

In this application friction is a very sensitive parameter. The forces observed are governed by the compliances and the friction between surfaces. During insertion, sharp edges may scrape against each other and result in surface finish variations between tests. We have observed this during many preliminary tests.

The sampling rate and accuracy of the 6-axis is 100Hz, +/-1 N (SRI M37 series 100N). The sensor provides forces necessary to analytically calculate friction during each test. Unfortunately, the sensor is very small and can only be used for lightweight end-effectors and small insertion forces (>100N). Hence it has not been possible to measure friction with the two DoF end-effector shown in Figure 3.14.

Assuming all parts are square, and the end-effector only has parallel compliance, in theory, we only need force in two directions to calculate friction. During sliding and one-point contacts within the hole, Given Fx and Fz from the F/T sensor the force equilibrium is solved for μ.
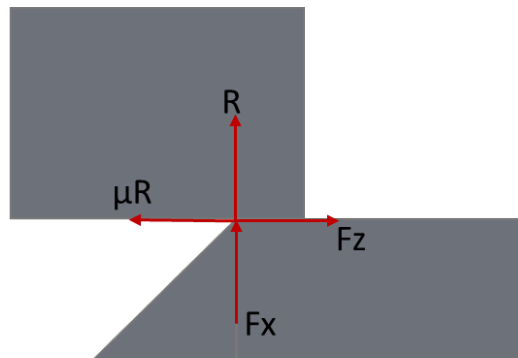
Figure 3.16 One-point contact inside the hole

$$\mu = \frac{Fz}{Fx}$$ (3.40)

During one point contact chamfer crossing before the mouth of the hole, friction is given by:
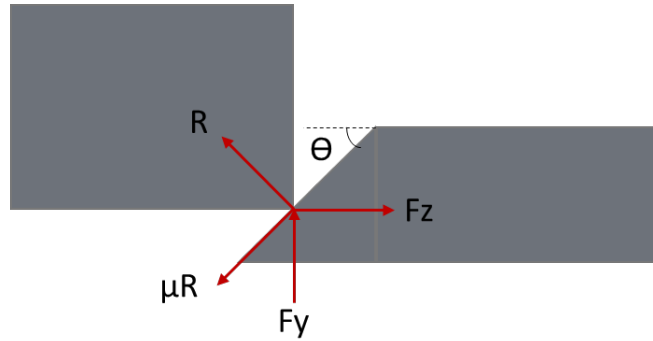
Figure 3.17 One-point contact on chamfer crossing

$$\mu = \frac{Fysin(\Theta) + Fzcos(\Theta)}{Fzsin(\Theta) - Fycos(\Theta)} \qquad 3.41$$

3.4.2 PRBM settings

SolidWorks Motion allows for the addition of various force and spring elements to imitate compliance. we will implement the 3R model shown in Figure 3.18 with the following simulation "elements" and settings.
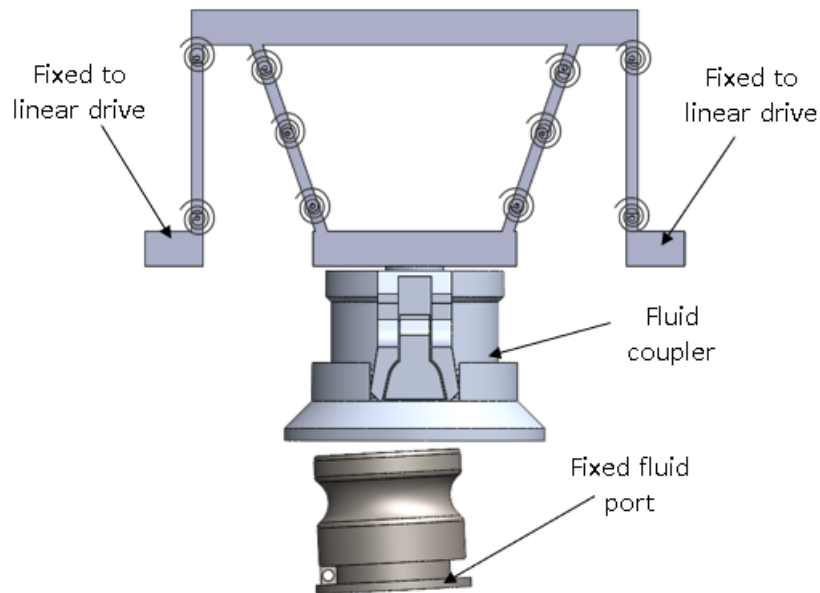
Figure 3.18 PRBM model with 3R springs for angular stage

1. Torsional springs: To imitate the rotational stiffness of the added springs.
2. Linear motor: this is the robot drive arm which follows a set path at a constant speed.

3. Solid-body contacts: this is defined between peg and hole. Friction coefficients are set as per material. we have found increasing stiffness and damping of contact provide more accurate results, for fluid coupling we use 200000N/mm and 100Ns/mm.

Other important settings are:

4. Contact resolution is set to "precise contact" with an integrator accuracy of 0.001 to ensure analytically sound results. The integrator used is WSTIFF which responds better to abrupt changes (eg impact and contact separation) during the simulation.

5. Frames per second are set to 50 for all insertions below 5>mm/s for higher speeds >5mm/s<15mm/s we use 100FPS.

6. SolidWorks motion analysis encourages no redundant DoFs resulting from the mating of components to provide accurate force results. When assembling the end-effector care must be taken to ensure this remains true. Often it may not be possible to achieve this, and redundant mates may be replaced with "bushings" with high stiffness, typically in the order of $10x10^7$ N/mm

7. A distinction should be made with friction coefficients. Most solvers require a static and dynamic friction coefficient. Depending on the solver this comes in many forms. In SolidWorks, there is an option to set a constant value of friction or implement friction with contact velocities according to Figure 3.19. We set parameters to achieve a constant frictional force.
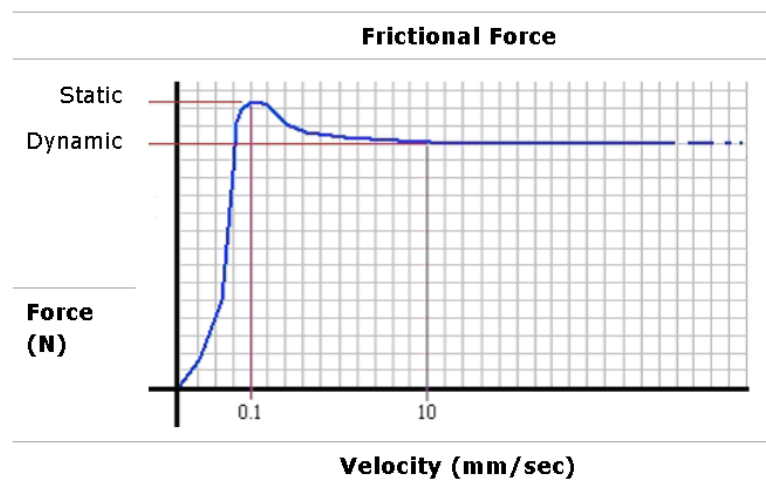
Figure 3.19 SolidWorks motion analysis, friction evaluation

The simulation takes around 13 mins with an Intel I7 processor H series, RAM of 16 GB and 6 GB GPU. There are many other controllable numerical and physical settings in this model

which can be calibrated to match a specific physical system i.e. CyberFluids (Eshraghi et al., 2020b). However, to maintain the generality of results such calibration will not be performed here. In fact, for the sake of validating the model, the physical setup up aims to fully replicate the simulation.

3.4.3 FEA (LsDyna) settings

The simulation package used is LS-Dyna, available with the Ansys workbench 2021, R2. See Figure 3.20 for a typical mesh setup used for modelling fluid coupling in LS-Dyna. Notice uniform mesh on the compliant mechanism, and refined mesh on the fluid couplers which are defined as solid rigid body surfaces. Ansys Quad shell elements are used for the compliant mechanism and Tetrahedral solid elements are used for the fluid couplers.

It is not possible to extract reaction forces at rigid bodies with displacement boundary conditions. Thus, in fluid coupling simulations conducted in this thesis, the boundary conditions are fixed supports (zero displacements) at the end-effector/robot mount point. Applied displacements (remote displacement option) at the fluid port. Contact is defined between all outer surfaces of the fluid port and all inner surfaces of the coupler. The contact formulation is Augmented Lagrange. The coupler is attached to the motion stage of the end-effector with rigid constraint joints. Connecting bodies are bonded with mesh adjustments which ensure common nodes between connecting surfaces. All materials are defined as isotropic and the time step is between is around $2.5*10^{-7}$. Simulations take between 18-28 hours on a PC with an Intel I7 H series processor, 16GB RAM and 6GB GPU.
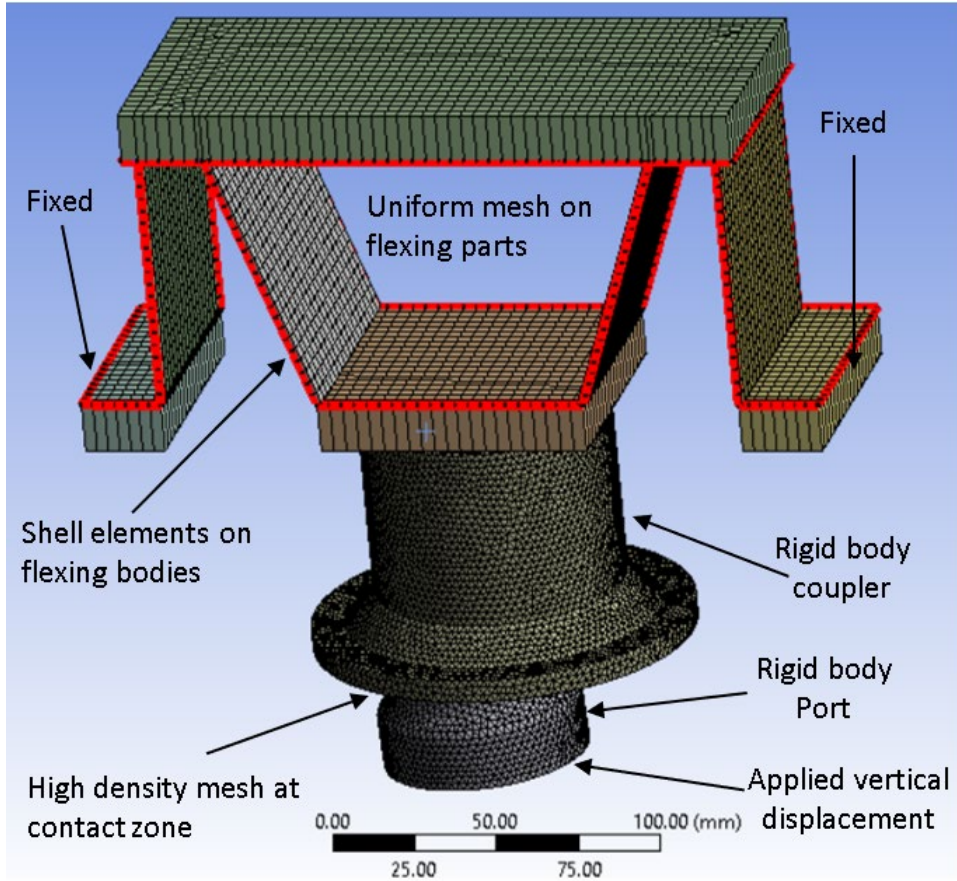
Figure 3.20 LsDyna FEA set up for fluid coupling end-effector.

The friction between contact pairs is set according to the dynamic friction equation below.

$$\mu = \mu_d + (\mu_s - \pi_d)e\^D|v| \qquad\qquad 3.42$$

Where D is the numerical decay constant and v is contact velocity. We input the same value for μ_s and π_d in order to keep friction constant.

$$\mu = \mu_d \qquad\qquad 3.43$$

3.4.4 Results.

3 tests are arranged as shown in Table 3.3, the nomenclature of parameters is found in Figure 3.7 and the end-effector design details are found in Appendix A2. For test 3 we will just compare the results of PRBM and FEA since we were not able to estimate friction for this setup. From Figure 3.21, we can see that there is generally a very good match between results, considering all the uncertainties and assumptions. For example, variation between physical parts and presumed CAD models. In physical experiments, the structure is subject to some

compliance and play. Hence, we see that generally physical experiments are less stiff. This is normal behaviour since, for the models, we assume rigid connections behind the end-effector. There are also unconsidered visco-elastic and creep effects of the PLA material, which may lower stiffness in physical experiments.

The general error of the PRBM model at the peak of maximum force is less than 5%. However, the FEA shows stiffer results with more errors up to 18 %. Nonetheless, these errors are consistent and reliable across all tests which indicates we can use these models in other analyses while taking note of the existing errors. One aspect which could be adding to errors in the FEA model is the meshing quality. The PRBM uses precise contact geometry as opposed to an approximate body mesh.

Table 3.3 Controllable parameters for validation experiments

Parameters	Test 1	Test 2	Test 3	Units
E	3	3	3	Gpa
L	80	80	80	mm
w	80	80	80	mm
t1	1.6	1.6	1.2	mm
t2	-	-	1.6	mm
hf	-	-	115	mm
Nominal ID	63	63	63	mm
Nominal OD	63.85	63.85	63.85	mm
Insertion Speed, V	3	5	7.5	mm/s
Friction coefficient, F	0.54	0.5	0.2	-
Linear misalignment, eo	5	10	5	mm
Angular misalignment, Θ	0	0	4	deg

Test 1

Test 2

Test 3
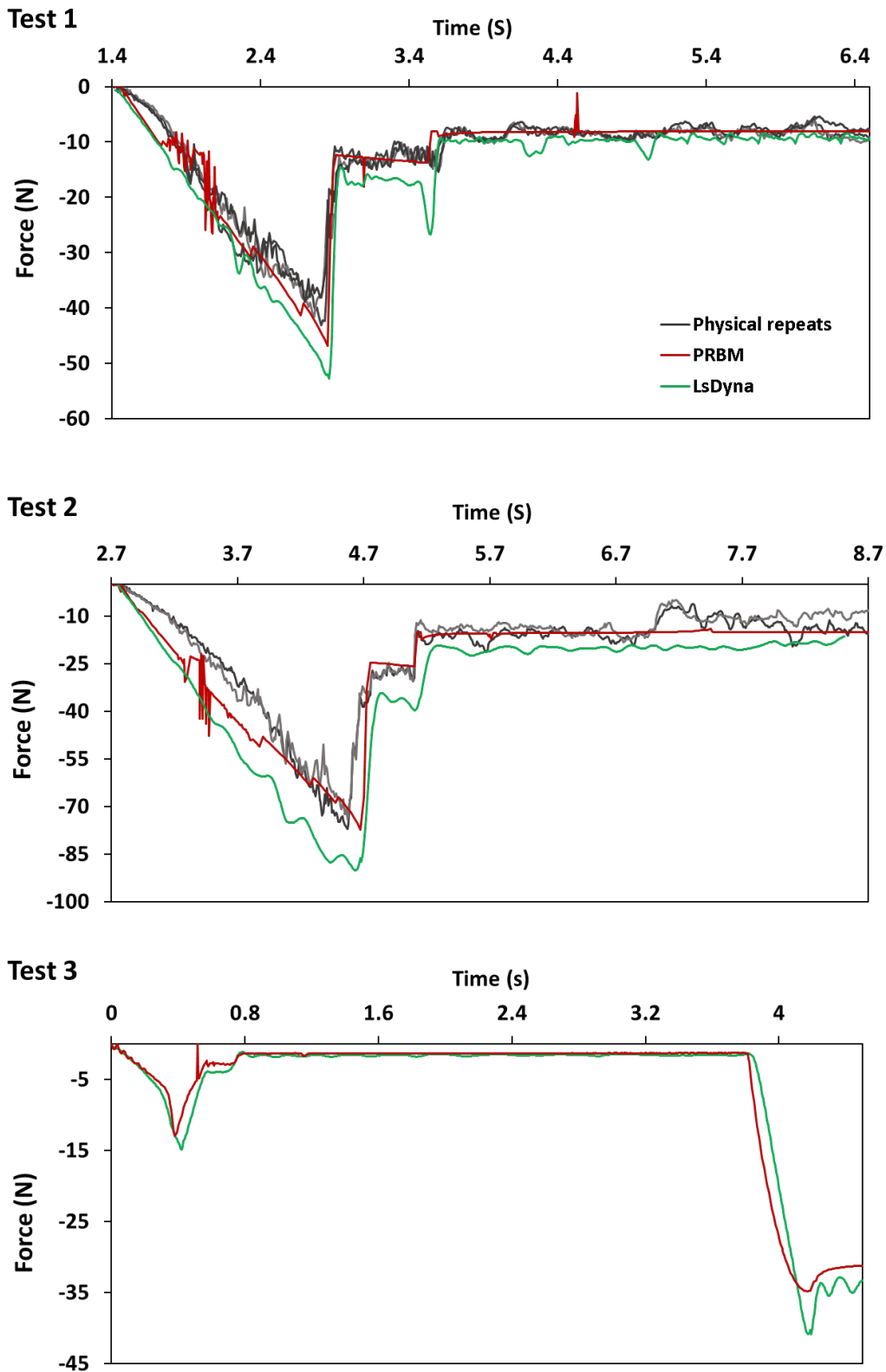
Figure 3.21 Model comparison results

3.5 Summary

We have discussed how to apply the RED methodology with a DoE framework for passive compliance design. Even though there is a focus on fluid coupling problems, we did discuss various performance measures applicable to other problems. Chapter 6 is a good example of how the method can apply to various applications of robust compliant mechanism design.

The two modelling approaches provide sufficient performance for our purposes of end-effector development, where physical experiments are not viable. However, we must consider some tolerance for errors in practical applications. This may translate to slightly upsizing the required actuators. At this stage, we can conclude that our modelling approach is reasonable. In the following chapters, we will implement the RED approach using various modelling approaches including Physical, FEA and PRBM in different case studies.

4. CYBERFLUIDS ROBOT: BENCHMARKING PERFORMANCE

Overview

This chapter introduces the CyberFluids robot we built at Brunel University London and, discusses the related train maintenance context. We also implement the methodology of Chapter 3 to evaluate the performance of an arbitrarily compliant end effector used in the Cyberfliuds system. The experiments conducted are all physical and require no numerical modelling. Using the proposed method we were able to improve the performance of this end-effector simply by varying some design parameters. However, this was not sufficient to meet our requirements of misalignment and insertion force. On the other hand, this has now provided a benchmark for comparison of future end-effector designs (eg Chapter 5).

4.1 Introducing the CyberFluids robot

Within our research group here at Brunel, (Hill et al., 2017) conducted an initial design study for train fluid servicing robots. In this work, the key design requirements of the robot were outlined, and design concepts were proposed. Subsequently, an economic justification study was conducted on these concepts (Atherton et al., 2020). The outcomes of these studies are:

1. Robots should operate outdoors in the maintenance shed.

   To save space inside the depot and keep depot, arrangements the same, managers would like to see a robot which operates outdoors of maintenance sheds on the trackside.

2. Need for standardised fluid ports and reduced fluid spills.

   In current (manual) train-fluid servicing operations, many different types of fluid couplers are used to completely service the train. For each type of port coupler, different combinations of linear and rotary motions are required to make the coupling. Therefore, there is a need to adapt and standardise train fluid ports for automated fluid servicing.

3. A cartesian-type robot is a more economical solution.

   The cartesian robot solution only has 3 Degrees of Freedom (DoFs) which makes it very simple and cost-effective. However, this brings along the trade-off of positioning accuracy and intricacy of motion provided by a robot with more DoFs. For the Cartesian solution to be feasible, a compliant end-effector must be able to accommodate intricate motions and misalignment compensations during the fluid port coupling.

For more information regarding the higher-level requirements and conceptualisation of a train fluid servicing robot, the reader is referred to the aforementioned studies.

Following the recommendations of our colleagues, we have built the CyberFuids system to demonstrate the feasibility of the robot design and overall concept. The track alongside the train carriage shown in Figure 4.1 is the robot's X-axis. The robot has 7 Degrees of Freedom (DoF) and provides 5-axis positioning for 3 end-effectors mounted on insertion arms (Z-axis). Two of the Z-axis arms accommodate fluid couplers and the third is for gripping the relevant dust caps. The nominal size of each train port (and cap) corresponds to the typical 2-inch fuel port and 3-inch CET port. The cap gripper has an adjustable jaw to accommodate both cap

sizes. On the train side, the 2-inch port is fixed to a manual 5-axis, non-back-drivable positioning stage that can be used to deterministically misalign the ports.
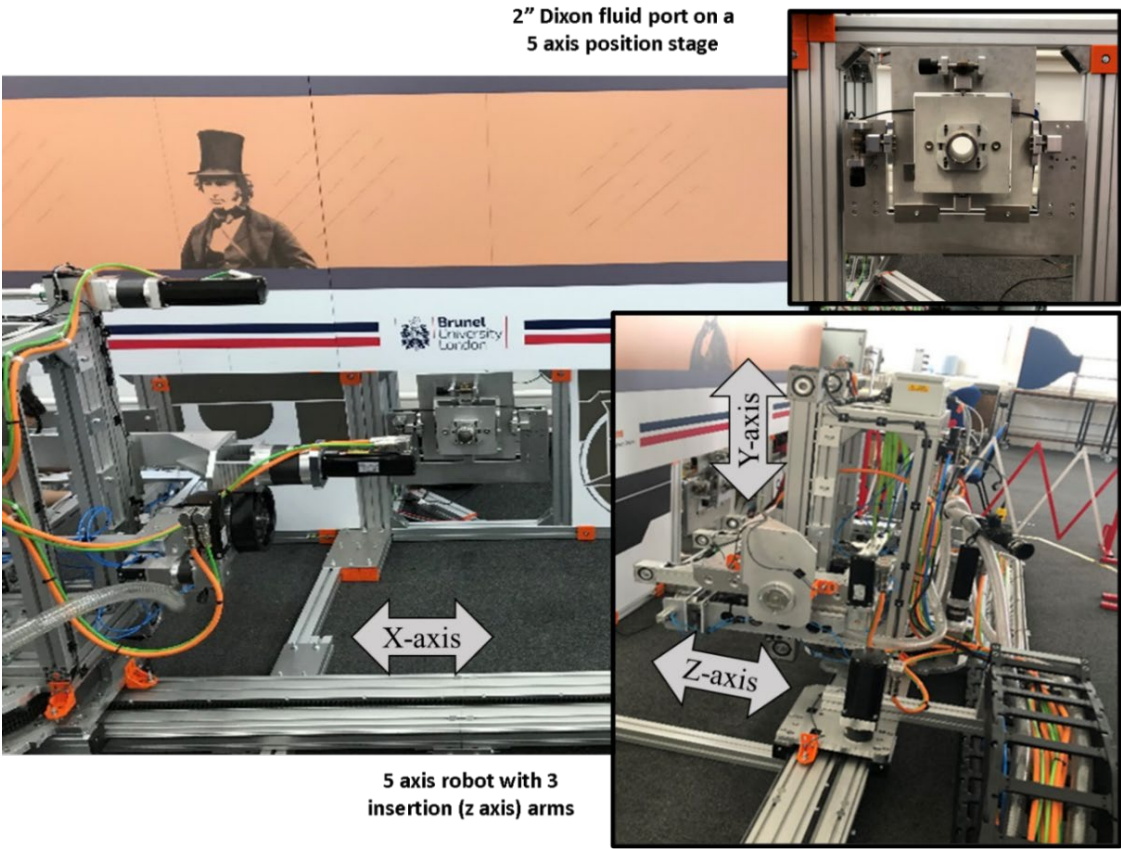
Figure 4.1 Arrangement of the CyberFluids train fluid servicing robot
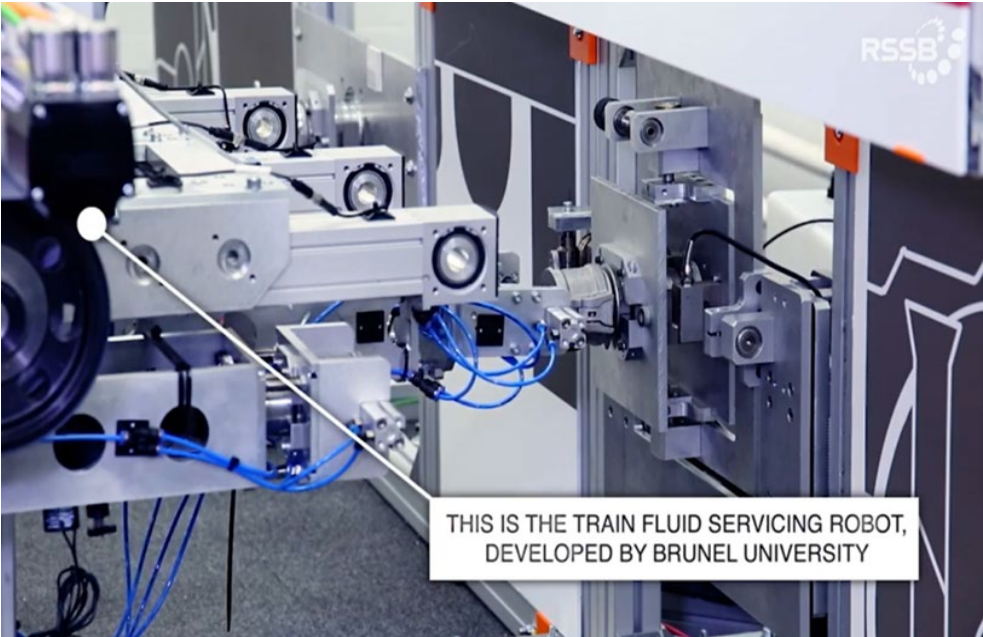
Figure 4.2 CyberFliuds in operation

4.2 Problem definition

To reliably make a secure and sealed connection Dixon Ez-link fluid couplers are selected for the CyberFluids robot. They only require a linear insertion motion to latch and make a leak-free connection. This linear motion will also be less demanding of the robot and end-effector while making the automated fluid servicing faster. This fluid port is a standard camlock port commonly found on most UK train fleets as the CET fluid port. It is expected that all other fluid ports on the train are retrofitted using adapters or this fluid port is incorporated for all other fluid on a train by manufacturers.

For demonstration purposes, we have built a fluid coupler end-effector (Figure 4.3) and dust cap gripper (Figure 4.4). The gripper-robot interface reduces the rigidity of the end-effector thus allowing for some misalignment compensation. Unfortunately, the misalignment capabilities of the gripper are negligible because the support flanges only accommodate caps in a particular position and the orientation problem is investigated in Chapter 6.

The 3-spring compliant interface has been found rather effective when integrated into the fluid coupler end-effectors. This is due to the nature of a cylindrical and chamfered male/female coupling which provides inherent funnelling guidance during the insertion process. This type of fluid port coupler is often rotationally symmetrical cylindrical shapes which are considered analogous to peg and hole shapes.
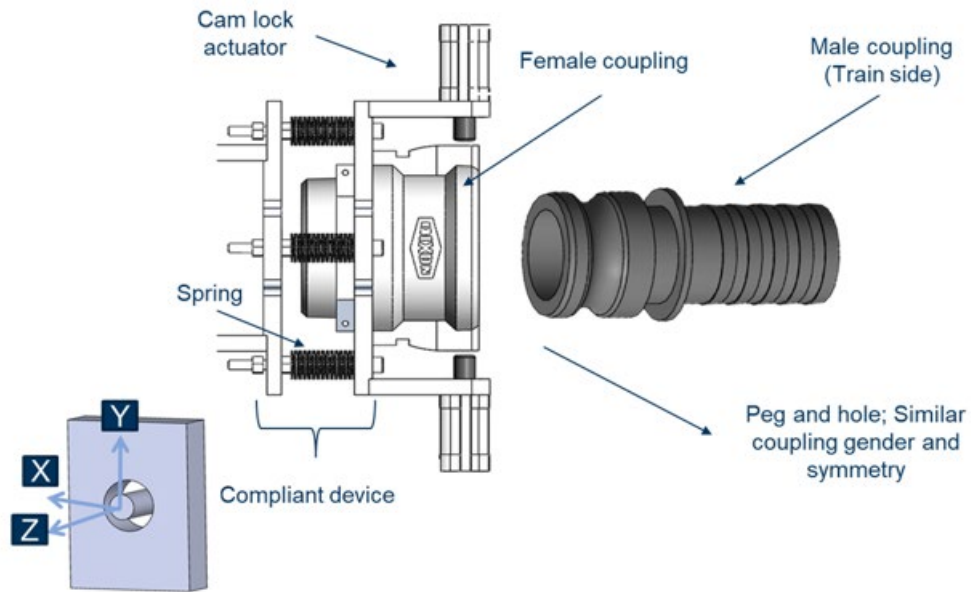
Figure 4.3 CyberFluid fluid port coupling end-effector
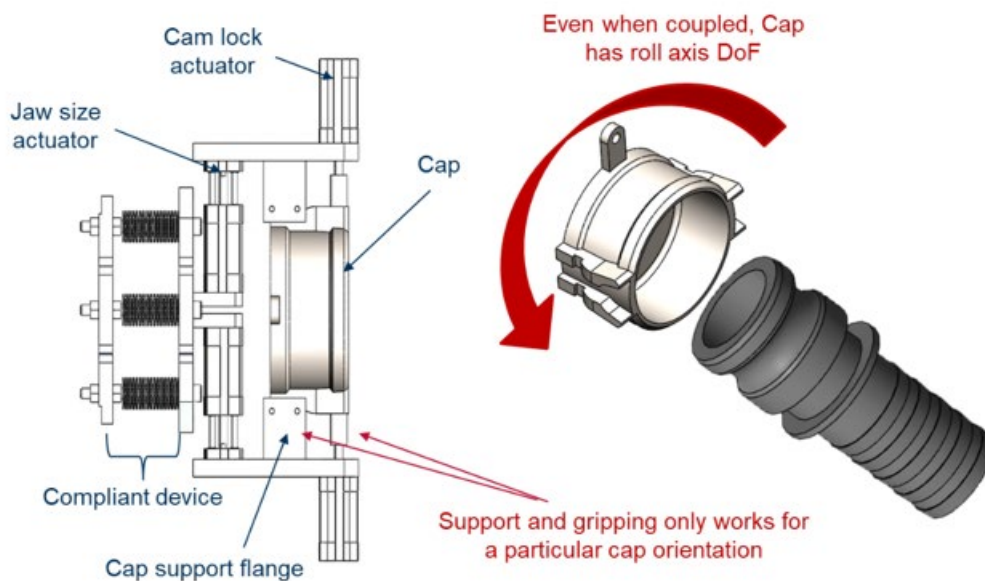
Figure 4.4 Arrangement of the gripper end-effector and dust cap

For an XYZ (3 DoF) Cartesian RAS (Atherton et al., 2020 and Hill et al., 2017) robot X and Y-axis misalignments lead to poor coupling. For these experiments train fluid ports are aligned parallel to the robot's Z-axis and the CyberFluids robots will only use XYZ motion to make the fit. We would like to investigate the robustness and performance of the fluid coupler end-effector design. The aim is to identify the range of expected forces and misalignments.

4.3 End-Effector design

The end-effector has passive compliance facilitated by spring elements, as depicted in Figure 4.5. It has 3 shoulder bolts encapsulated by springs, the threaded part of the bolt is fixed to the coupler flange while the bolts are free to pivot and slide within corresponding clearance holes located in the arm flange. In this arrangement when all bolts slide simultaneously, the motion is linear in the Z-direction. The clearance holes effectively act as spherical joints that have corresponding angular motions, which are amplified along the bolt length. The bolts are equally spaced around a pitch circle (radius, *PR*) that coincides with the centre of the coupler. Spring pre-compression ensures that the end-effector returns to its original position after a misaligned insertion. Maximum linear sliding in Z is determined by the compressed length of the springs. The coupler and its flange rotate and slide relative to the arm flange. The maximum rotation occurs when the bolts have two-point contact in the hole. The below equation is based on simple geometry and can be solved nonlinearly to estimate this maximum angle.

$$b\sin(\vartheta) + l\cos(\vartheta) = t \qquad\qquad 4.1$$

Where b is hole diameter, l is hole length, t is bolt diameter and θ is the maximum angle of rotation.

The coupler has 3 DoF (θ_{YZ}, θ_{XZ} and Z). The X and Y linear motions of the coupler are coupled to the rotations in yaw (θ_{XZ}) and pitch (θ_{YZ}). Hole clearance can encourage small, non-elastic motions in the remaining directions (X Y and θ_{XY}) however, keeping the clearance to a minimum, these motions can be neglected as relatively small. The maximum range of linear motion is not symmetrical on either side of the X-axis i.e. in pitch motions. This is because bolts and springs on either side of the X-axis have different distances to the coupler centre. This means that when the plate pivots the amplification effect will be different depending on the direction of motion. For similar reasons, compliance in the pitch axis is also not symmetrical.

4.3.1 Controllable design factors: compliance

We are interested in understanding the effects of spring stiffness, *K*, pitch radius of the bolt holes, *PR* and the orientation of the set of holes, *O*. As discussed in the previous section, clearance will remain a constant and bolt length is not considered (or distance between the arm and coupler flanges) in order to reduce the number of variables and experiments. Table 4.1 lists

the experimental parameters and Figure 4.6 shows the modified experimental end-effector that can accommodate up to 5 adjust levels for hole orientation, *O,* and pitch radius, *PR*.
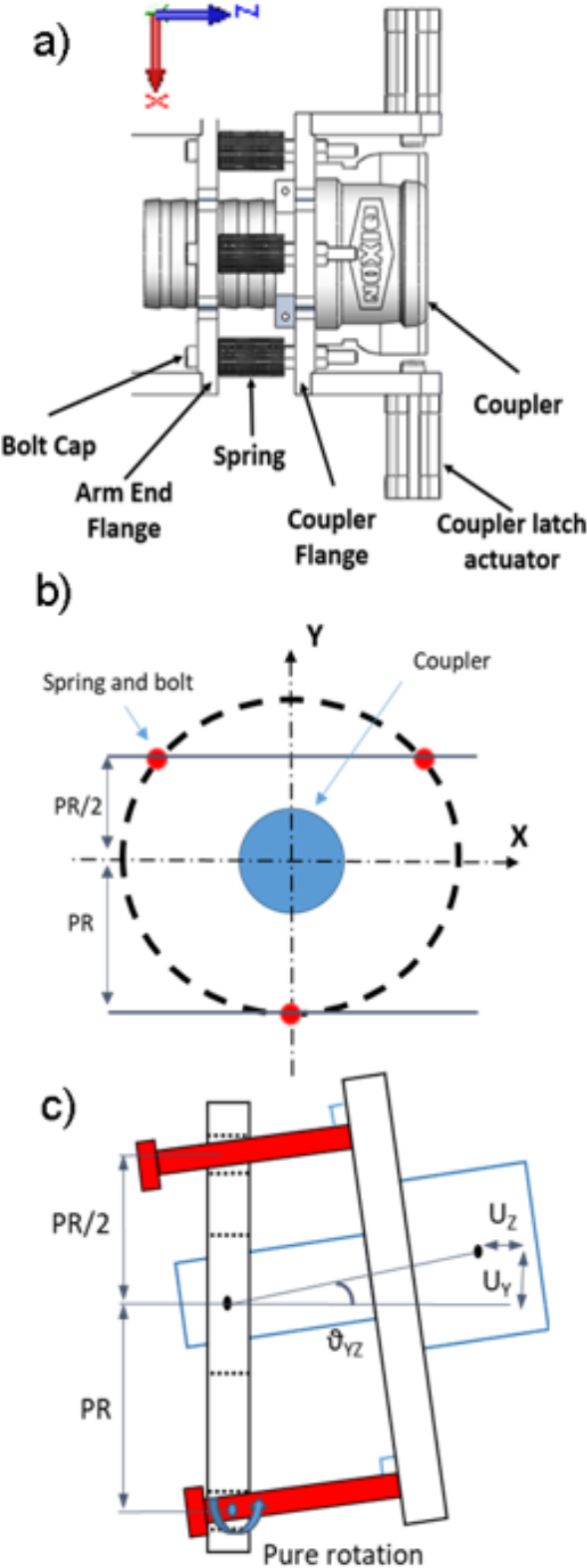
Figure 4.5 Mechanical arrangement of the CyberFluids coupler end-effector

Table 4.1 Experimental variables

Parameters	Nomenclature	Nominal Value	Experimental Range	Units
Spring Eq. Stiffness	K	4.6	3.2 to 6	N/mm
Pitch Radius	PR	91.5	65 to 118	mm
Bore Orientation	O	0	-25 to +25	°
Bolt Length	L	110	Constant	mm
Bore Clearance	C	0.5	Constant	mm
Coupler/port Clearance	CC	0.7	Constant	mm
X-axis Misalignment	XM	≈0	-5 to 5	mm
Y axis Misalignment	YM	≈0	-5 to 5	mm
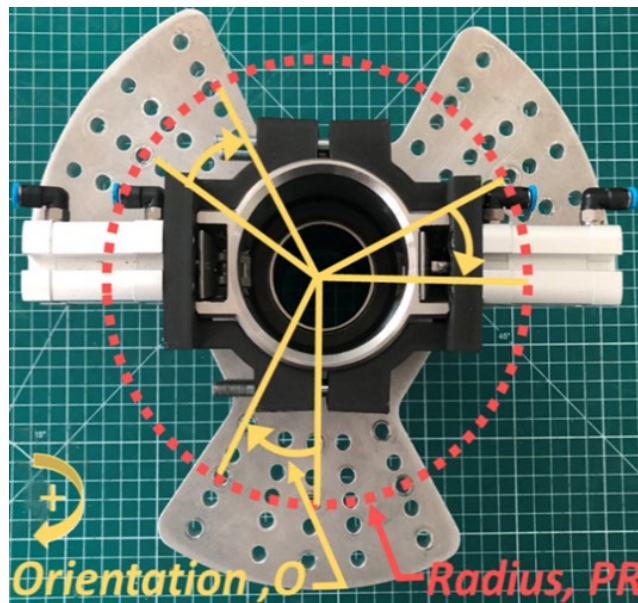
Figure 4.6 Physical prototype of the experimental end-effector

Spring Parameter	Value (mm)
H	0.8
h	0.45
t	0.35
O.D	12.5
I.D	6.2
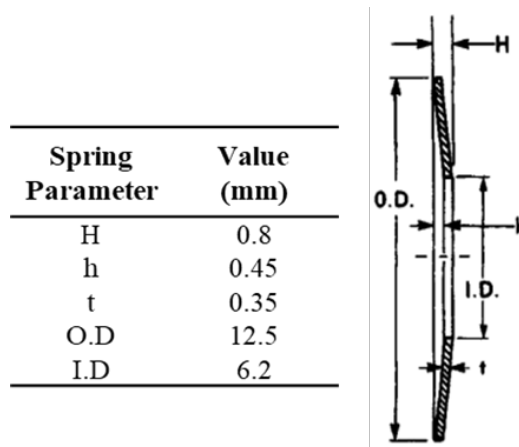
Figure 4.7 Belleville washer parameters

In order to easily adjust the spring stiffness, *K*, it was decided to use Belleville spring washers (Figure 4.7). A number of these spring washers can be stacked in parallel or in series to achieve. a large range of stiffness, deformation or load characteristics. The selection of Bellville springs is not only constrained by the required range of stiffness or deformation but also by bolt diameter. If the clearance between the washer and bolt is too large, even when the spring is compressed, washers can slide in the radial direction. This is undesirable as washers will not make contact at consistent points and this will cause an indeterminate change in spring parameters that will induce experimental error. It is also crucial to prevent the washers from jamming in the screw thread. Thus, bolt length, *L*, is selected to accommodate the longest spring washer stack. For spring arrangements with a lower free length, standard spacer washers are included in the stack to fill the remainder of the bolt length. All spring arrangements are pre-compressed to 15% of the total stack deformation (lower bound spring operating range recommended in DIN2093). The selected spring has a nonlinear force-displacement relationship thus:

$$\frac{df}{dx} \neq Constant\ K \qquad\qquad 4.2$$

In order to derive a single parameter that serves as the stiffness constant (design parameter, *K*), the force-displacement relationship shown in Figure 4.8 is linearised. This will reduce the number of variables associated with the stiffness parameter and streamline the DoE. Since the relationship between the number of washers and deformation/load is linear, the regression fit is independent of the number of washers stacked. With R^2=0.898 and *P-Value*= 0.00404, the regression model has a good fit. Hence linearisation is a simple and reliable method of comparing the stiffness of various washer stack arrangements. The below equation is used to identify the number of washers (in series) that will deliver the required linear stiffness.

$$N_{series} = \left(\frac{Linear\ Stiffness\ of\ 1\ washer}{Required\ Linear\ Stiffness}\right)^{Integer} \qquad\qquad 4.3$$

The number of washers must be a discrete value and thus, due to rounding up/down, there are errors in achieving the exact required linear stiffness. If a large number of washers are stacked in series this error becomes very small. Using the selected spring, for a range of 3.2 to 6 N/mm (91 to 49 spring washers) maximum error in the stiffness is 0.064%
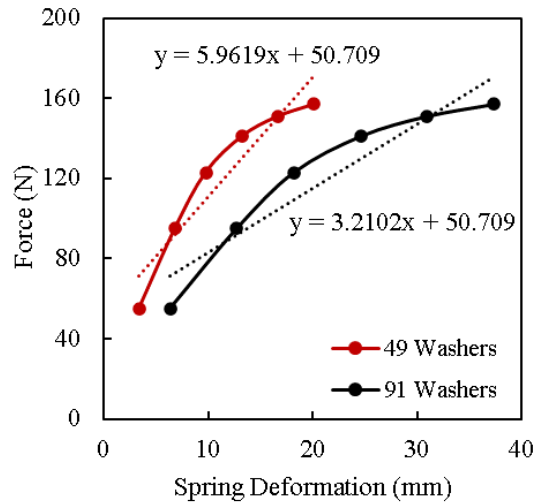
Figure 4.8 Force-displacement relationship of the selected Belleville washers

4.3.2 Performance measures

A perfectly aligned fluid coupling is expected to couple with minimal force; a high insertion force will indicate high friction and/or physical clash that will occur due to misalignment between the coupler and fluid port. Therefore, considering the complete insertion cycle, we can use the energy quantity 'work done' by the motor, as a scalar measure of coupling performance. Insertion force is also monitored, as this is important for sizing actuators, and robot structure and preventing damage to the robot or train parts. Robot servo-drives can monitor motor current and position, which is used to determine insertion force and linear position of the end-effector arm. The relationship between motor current and torque is linear and defined by a motor torque constant specified by the manufacturer. To obtain work done, torque must be converted to force and integrated over the linear distance travelled.

$$\text{Motor Torque}, T_M = k_M * I_{RMS} \qquad 4.4$$
$$\text{Gearbox}, T_G = T_M * 5$$
$$\text{Insertion Force}, F_z = T_G/r$$
$$\text{Work}, W = \int F_z d_Z$$

Where k_M is the motor torque constant, Irms is the root mean square of the 'torque generating' current and r is the radius of the pulley drive in the insertion arm.

The servo-drive is capable of recording 200 samples for motor position and current. The robot insertion speed was set to a nominal value of 25mm/s, and a sampling rate of 20ms was used to capture the entire event of coupling with sufficient precision.

4.4 RED Experiment plan

A second-order regression model is chosen as the non-linear behaviour of its response upon factor changes is expected. Each factor in an FCCD is configured to three levels: low, medium and high. These levels are generally codified as -1, 0 and 1 respectively. Actual settings for each factor were then interpolated referring to their actual limits. Table 4.2 the experimental plan in actual values using FCCD with a revised order to minimise human effort in changing end-effector configurations. Furthermore, centre runs were performed at different points during the experiments in order to effectively capture more of the experimental errors. Initial experiments determined that ports do not couple when X and Y axes are misaligned more than 5 mm, the angular misalignment is negligible.

Table 4.2 Design of experiment plan

Order	K	PR	O	XM	YM	Work (Nm)	Max Force (N)	Order	K	PR	O	XM	YM	Work(Nm)	Max Force (N)
1	4.6	91.5	0	0	0	1.89	49.64	19	6	65	-25	-5	-5	4.20	329.85
2	4.6	91.5	0	0	0	2.03	60.85	20	6	65	-25	5	5	6.05	521.99
3	4.6	91.5	0	0	0	1.94	59.24	21	6	65	25	-5	5	8.92	611.66
4	4.6	91.5	0	0	0	1.89	51.24	22	6	65	25	5	-5	3.42	209.76
5	4.6	91.5	0	0	0	1.89	49.64	23	3.2	65	25	-5	-5	3.73	285.01
6	4.6	91.5	0	-5	0	4.92	414.71	24	3.2	65	25	5	5	7.46	542.81
7	4.6	91.5	0	0	0	1.98	60.85	25	3.2	118	-25	-5	-5	4.30	344.26
8	4.6	91.5	0	0	0	1.89	48.04	26	3.2	118	-25	5	5	10.78	643.68
9	4.6	91.5	0	5	0	3.04	163.32	27	6	118	-25	-5	5	11.13	648.49
10	4.6	91.5	0	0	-5	2.66	118.49	28	6	118	-25	5	-5	3.86	291.42
11	4.6	91.5	0	0	5	5.67	493.17	29	6	118	25	-5	-5	9.34	630.87
12	3.2	91.5	0	0	0	2.04	60.85	30	6	118	25	5	5	9.03	650.09
13	6	91.5	0	0	0	2.06	67.25	31	3.2	118	25	-5	5	9.30	570.03
14	4.6	91.5	-25	0	0	2.01	60.85	32	3.2	118	25	5	-5	3.68	257.79
15	4.6	91.5	25	0	0	2.17	76.86	33	4.6	118	0	0	0	2.06	68.85
16	4.6	65	0	0	0	2.08	73.66	34	4.6	91.5	0	0	0	2.09	73.66
17	3.2	65	-25	-5	5	9.32	611.66	35	4.6	91.5	0	0	0	1.96	59.24
18	3.2	65	-25	5	-5	3.41	261.00	36	4.6	91.5	0	0	0	1.95	57.64

4.5 Results and discussion

The trapezium rule of integration was employed to numerically calculate the work done. Two independent regression models were developed based on work done and maximum insertion force (Max-Force). The model fit statistics are listed in Table 4.4 Both models are significant (*P-value* < 0.05) and express very good prediction capability with R^2 values close to 1. Table 4.3 shows the regression coefficients and *P-values* that represent the significance of each term in the regression model. The main and quadratic effects of misalignments are very sizeable. Spring stiffness, *K,* and pitch radius, *PR,* are effective design parameters while hole set orientation, *O,* is not. The quadratic effect of design factors is insignificant however, most interaction terms, especially those involving *K*, are significant.

Table 4.3 Regression terms and P-values

	Work		Max-Force	
	B	**P-Value**	**B**	**P-Value**
(Intercept)	1.932	0.000	67.366	0.000
K	0.221	0.045	21.349	0.042
PR	0.827	0.000	36.561	0.002
O	0.111	0.290	6.761	0.492
XM	-0.801	0.000	-50.260	0.000
YM	2.170	0.000	142.507	0.000
K^2	0.141	0.615	-16.272	0.539
PR^2	0.163	0.560	-9.066	0.731
O^2	0.182	0.516	-11.468	0.664
XM^2	2.072	0.000	208.697	0.000
YM^2	2.254	0.000	225.509	0.000
K.PR	0.414	0.002	27.020	0.018
K.O	0.570	0.000	32.224	0.006
K.XM	-0.619	0.000	-27.621	0.016
K.YM	-0.465	0.001	-15.612	0.146
PR.O	0.048	0.661	16.012	0.136
PR.XM	-0.055	0.613	-3.002	0.772
PR.YM	0.130	0.243	-13.410	0.207
O.XM	-0.178	0.118	-13.810	0.195
O.YM	-0.435	0.001	-13.010	0.220
XM.YM	0.116	0.299	30.423	0.009

Table 4.4 Fit statistics of the regression.

Statistics	'Work' Model	'Max-Force' Model
Error Degrees of Freedom	15	15
Root Mean Square Error	0.429	40.7
R²	0.991	0.986
Adjusted R²	0.98	0.968
P-Value	5.91e-12	1.45e-10

Figure 4.9 is a typical experimental reading in which it is possible to see the force-displacement relationship of the robot arm. Typically, 45 N is required to drive the arm at the set speed of 25 mm/s. Based on the Max-Force prediction model, Figure 4.11 shows that when both misalignments are large, the maximum force could reach up to a value of 660 N.

Figure 4.10 shows the mean effect of the significant factors in terms of the observed work done. By averaging, the observed responses when each factor was at its higher or lower limits, the typical effect of a design factor is determined. Softer springs and lower values of *PR* result in lower work done. Coupling with large misalignments should produce a higher value of work done. However, the mean response is significantly lower in the *−Y* and *+X* directions. This is understandable for the Y-direction as pitch compliances are not symmetrical. It is interesting to have observed this in the X-direction as this could indicate systems' (end-effector, robot and fluid port) preferred directions of compliance. This phenomenon and the lack of symmetry are also observable in Figure 4.11 as the red and blue lines do not overlap, and the minimum point of the curve is slightly away from the zero-misalignment point.

Figure 4.12 is a model-based surface plot showing the effects and interactions of *PR* with *K*. When both parameters are at their lower level, significantly less work is required to make the coupling. The plots of Figure 4.13 are based on the Max-Force prediction model. Again, the quadratic effect and lack of symmetry are very clear. Design factors *K* and *PR* reduce Max-Force significantly. When using the softest springs, the average reduction is 43 N, when the pitch radius is minimum this value is 73N, when both parameters are set to their lower values its 115 N with a maximum reduction of 170N at -5mm misalignment in the X-axis. Note that in cases of Y-misalignment, Max-Force reaches values below zero. These regression model predictions are inevitably not an exact representation of physical reality. This is due to the fit

of the regression model and in Figure 4.14 the residuals (difference in real and predicted response) for each observation highlight that some of the experiments have large residuals.
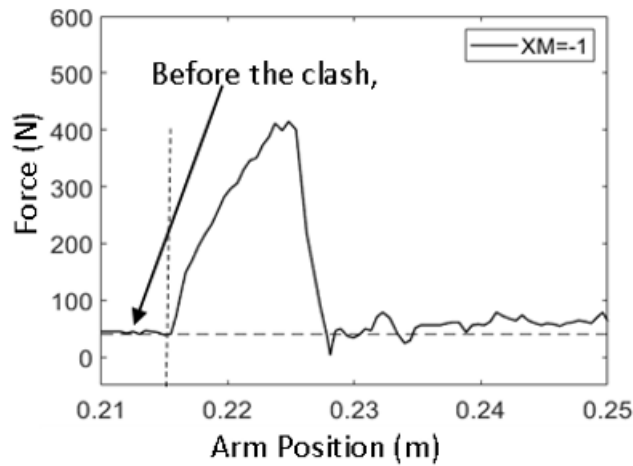
Figure 4.9 Experimental Force-Position curve for misaligned insertion
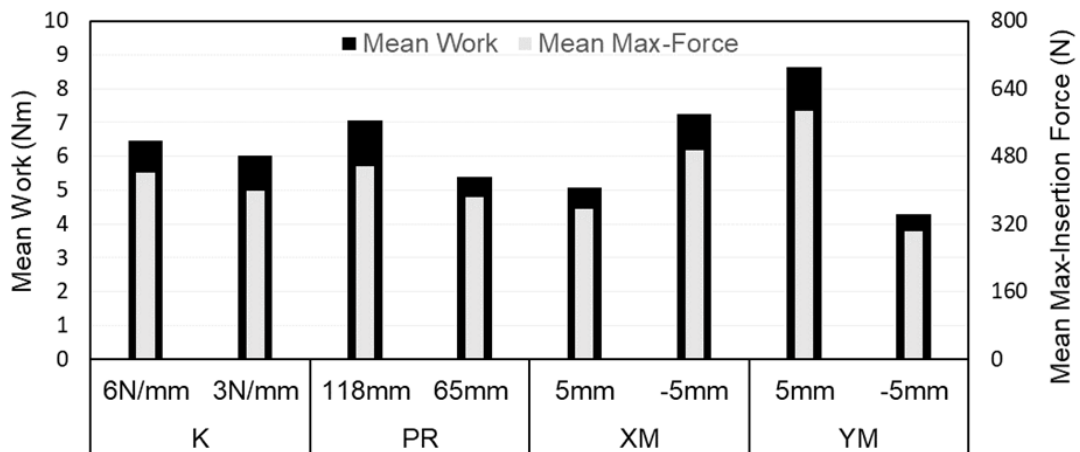
Figure 4.10 Mean effect of experiment factors based on physical data.
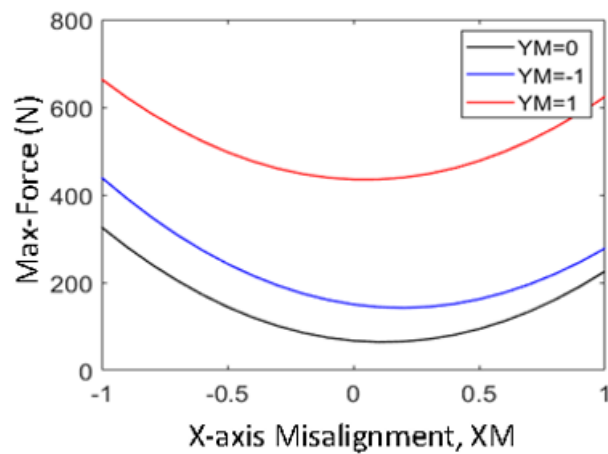
Figure 4.11 Prediction of Max Force at nominal design condition and varying misalignments
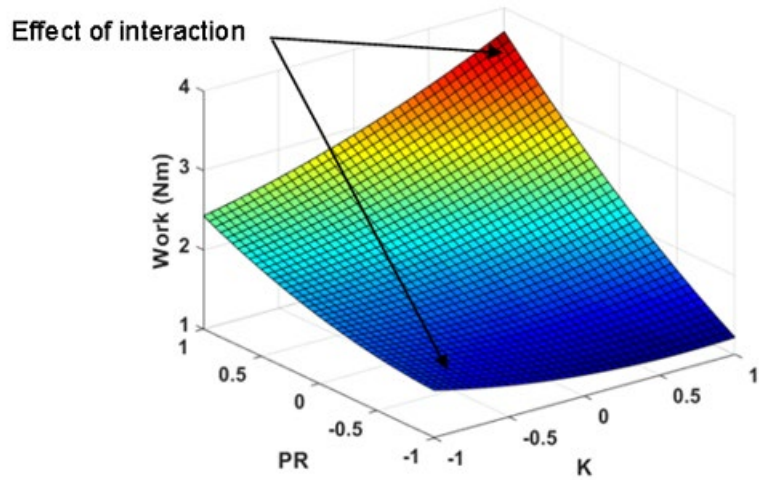
Figure 4.12 Predicted response surface showing the interaction effect of design factors.
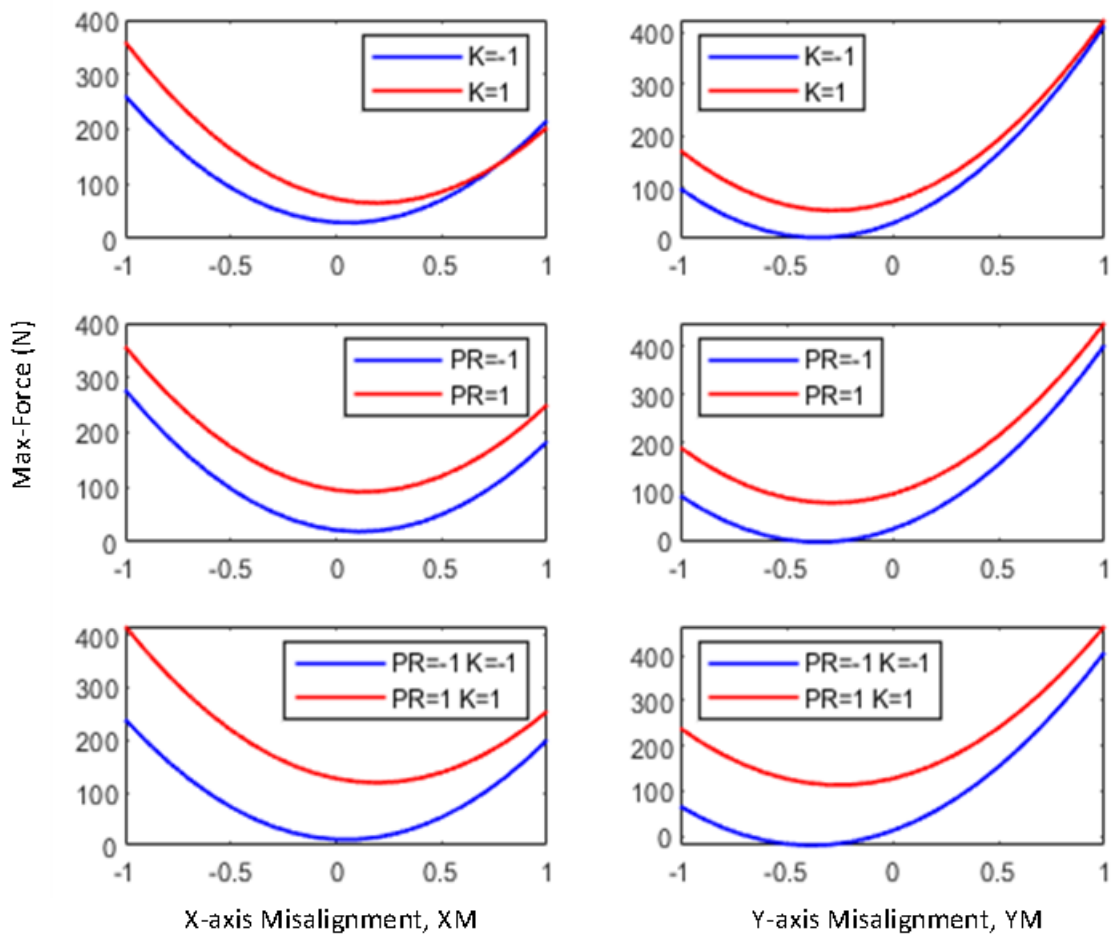
Figure 4.13 Prediction of maximum force at various design factors and noise conditions
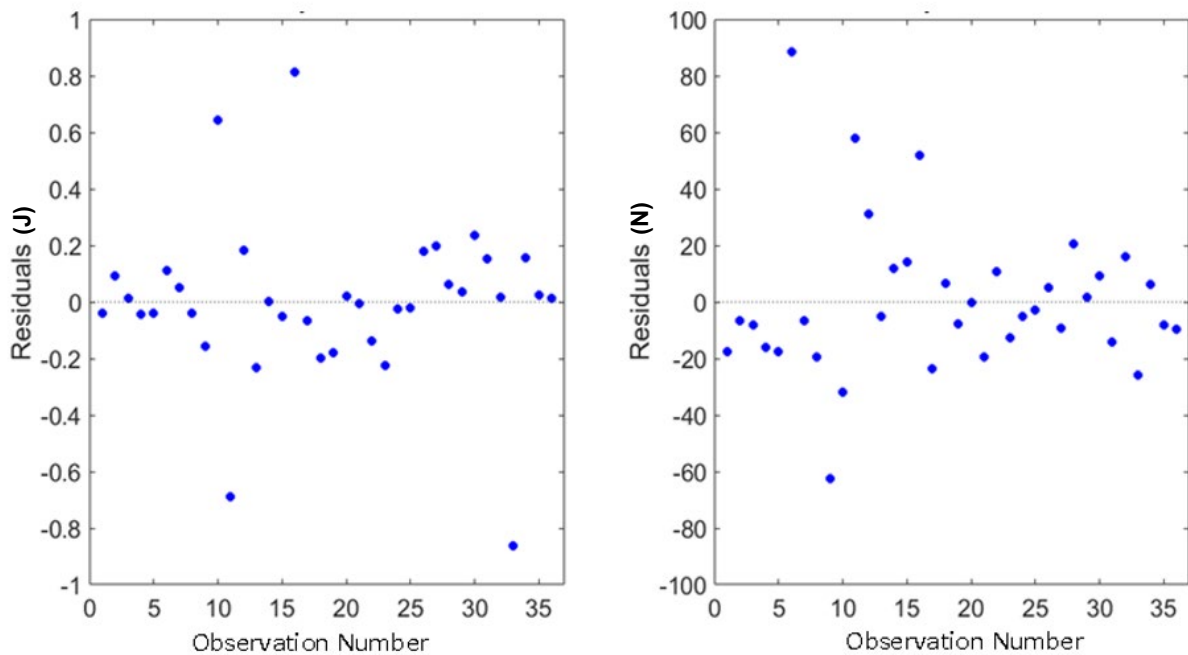
Figure 4.14 Plots of error in real and estimated responses (plot of residuals)

From the results we can see that compliances of the end-effector are not symmetrical in pitch motions. When the coupler pivots downwards it only deforms one spring, if it pivots upwards it will press on two springs. Thus, pivoting downwards due to a corresponding misalignment requires less work or force. This has encouraged a lack of symmetry in the results which is also augmented by experimental error, robot inherent compliance, backlash and other hysteresis that create preferred directions of motion. Robot compliances could overshadow the end-effector compliance and explain the relatively lower mean effect of design parameters. For future experiments, where only end-effector compliance is of interest, fixing and rigidising all but the insertion axis of the robot will be beneficial in isolating the effects of the end-effector compliance. Nevertheless, testing the end-effector 'in-situ' is important for representing the real application.

It can also be observed that the second-order regression model has a limited ability to capture the actual non-linearity. Although the regression statistics suggest a very good fit, when the work done, or forces are low the predicted response can go negative in cases of Y-misalignments. Other than the highly nonlinear profile this could have been exited by the lack of symmetry in the end-effector compliance. Increasing the number of experimental levels from 3 to 5 could improve the model and resolve this issue.

Overall results show that generally more compliant springs reduce the work done. We also observed an interaction between pitch radius and spring stiffness. When both are at their lowest values, a significant increase in performance is observed. This is intuitive in that moments exerted by the spring are reduced at a lower pitch radius. When there are no misalignments, a force of about 45 N is required to drive the robot arm at the nominal speed. Force observed beyond this value is due to contact friction and physical clash. When the port is misaligned 5mm in X and Y, the maximum insertion force is around 660N. This value is very large when compared to the typical force exerted manually by a human. Train fluid ports are not designed for such loads, which also increases requirements on the robot such that larger motors and structures become necessary.

As understood from a typical PiH problem when the misaligned peg travels across the chamfer and into the hole, angular motions of the peg could result in 2-point contacts that encourage jamming. The current end-effector only moves in pitch, yaw and insertion directions and thus coupling is prone to jamming as misalignments are linear. The CyberFluids robot can generate large enough forces that exceed the jamming force. As this occurs, the robot arm bounces forward and the springs release energy hence the sudden drop of force in Figure 6. There was no need to evaluate variance due to noise since the mean force value is so high and unfeasible.

Simple modifications to the CyberFluids end-effector can increase its performance and help to prevent and reduce insertion forces. By incorporating clearance holes in the coupler flange, and removing the locking nuts from the spring side, the coupler will attain pivoting capabilities relative to the bolt. In 2D, this arrangement becomes analogous to a parallelogram linkage. The double pivoting action stacks allow linear motion in X or Y. It is also desirable to have symmetrical compliance in the X-Y plane, thus 4 equally spaced springs should be incorporated. 2 along the Y-axis and 2 along the X-axis. Compliance in the insertion direction is not necessary but it is inherent to this end-effector design concept. Nonetheless, this feature could be useful as a safety feature for robots that cannot limit the force/torque of actuators.

Flexure mechanisms have become very popular over the last two decades. There are many inherent advantages to solving the same design problem using monolithic, distributed compliance mechanisms. Good examples are Constant Force Mechanisms (CFM) that regulate surface contact forces and generate compliance at the end-effector. Therefore, in developing new compliant end-effectors, a flexure-based mechanism incorporating passive compliance

capable of handling a larger range of misalignments will be developed for a peg-in-hole scenario. Such an end-effector can solve another limitation of our work; where we assumed ports would be horizontally located on the train. Depending on how the rail industry goes forward with modifying the fluid ports, simple robots with compliant end-effectors could deliver a better economic solution than very sophisticated robots with many sensors and DoF.

4.6 Summary

Automated servicing of trains is being seriously considered by the rail industry to release humans from unsuitable tasks and improve health and safety in maintenance depots. The benefit of having passive compliance in a robot end-effector will help to improve the robustness of fluid coupling whilst reducing the reliance on accurate robot end-effector positioning systems. In this work, we have investigated the role of end-effector compliance in enhancing the mechanical connection of fluid ports under positional uncertainties. Results show that misalignments have an exponential effect on the work done and the maximum force of insertion. When the fluid port is misaligned, having softer springs at a lower pitch radius can reduce the maximum insertion force by up to 160N. Likewise, there is a reduction of work done by the insertion motor indicating an overall better coupling. Yet still the forces involved are too large (more than 600N) and need to be reduced. Our research on end-effector compliance design, which focuses on relaxing the insertion force relationship to misalignments can benefit from new compliant mechanism designs.

5. A LARGE MISALIGNMENT RCC END EFFECTOR FOR FLIUD COUPLING

Overview

In this chapter, we compile a specification for a large motion train fluid coupling end-effector. Design concepts are then proposed and qualitatively discussed. The chosen design is modelled using the approaches previously discussed in Chapter 3. Two robust design approaches are conducted here, the Taguchi and RSM. The former results in an improved design that is physically prototyped and compared with the previous CyberFluids end-effector. The RSM approach results in generalised design charts discussing the performance of this design in variance fluid coupling applications.

5.1 Problem definition

It is expected of the train driver to park the train within the "servicing zone" with an accuracy of +- 1m. The robot sequence begins by performing a prescheduled search pattern for the RFID tag on the train carriage. It then centres on the RFID tag which is defined as home position. The train tag provides information regarding the train model, the location of fluid ports, and other maintenance schedule data. Knowing the presumed location of fluid ports the robot begins fluid servicing by addressing various tasks. below is a list of uncertainties that may cause misalignments between the robot and the train.

1. Inaccuracy of robot mechanical movement +-1mm.

    Typically, industrial Cartesian systems of this scale can provide an accuracy of +-1mm which is a liberal estimate.

2. Inaccuracy of robot centring on the RFID tag +-1mm

3. Unintentional dimensional change of train parts i.e., due to wear, damage manufacturing tolerances +-1mm, 1deg

    Train parts that are exposed are subject to damage and wear. We assume a feasible uncreate of +-1mm and 1dgree which will not affect the performance of the part such as the fluid port.

4. Train suspension motion due to wear, weight load, or other factors

    Usually, tarins have two sets of suspensions, primary and secondary, and the carriage rides on both suspensions. Wear on the springs could cause the carriage to level higher or lower than expected. Furthermore, fluids and sand also contribute to the weight of the carriage. As the fluid port is coupled and fluid dispensed or extracted the suspension moves to accommodate new weight. The total motion of suspension is assumed to be +-10 mm and 4 degrees. It is possible to reduce this uncertainty by re-evaluating the position of the RFID between each fluid extraction and dispensing task. Placing the RFID tag and fluid couplers where it is not affected by suspension height, however, this complicates the robot's work schedule and causes other difficulties such as moving components on the train.

Another source of uncertainty is the contact interaction between the robot and the workpiece. Surfaces of the fluid ports and caps may be subject to dust, debris and fluids, which affect the friction coefficient between surfaces.

Table 5.1 Sources of Misalignment

Source of misalignment	Linear amount	Angular amount
Inaccuracy of robot mechanical movement	+/-1mm.	+/-0.5
Inaccuracy of robot centring on the RFID tag	+/-1mm	+/-0.5
Unintentional dimensional change of train parts i.e., due to wear, damage and manufacturing tolerances	+/-1mm	+/-1deg
Train suspension motion due to wear, weight load, or other factors	+/-10mm	+/-3deg
Sum of misalignments	+/-15mm	+/-5deg

The design purpose of the end-effectors is clear, accordingly, the mission state of Table 5.2 is produced. The next step is conducting further analysis of the requirements and specifications for the design. There are some key metrics that we must consider.

Table 5.2 Mission statement for end-effector design

Design description	• Compliant end-effectors for coupling of hoses and dust caps in train fluid servicing
Benefit proposition	• Reduced cost and requirements on the robot side i.e., a less complicated system with reduced DOFs and payload • Reduced operational forces for reduced health and safety risks
Goal	• Feasible end-effector designs with misalignment range of +/15mm linear, 5 deg angular. • Reduced operating forces to 150 N • Incorporate compliant mechanisms to take advantage of their inherent benefits (i.e., cost benefits)

Primary market
 	
Secondary market
	• Rail industry
	
	• Other servicing and maintenance industries
	    o Car refuelling,
	    o Satellite servicing
	    o Modular robots.

Assumptions	• Robot-carrying end-effectors are a cartesian system similar to the CyberFluids system. • Dixon fluid ports are used in the end-effector, and train fluid ports are standardized using adapters.
Stakeholders	• Rail Safety and Standards Board (RSSB) • Chiltren Railway • Brunel University London

5.1.1 Target specification metrics: Fluid coupler end-effector

The key requirements for a compliant fluid coupler end-effector relate to metrics which affect robot payload, precision and DoF requirements. An end-effector which reduces these requirements on the robot side can significantly reduce cost which becomes even more pronounced in mass production.

Coupling or insertion forces, the mass of the end-effector, and its misalignment ranges can be considered the most attractive metrics for industrial applications. There are some other key requirements, for example, fatigue life or compactness which also increase the desirability of the design solution. To include elementary requirements for example capability of horizontal or vertical insertion, having means of operating fluid port cam locks, ensuring secured fluid port connection etc would be useless. Such requirements are inherent to the function of the end-effector hence no need to include in the specification.

We should also consider contact surface wear and resistance to fluids as requirements; however, these requirements relate to the fluid coupler and not so much the compliance of the end-effector, we assume existing fluid coupler designs (i.e. Dixon couplers) satisfy those requirements. We focus on measurable performance which discusses the compliance capability of the device.

See Table 5.3 for the mapping of metrics and requirements. it is also worth mentioning set input variables are the architecture of fluid ports, that is geometry and material properties which manifest themselves into:

    S1.1.   Nominal diameter

    S1.2.   Clearance

    S1.3.   Contact Friction coefficient

It is assumed these parameters cannot be controlled as part of the design and are application-specific. In this regard, some analysis has been conducted to produce design charts considering these parameters.

Table 5.3 Specification for the train fluid servicing compliant end-effector

Need	Metric	Importance	Target	Units
R1.2. Reduces forces	M1.2 Max insertion Fz	1	100	N
R1.3. Large misalignments	M1.3 Max possible misalignment	1	15, 5	mm/°
R1.4. Robust/durable	M1.5. Stress factor	3	1.5	-
R1.5. Lightweight	M1.6 Mass	2	5	Kg
R1.6. Compact	M1.7 Max misalignment / characteristic length	4	0.1	-

Modelling these performance metrics is the subject of the upcoming sections. At this stage, it is worth noting the coupled nature of requirements and metrics. Generally, the most desirable scenario is where each requirement is only associated with one specific metric. However, in many cases, this is unattainable, the author believes this is especially true in the case of compliant mechanisms. This is because of the highly coupled nature of the mechanism itself, in many cases, motion across various axis will affect other axes, i.e. motion is coupled, and this can increase the coupled nature of metrics and requirements. In such case couple of the most important metrics can be chosen to steer the design, the specification should be updated on each iteration of the design to ensure other metrics are within bounds.

5.2 Conceptualisation

Generally, an RCC device for cylindrical peg and hole shapes requires 4 DoFs two translational and 2 rotational. The insertion axis must be constrained and stiff to accommodate insertion forces. Since a cylindrical shape is rotationally symmetrical with a circular profile, the roll axis may be constrained or free. It is often the case that compliant mechanisms with many degrees of freedom have coupled motion. Recently researchers have been pursuing decoupled compliant mechanisms (Awtar et al., 2013) however their designs tend to be very bulky and generally have a low compactness ratio. Due to the coupling, it is crucial to incorporate stiffer angular stages which result in only translational movements when crossing the chamfer of the peg. This prevents angular movement which maybe increase misalignments. Followingly when the peg is inserted in a hole which has relatively low clearance, translations are confined by peg and hole geometry. Hence rotations become dominant and angular misalignments are resolved.

Typically (for small misalignments), the stiffness ratio between the linear stage and angular stage of an RCC mechanism is in the range of several hundred around 200 times (Whitney and Rourke, 1986).

Angular misalignment may be slightly augmented or corrected during chamfer crossing depending on the position of the RCC point. Figure 5.1 presents the two possible misalignment scenarios which may occur, there are 4 possible cases (in 2D) however due to symmetry, analysis across two cases is sufficient.
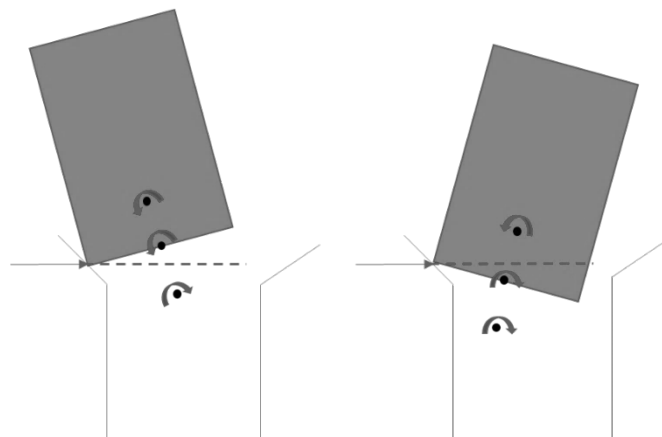
Figure 5.1 Various positions of RCC point in Peg-in-Hole insertion.

3 possible positions for the RCC point are shown on the peg. Due to the horizontal contact force, different types of turning moments are imposed upon the three various RCC points. If the RCC point is far from the tip (in either direction) the resulting turning moment is larger, for one scenario this causes more corrective motion but for the other, this causes more angular misalignment. By setting the RCC point exactly at the tip of the part, in both cases the turning moment is equally disruptive. However, the disruption is minimized since the moment arm is minimized for both cases. Furthermore, since the angular stage is significantly stiffer than the linear stage, a slight variation of the RCC point from the tip of the peg will not have a pronounced effect. For the case where the hole is being carried by the end-effector RCC can be set halfway through the chamfer to achieve a similar effect.

A remote centre of motion can be attained through various linkage arrangements (Zong et al., 2008). For cross-flexure-based compliant mechanisms, beams arranged with an instantaneous centre of rotation create an RCC effect. Constrained-based design better elaborates on this.

Based on these principles the location where all constraint lines coincide will have a rotation DoF. Hence By constraining all irrelevant DoFs, RCC can be attained.

Various building blocks (or compliant elements) with known degrees of freedom and constraint can be arranged to achieve the desired motion (Hopkins and Culpepper, 2011). For example, parallelogram-guided beams provide a single translational DoF, folded flexures constraint motion in one direction and cross flexures provide rotational DoFs. More recently we have seen that circularly curved beams can also provide a rotational DoF which may be considered remote (Parvari Rad et al., 2018).

Figure 5.2 shows a series of compliant mechanism building blocks that can be used for the linear and angular stages. These elements make use of distributed compliance to better perform in large motions hence there are no hinges or small length flexures. Due to large stress concentrations hinges and small flexures do not perform well in large displacement cases and have not been considered as an option.

Linear stage	Parallelogram	Folded flexure
Angular (RCC) stage	Cross flexure	CCB
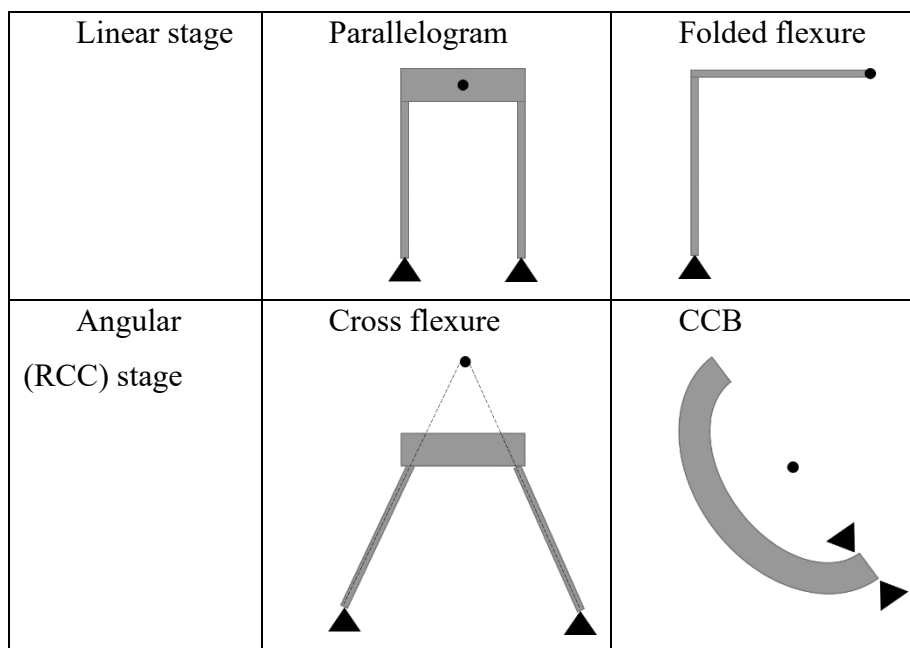
Figure 5.2 Various compliant elements considered for end-effector design.

Of course, the arrangement of these building blocks and their parametric design will have a significant impact on their performance. Evaluating the performance of various concepts is not the objective of this chapter nonetheless the key performance criteria can be listed as

1. Range of motion
2. Motion axis drift
3. Off-axis stiffness or drift
4. Stress concentration

In reality, all these qualities relating to the end-effector's compliant mechanism will impact the coupling performance. However, the key design factor affecting insertion performance in fluid port coupling is the compliance or stiffness characteristics of the motion axis. The requirements for all other quantities are clear i.e., any kind of axis drift must be minimised, stresses must be highly distributed such that material can withstand failure and range motion must suffice misalignments. Given motion axis stiffnesses for a successful coupling, other quantities can be achieved through well-constrained designs using distributed compliance mechanisms. Furthermore, the compliant parts of the end-effector must be able to handle the end-effector weight. This may be done in many ways e.g., via auxiliary locking mechanisms, stiff compliant members which ensure minimal deformation due to gravity or the addition of a new decoupled mechanism or springs which compensate for gravity. A simple and cost-effective solution would use a stiffer linear stage instead. However, this increase in stiffness is also followed by higher insertion forces. An addition of a constant force spring which offsets the weight of the end-effector is more desirable. Since the angular stage is significantly stiffer than the linear stage motion induced by gravity on the angular stage can be neglected.

5.2.1 Gravity compensation

If we do not compensate for gravity, then displacement due to gravity should be considered and deducted from the maximum misalignment range. However, the stiffness of the compliant mechanism must be raised to mini minimise displacements. This option will significantly increase insertion force so it's inefficient. It's possible to compensate for the weight of the end-effector and arm around a pivot with a simple coil spring (Rahman et al., 1995). This idea applies parallelogram stages identical to the linear stage in Concept 3.
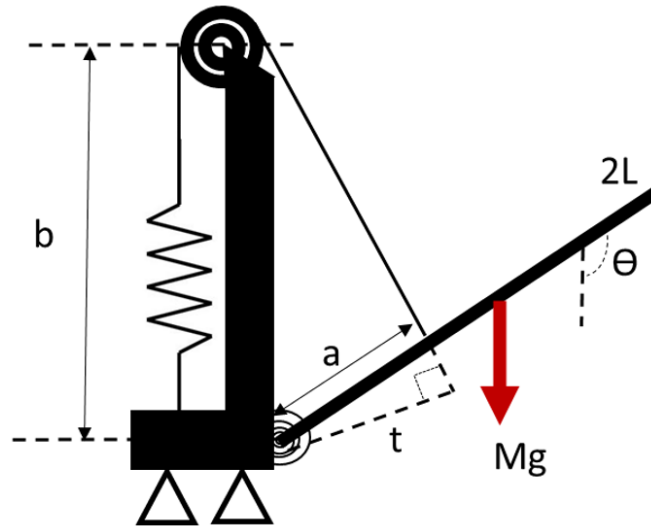
Figure 5.3 Gravity compensation spring arrangement

$$M_o = mgLsin(\theta) - K(x - x_o)t = 0 \qquad 5.1$$

For $\theta \neq 0$ and $x_o = 0$, K can be isolated

$$K = \frac{mgL}{ab}$$

Note K Is not a function of theta θ or x, thus irrespective of displacements K will always balance weight. However, to achieve this for a very large range of motion, a spring with zero initial length should be realised. Of course, physically a spring cannot have zero length, a simple way to do this is by arranging springs and pulleys as shown in the figure. This will not be necessary since relative to a manipulator arm displacement achieved by a compliant end-effector is magnitudes small. A spring with stiffness K directly satisfies gravity compensation.

5.2.2 *Material, manufacturing, and concepts selection.*

Various concepts have been proposed see Figure 5.4 to Figure 5.8. Generally, designs consist of a linear stage and an angular stage coupled to each other. The end-effector is inserted towards the train fluid port requiring only a single line of motion from the robotic system. The fluid port on the train side will contact the end-effector somewhere within the vicinity of the funnel. There is a through hole along the linear and angular stages, to allow for the fluid hose to run through. A funnelling tip is fixed to the fluid coupler, this provides a 25mm 45-degree chamfer up which the misaligned fluid port can be guided to the fluid coupler. Small pneumatic cylinders (not shown in figures) may be added to operate the fluid coupler cam locks which are carried by the angular stage. Figure 5.7 is a physical realisation of concept 3 which has been 3d printed in 1 piece. This prototype has been used in the CyberFliuds+ system, see Appendix A5.
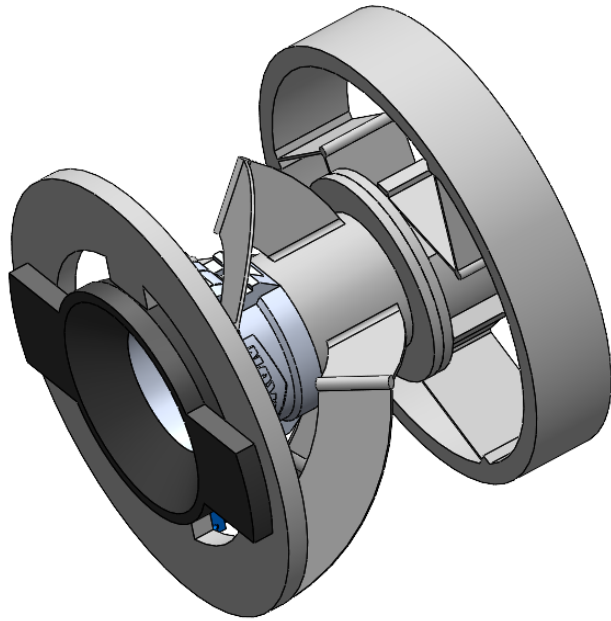
Figure 5.4 Train fluid servicing RCC end-effector concept 1
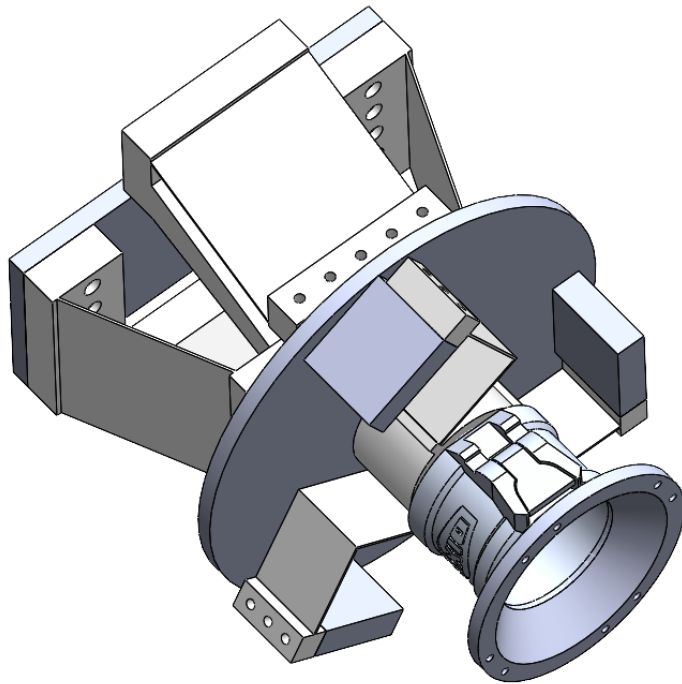
Figure 5.5 Train fluid servicing RCC end-effector concept 2
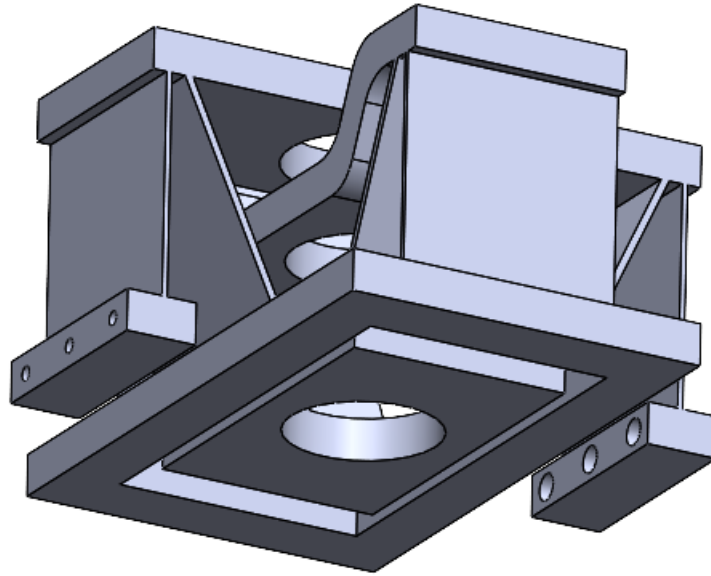
Figure 5.6 Concept 3 compliant mechanism of the end-effector
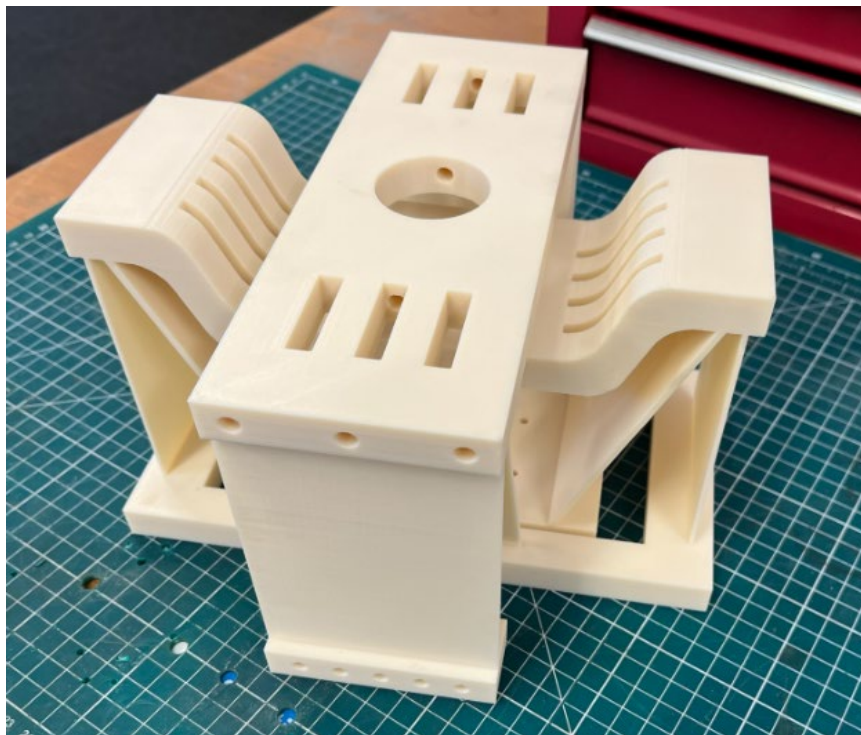
Figure 5.7 Concept 3 prototype
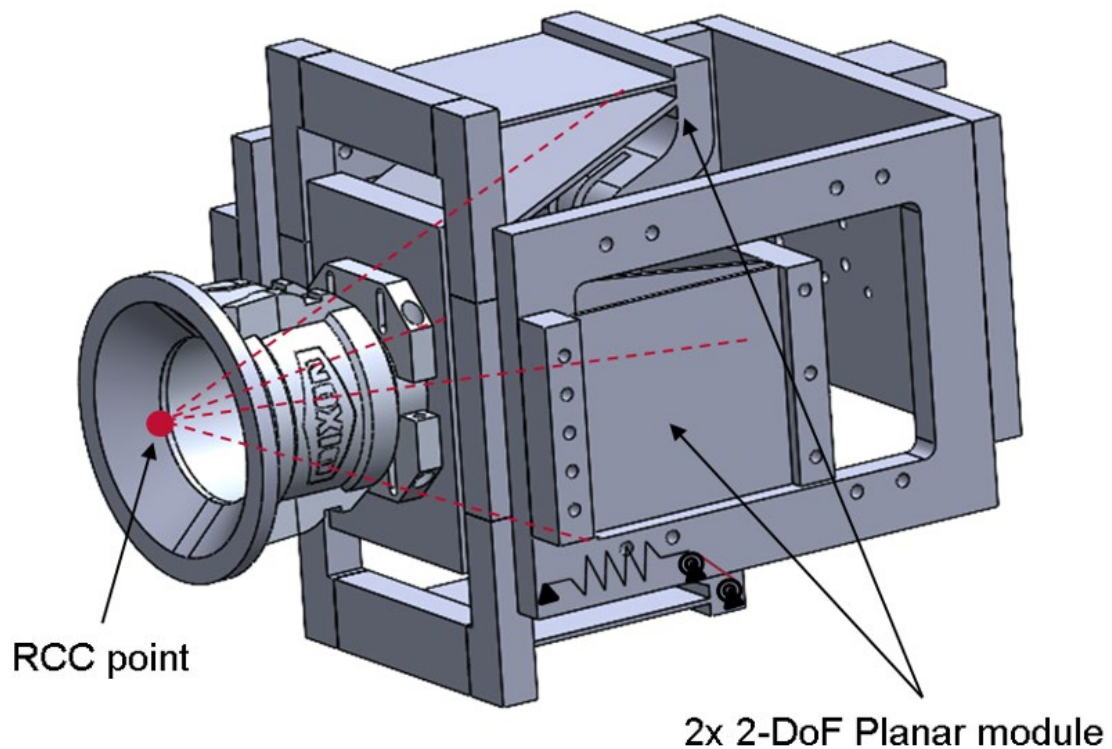
Figure 5.8 Concept 3 with robot end-of-arm adaptor

According to Table 5.4, we have selected Concept 3. The ratings are mostly qualitative based on intuition and experience. However, we can confirm that in terms of manufacturing, compactness and gravity compensation ease, Concept 3 is the top candidate. It can be manufactured with the assembly of multiple planar parts. Each module can be moulded, extruded, Electrical Discharged Machined (EDM) or assembled with sheet metals and connecting elements. For Concept 3 the modules are sitting compactly on top of each other reducing the characteristic length of the device and resulting in increased compactness. In terms of other metrics, the flexure-based RCC device used in Concepts 3 and 2 has a larger motion axis drift due to the movement of the instantaneous centre of rotation. In this regard, concept 1 performs best since it has more constraint lines coinciding with the centre of motion. Accordingly, it may also perform better on stress metrics.

Table 5.4 Concept selection (higher is better)

Comparison parameter	Concept 1	Concept 2	Concept 3
Ease of production manufacturing	1	3	3
Compactness	1	1	3
Motion axis drift	3	1	1
Stress concentration	3	3	3
Ease of gravity compensation	1	1	3
Sum (rating)	12	9	13

The selected material should have good corrosion characteristics but more importantly a high yield strength-to-flexibility ratio. This means more range of motion can be achieved without failure. Table 5.5 shows a list of generally less corrosive materials rated against this characteristic and others. We can see that Titanium is the top candidate. Generally, plastics are not used for heavy-duty applications due to low creep performance and high-temperature sensitivity. However, in this work, we are bounded by 3D printed prototypes, hence the material selected is ASA.

Table 5.5 Material selection (lower is better)

Material	Elastic modulus,E	Yield strength,σy	$10^3 *$ σy/ E	σy/ E rating	Durability rating	Creep rating	Cost rating	Total rating
Titanium V	115	1100	9.6	3	1	1	7	12
Aluminium 7075	70	490	7	4	3	2	6	15
Aluminium 2014	75	400	5.33	5	5	5	3	18
Aluminium 6151	70	255	3.6	6	4	4	4	18
Stainless steel 304	200	200	1	7	2	3	5	17
PLA	3	50	16.7	2	7	6	1	16
Nylon 66	2	60	30	1	6	7	2	16

5.3 Modelling

Performance evaluation is conducted in the PRBM model where insertion forces can be minimised hence also stresses reduced. This certainty can be granted using a single post-FEA run which can ensure stress limits are respected. In this approach, we capitalise only on the benefits of each model. Figure 5.9 shows the mapping of requirements and metrics as related to various models which may be used in conjunction.
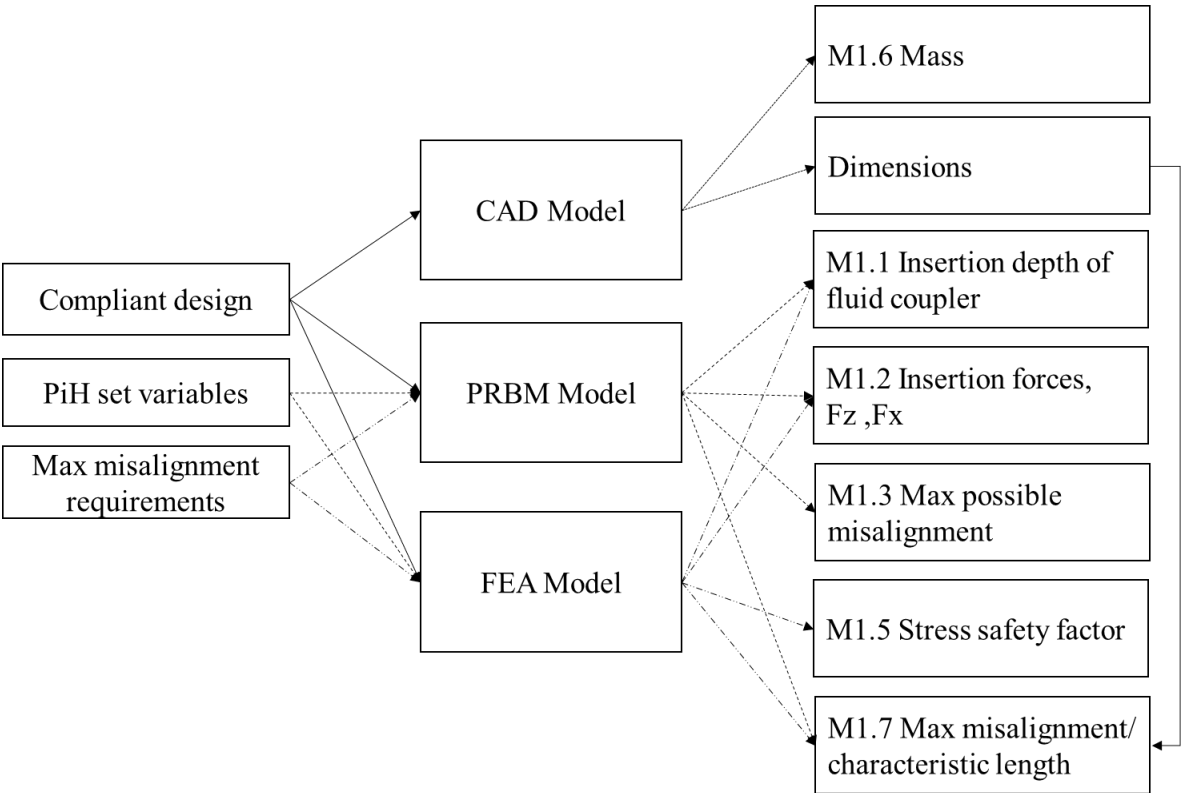
Figure 5.9 Model input/output and metric mapping

5.3.1.1 *Ball parking stiffness and stress with PRBM*

A simpler stiffness model (not shown in Figure 5.9) will prove useful for quick calculations which put the design configuration in an approximate operation zone. A simple calculation including maximum misalignment ranges (displacement) and stiffness of stages can give an idea about the range of expected forces during the insertion. Actual insertion forces will be larger than these approximations. This is due to the force in the insertion direction, contact friction and geometrical conditions. Hence if at this early stage forces observed are not desirable

then the design should be reconfigured to fall into a feasible range. We discussed this approach in3.3.1.2 as Formulations 3.21 to 3.36. We can recall some of those Formulations for this problem as follows.

$$F_{lateral} = Max\ linear\ misslaigments * stiffness\ of\ linear\ stage \qquad 5.2$$
$$M = Max\ angular\ misslaigments * stiffness\ of\ angular\ stage$$

K is given for a fixed-guide beam and is substituted here. To consider the stiffness of two identical beams stiffness is multiplied by 2. This yields the system force-displacement relationship

$$F_x = \frac{8K_\emptyset EI\theta}{l^2 cos(\theta)} \qquad 5.3$$

The angular stage is simplified to a pin joint and link for which moment is given

$$M = \left(\frac{8EI(H^2 + Hh_f + h_f^2)cos(\varphi)}{(H - h_f)^3} cos\left(\frac{h + 8h_f}{8(H - h_f)} \theta \right) \right) \theta \qquad 5.4$$

The maximum stress due to bending occurs at both ends of a fixed guided beam given by (Howell 2001)

$$\sigma = \frac{F_x ac}{2l} \qquad 5.5$$

c is the distance from the neutral axis to the surface of the beam. a is the deformed length of the beam. Table 5.6 illustrates the results of the above analysis, we can see that we are operating in a suitable range with physical stress and force values.

Table 5.6 Results of preliminary design analysis with PRBM

Initial configuration	Value	Units
Input parameters		
E	2.6	Gpa
L	90	mm
w	85	mm
t1	2	mm
t2	2.7	mm
hf	120	mm
φ	47.92	deg
λ	0.834	mm
KΘ	2.65	-
Spec linear miss, eo	15	mm
Spec angular miss, Θ	5	deg
Output parameters		
Miss. Lateral force	79	N
Miss. Moment	25.3	Nm
Linear stage beam stress	11.5	MPa

5.3.2 Simulation models

Since end-effector compliance is symmetrical, a simplified version of the end-effector will suffice the modelling approach, The simplified model is only of the identical modulus in the two-module configuration of concept 3. The module has 2 coupled degrees of freedom with a set of cross flexures to create an RCC point at the instantaneous centre of rotation. Linear motion is guided by the parallelogram mechanism. The PRBM and FEA settings are the same as those used in the model comparison of Chapter 3. The nomenclature of parameters used in upcoming sections is also illustrated there in Figure 3.7.

5.4 RED plan

If reaching specification metrics is the only goal, a small set of experiments will suffice this process. fractional factorial or Taguchi's method is ideal for this purpose. If a more thorough analysis is required, Response Surface Methodologies (RSM) will produce more comprehensive results with second-order predictors. This will be at the cost of more simulations. This chapter will implement both approaches.

5.4.1.1 The Taguchi approach

In the following, we use a Taguchi-type approach since it requires minimum statistical effort with a small number of runs for 2 design factors and 2 noise factors. The 2 noise factors are linear and angular misalignments. This "crossed array" approach contains noise factors outside the orthogonal array of design factors. Each factor at 2 levels yields a total of 16 runs with either the PRBM or FEA models. Mean and standard deviation are directly calculated from the results of experiments without significant statistical analysis that is required for factorial or RSM plans. The aim is to identify the most suitable configuration that yields the best mean performance with the least variability for a prototype (3D printed ASA) end-effector. The 2^4 factorial design (combined array) is a suitable experiment design, given the practitioner can effectively explore the statistical endeavours required for the analysis. Mean and variance (or standard deviance) can be analytically approximated from first-order response equations according to Chapter 3. It can also be used to derive the first predictor models and conduct the steepest/deepest ascend study to drive design factor ranges to a more suitable level. For the sake of conciseness of results and simplicity, we will stick to the Taguchi design to illustrate how a small number of runs and a little statical effort can lead to a robust design.

Taguchi design is arranged with 16 total runs, 2x 2^2 factorial arrays arranged in a cross formation. Table 5.7 shows the details for each run. We consider high (1), and low (0) settings to correspond to the top, and bottom of the range bounds respectively. Y is the response measured at each combination of noise factors. Taguchi's Signal-to-Noise Ratio (SNR), which indicates the most desirable solution for our case translates to the 'smaller is better' formula:

$$\frac{\text{S}}{\text{N}} \ = \ -10 \ * \log\left(\frac{\sum_{i=1}^{n}(Y_i^2)}{\text{n}}\right) \qquad\qquad 5.6$$

Table 5.7 Parameters for Taguchi DoE

Experiment variable	Symbol	Range	Units
Overall length	L	0.7 to 0.11	N/mm
Thickness ratio	T2/T1	1.2 to 1.5	-
Linear misalignment	e_0	5 to 15	mm
Angular misalignment	Θ	-5 to 5	deg
Thickness	T1	2	mm
Friction coefficient	F	0.15	-
Nominal ID	63	63	63
Nominal OD	63.8	63.85	63.8
Insertion speed	V	5	mm/s
Elastic modulus	E	2.6	Gpa

The design factors selected for his study are the overall effective length L and the thickness ratio of the angular and parallel beams. Please refer to Figure 3.7 for illustration and nomenclature. Note parameters such as effective overall length, L and width w, are shared between the linear and angular stages, L, geometrically constraints La. The RCC point is kept in the middle of the funnel 10mm outside the mouth of the hole. To identify suitable ranges for these design factors, we first implement the simplified PRBM approach from the previous section Table 5.6. The initial design configuration satisfies target force and stress limits. Thus, the design factor ranges selected for the design of experiments will revolve around this initial configuration. The selected material is ASA with E=2.6Gpa. We measure the maximum insertion force using the PRBM rigid solver.

5.4.1.2 Response Surface Method

The RSM method is used to conduct a thorough analysis of the proposed design. Charts have been produced describing end-effector performance. Factors will also include the nominal size of fluid ports and friction between which would be different in each application. This results in several performance contours and charts which will help to find optimal design configurations for various scenarios. Given the range of factors that suit the user's application, they may directly refer to these results. If the range is beyond what is available, the user can follow the didactics of these sections to construct their search for a feasible design.

Let's take 2 design factors, 2 signal factors and 2 noise factors, that's a total of 6 factors in a combined array. We will use the CCD design with 90 runs Appendix A3 shows the run order in coded and uncoded values. We sought the effect of design factors and noise factor levels and used them to evaluate the mean and variance of performance and plot this against the signal factors. Again we used the PRBM rigid solver to model insertion force Fz.

The design factors were selected to maintain a sense of generality while satisfying a feasible number of experiments. As will be shown in the results section, we identified from Taguchi experiments that larger values of T2/T1 have a significant effect in reducing the standard deviation of maximum force due to noise. In order to maintain the generality of results we will try to normalise the factors to relate to more applications. Thus, instead of T2/T1 will use I1/I1/L which is the beam length normalised section ratio. Accordingly, we will pick a range higher than what translates from Taguchi experiments.

Since in different applications projection of the RCC point will be different we have also introduced a normalised projection ratio. That is the amount of projection over the largest width of the RCC angular linkage and overall length, L. Clearance ratio and friction also include signal factors which are different in various applications.

Table 5.8 Response surface plan showing the range of variables for the RCC mechanism.

Experiment variable	Symbol	Range	Units
Normalised section ratio	I2/I1L	8.6-17.2	N/mm
Normalised projection ratio	P/WL	10-15	-
Linear misalignment	e_0	-15 to 15	mm
Angular misalignment	Θ	-5 to 5	deg
Clearance ratio	C/ID	6 to 8 $*10^{-3}$	mm
Friction coefficient	F	0.1-0.3	-
Insertion Speed	V	5	mm/s
Elastic modulus	E	3	Gpa

5.5 Results and discussion

5.5.1 Analysing the Taguchi results

The SNR often indicated the best performance considering variability due to noise and mean performance. Looking at the results of Table 5.9, configuration 2 has the best SNR and the best mean performance. However 50 % lower standard deviation is achieved in configuration 1, this is at the cost of a 43% decrease in mean performance. We can also see that SNR for configurations 1 and 2 are very close. Thus, if the reduction in performance is feasible then configuration 1 is a more robust design. Accordingly, it is always best practice to evaluate mean and standard deviation alongside the SNR for more informed decisions. This becomes more apparent when looking at Figure 5.10 which discusses the mean of force and mean of standard deviations, at given factor levels. We can confirm that higher values of T2/T1 reduce standard deviation but also decrease performance (higher force). For the given experimental range of variables, we can conclude that both T2/T1 and L have a high impact on both standard deviation and mean.

In terms of guidance on sizing actuators we can estimate in terms:

$$F_{actuator} = (F_{mean} + n * Y_{sd}) \qquad\qquad 5.7$$

Common practice will use a "3 Sigma" rule setting n=3 to ensure a 99.73 % chance that the maximum possible force is accounted for. We should also allow up to 10% due to simulation inaccuracies and up to 10% oversizing. We should also allow 5-10% due to simulation model inaccuracies. Hence as an example, for design configuration #1, we need a robot payload of at least 135.61N which can be rounded up to 150N. We selected this configuration for our prototyping since it has a lower standard deviation and the actuator force is feasible for our applications. This is a significant improvement against existing CyberFluids end-effectors which require a payload of upwards of 600N only for 5 mm parallel misalignment.

Table 5.9 Taguchi DoE arrangement and results

		e_0	1	1	0	0			
		Θ	1	0	1	0			
Config#	L	T2/T1	Y1	Y2	Y3	Y4	Mean	Ysd	S/N
1	1	1	91	116	100	107.5	103.63	10.66	-35.01
2	1	0	103	69	54.5	61	71.88	21.58	-32.85
3	0	1	243	315	250.5	281	272.38	32.83	-42.73
4	0	0	255	237	152	178	205.50	48.51	-42.21
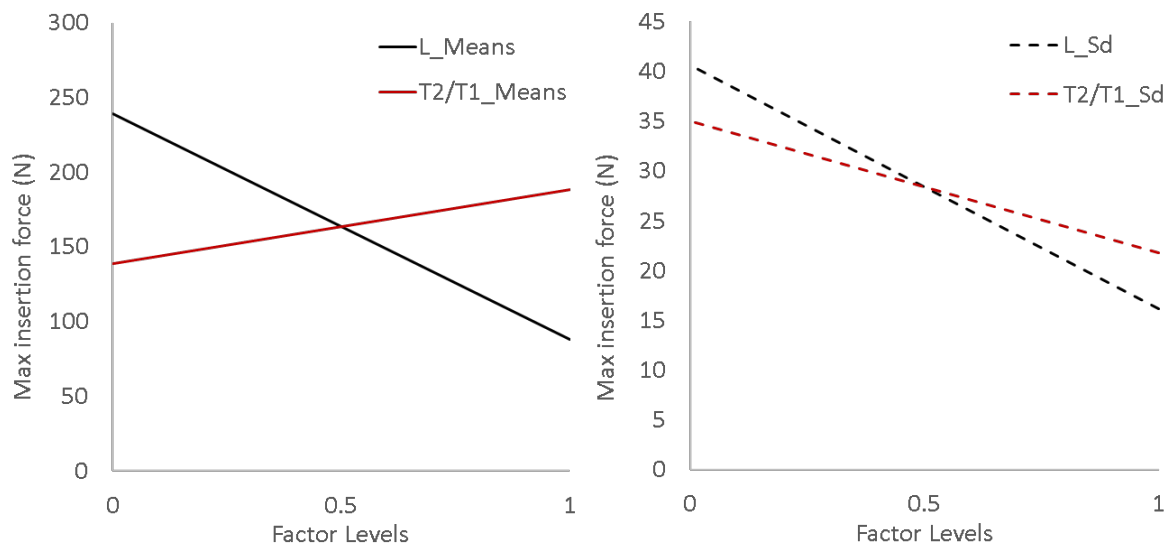
Figure 5.10 Mean force and mean standard deviation against factor levels.

Table 5.10 Updated specification.

Need	Metric	Importance	Target	Actual	Units
R1.2. Reduces forces	M1.2 Max insertion Fz	1	100	150	N
R1.3. Large misalignments	M1.3 Max possible misalignment	1	15, 5	15, 5	mm,°
R1.4. Robust/durable	M1.5. Stress factor	3	1.5	1.3	-
R1.5. Lightweight	M1.6 Mass	2	5	1	Kg
R1.6. Compact	M1.7 Max misalignment / characteristic length	4	0.1	0.12	-

5.5.2 Response surface analysis

We can see that the regression equation obtained has a very good predation capability with R^2 =96.8%. Residuals are typically around 50 N, higher ones can be observed outside the range bounds (<-1 and >1), we will only use predictions within the bound range since they are generally more reliable. This RSM model is useful in predicting insertion forces.

From Table 5.11 it's clear that design factors and frictions are significant, clearance ratio is just outside of the significance acceptance range of 0.05. the exponential effect of misalignments is highly significant and most of their effect is exponential. This is also apparent from Figure 5.12 which shows the mean effects of the design factors (Montgomery, 2012). Here we can see that generally better results by reduced (-1) values of design factors.

Table 5.11 Fit statistics (P-value and coefficients) of the model

Term	Coef	P-Value
Constant	7.69	0.411
l2/l1 L	24.88	0.000
L P/d	11.03	0.008
e0	2.15	0.594
ϴ	-1.14	0.777
C/D	-6.97	0.088
F	23.01	0.000
l2/l1 L*l2/l1 L	2.40	0.470
L P/d*L P/d	2.40	0.470
e0*e0	52.40	0.000
ϴ*ϴ	127.40	0.000
C/D*C/D	2.40	0.470
F*F	2.40	0.470
l2/l1 L*L P/d	19.54	0.000
l2/l1 L*e0	-2.67	0.555
l2/l1 L*ϴ	1.43	0.751
l2/l1 L*C/D	-3.47	0.443
l2/l1 L*F	0.19	0.967
L P/d*e0	-2.04	0.651
L P/d*ϴ	0.90	0.841
L P/d*C/D	-3.44	0.447
L P/d*F	4.89	0.280
e0*ϴ	34.51	0.000
e0*C/D	-0.28	0.950
e0*F	0.46	0.920
ϴ*C/D	-0.36	0.937
ϴ*F	-1.49	0.742
C/D*F	1.77	0.695
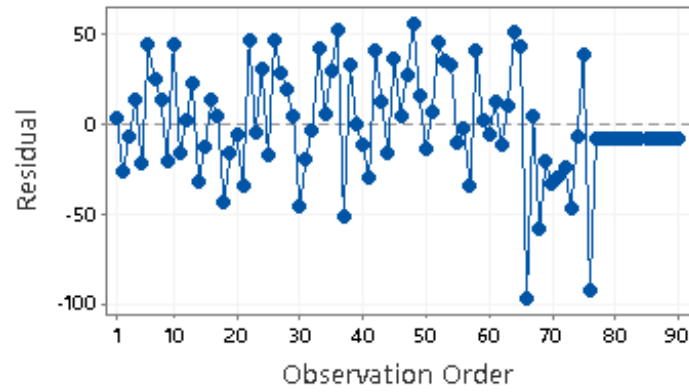
Figure 5.11 Regression model residual vs actual observation
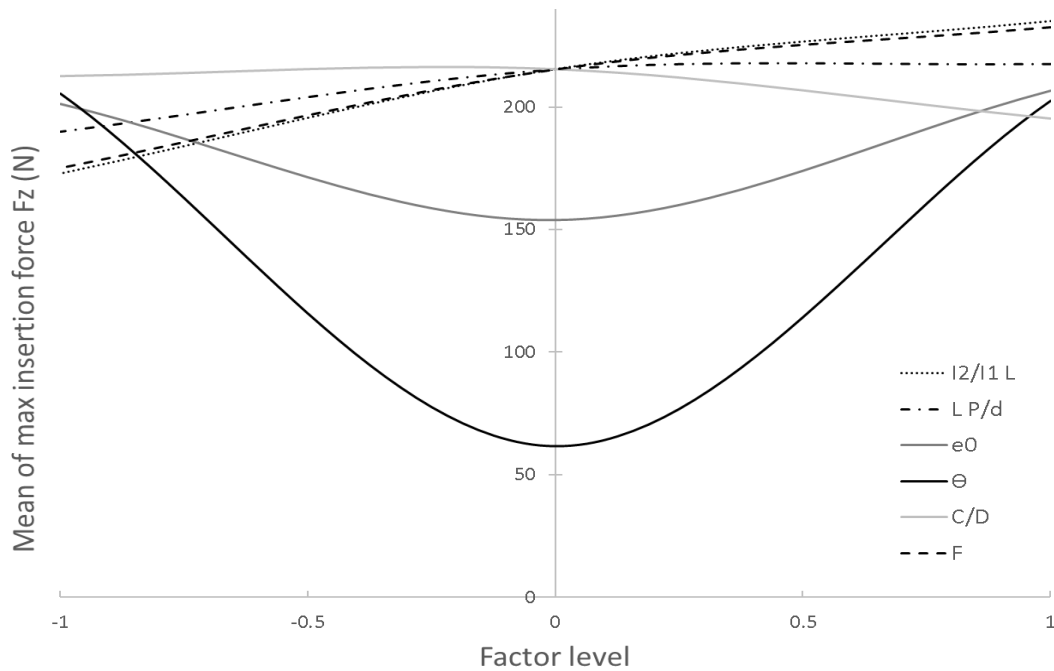
Figure 5.12 Mean effect of factors.

Figure 5.13 and Figure 5.14 show contour plots (from regression equations) of averaged maximum force and its standard deviation across noise factors, for various operational conditions. Figure 5.13 shows the change in mean performance vs design factors at various clearance ratios and frictions. Figure 5.14 sets the design factors at the point where the best performance is observed and illustrates the performance at various friction and clearance ratios. From the plots, we do not see a change in standard deviation which indicates design factors have no contribution to changing variance due to noise. This coincides with the p-values of design/noise factor interactions which are not significant. Indicating for the chosen range of variables, design factors will not increase robustness by significantly reducing forces given misalignments. However, when we did the Taguchi experiments, we observed that T2/T1 has a significant effect in reducing standard deviation. T2/T1 is related to I2/I1L as the thickness of

the beams is the most sensitive parameter (cubed) in determining the moment of inertia, I. Thus, the design factor is effective but not in the particular range selected for this experiment.
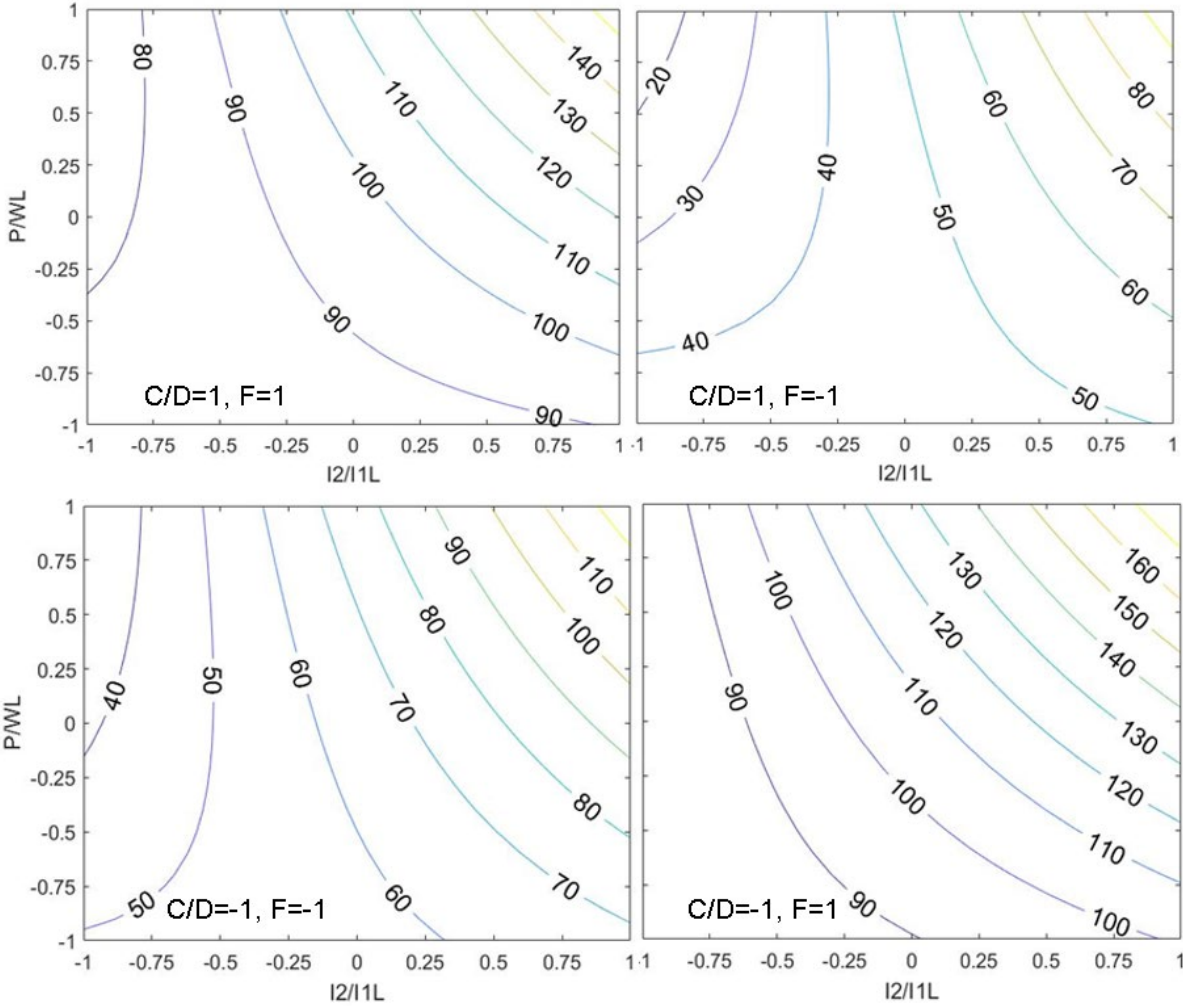
Figure 5.13 Contour plots averaged force (across misalignments) vs design factors, at various clearance and friction conditions. Sd across misalignments is 46.5 N

Ideally, more experiments would have further demonstrated the validity of results, this was not possible due to a lack of resources. To this end, we rely on the PRBM model validity and RSM cross-validation. The PRBM comparison with physical experiments (Section 3.4.4), showed a 5 % simulation error. Given the residuals of the RSM model shown in Figure 5.11 the prediction error is +/-50N. Including the 5% simulation error on top, the total equates to +/-52.5N. As shown in Formulation 5.7, a useful estimate of the actual maximum force for sizing robot actuators and payload, multiplies the predicted average force by 3 times the standard deviation (sd). Accordingly, the resulting figure must be further upsized by 52.5N.
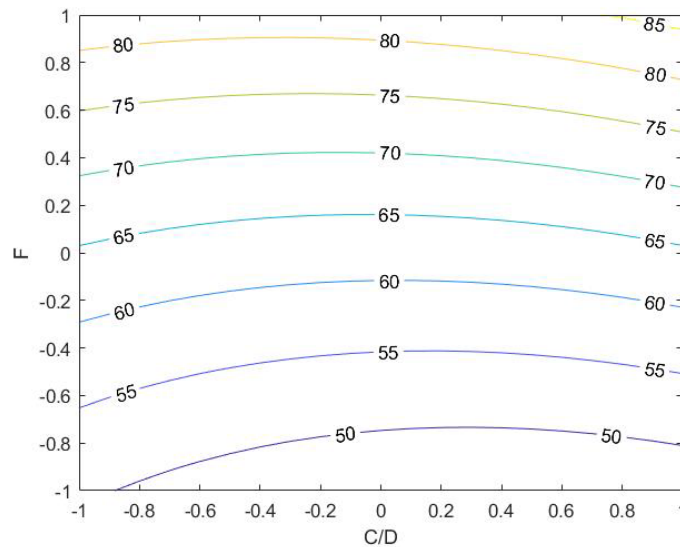
Figure 5.14 Contour plots of averaged force across misalignments at I2/I1L =-1 P/WL=-1 Sd across misalignments is 47 N

5.6 Summary

The proposed methodology was implemented to embody and analyse a new RCC end-effector for large misalignment application of train fluid servicing. We demonstrated how to achieve a robust design configuration of the end-effector for our specific application. Compared to the existing device on the CyberFluids robot (see Chapter 4), maximum forces were reduced up to 75% from 600N to around 150N, while the misaligned range increased at least 3-fold to 15mm parallel and 6 deg angular. This also satisfies the target design metrics specified in Table 5.3. The Taguchi analysis revealed that beam thickness ratio T2/T1 and length, L, both have a significant effect in reducing the standard deviation of maximum force, indicating a more robust design. Using RSM, more generalized results were obtained for various applications that incorporate cam and grove-shaped pegs and holes. Charts were developed showing predicted average maximum force, and standard deviation under various system configurations. Even though we found the normalised design factors to be significant in reducing the average maximum force, we did not see a reduction in standard deviation. This may be due to the selected range of factors which are not positioning us well in the design space. However, we cannot confirm this, a larger range of factors should be selected to see improvement followed by a plateauing of performance. Such effort should also aim to reduce residuals and increase the prediction accuracy of the regression model, by increasing the number of experiments and order of the model. This will in turn provide more confidence during the downsizing of the robot payload.

6. A COMPLIANT INTERFACE FOR TRAIN SERVICING GRIPPERS

Overview

In this chapter, we will use our methodology to solve a different type of problem. Here we deal with a type of passive compliant mechanism which is required to transfer load from an uncertain input load position. The aim is to illustrate the generality of the method and how it can easily be applied to various compliance design problems.

Even when coupled, the dust caps on the train fluid port are free to rotate around their roll axis. The existing CyberFluids gripper can only operate dust the caps if they are in a particular roll angle. A novel compliant mechanism is proposed to accommodate all roll angle misalignment between a parallel jaw gripper and the train fluid dust cap. This gripper interface is retrofitted on the dust caps and transfers grip force to unlatch the dust caps. Here we implement a response surface approach and discuss the results.

6.1 Problem definition

The fluid port dust cap on the CyberFluids rig has two buttons (levers) on each side which operate a cam lock that latches onto the fluid port groove. In order to remove the cap these levers must be pressed however when refitting the dust cap these levers need not be pressed since the cam lock can glide over. Due to the rotational symmetry of the fluid port and dust cap, the cap may be coupled to the port at any roll angle. Thus, the position of the unlatching levers is uncertain. Figure 6.1 also shows an existing parallel jaw gripper which can only operate the cap at a particular orientation. The pneumatic cylinders are responsible for proving the grip force on the CyberFluids robot rated at 8 bars with a piston diameter of 18 mm which yields 203 N per cylinder.
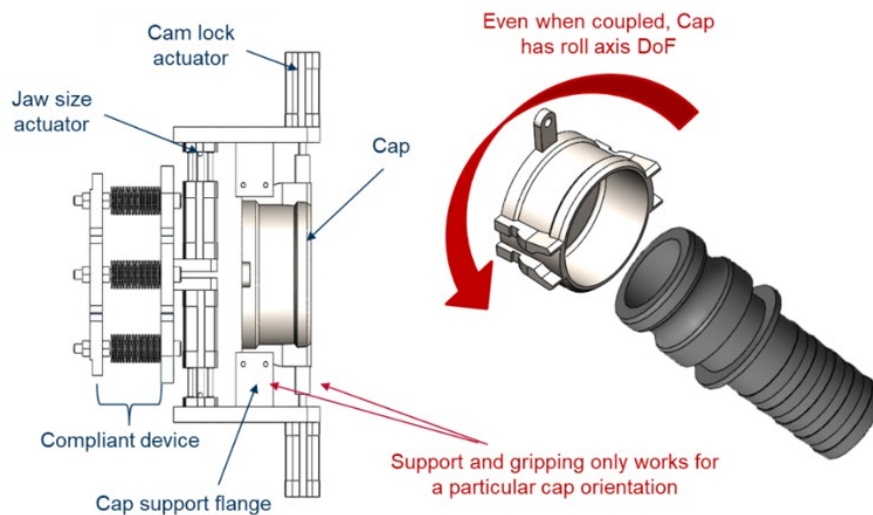
Figure 6.1 CyberFluids fluid port dust cap gripper
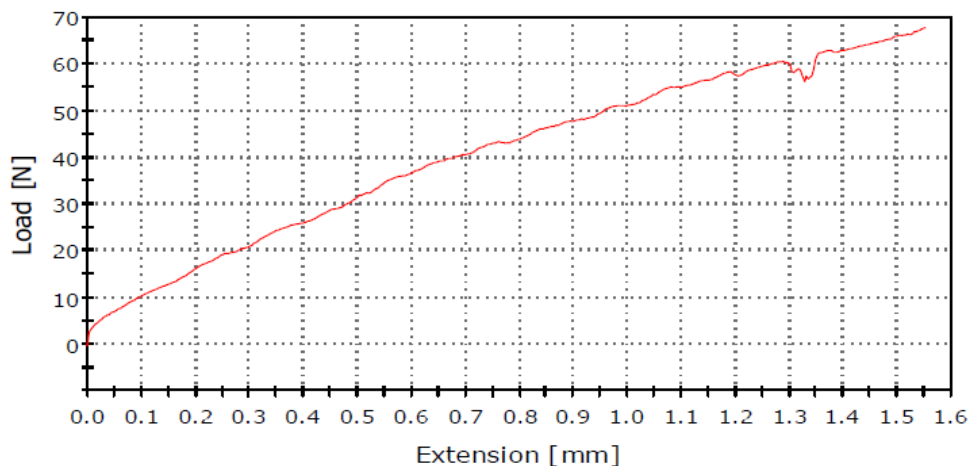
Figure 6.2 Graph force required to press unlatch buttons on the fluid port cap.

Regarding the latching system installed on the fluid couplers, an Initial test using a 5500 series Instron machine has shown that buttons on the fluid couplers and caps require a force of 60N to unlatch when coupled to a port. However, when the cap/coupler is pushed in the insertion direction to compress the inner gasket, pressure is released on the latches. Eliminating latch contact and frictional forces and eventually reducing the force required to unlatch. This force is approximately 10 N which is chiefly dependent on the torsional spring used for the spring return action of the latch. To reduce overall forces, it is very easy to schedule the robot to lightly press anywhere on the cap before gripping.

Considering that a standard parallel jaw gripper is operating the cap, the proposed design must be able to transfer forces and motion from the gripper to unlatch the cap. The design can lie on the effector or alternately retrofit onto the fluid port cap. The proposed design is planar, which eventually makes it very easy and cheap to manufacture. This device will clip on over the existing dust cap to create an interface for the robot gripper. This is a contact-aided compliant mechanism based on a cross-flexure design. It has 4 cross flexure mechanisms a pair for each button. The cross-flexure coupler link (outer rim) contacts a slider which has a single degree of freedom and presses on the buttons. However, due to misalignments the location and thus effective magnitude of gripper force (Fin) is uncertain. Assuming the robot gripper moves radially towards the centre of the cap (i.e. no other misalignment present) the force input position can be anywhere along the rim.

6.2 Conceptualisation

Several concepts are generated, some guided by topology optimisation, and some based on intuition. The idea behind this design is that it serves as a compliant interface between a parallel jaw gripper and any component which latches, in our case the dust cap. If the gripper manages to compensate for all other misalignments, the proposed device will completely accommodate roll axis misalignments between the gripper and latches. The gripper may accommodate other misalignments for example with a cylindrical or tapered PiH interface with this device. The gripper must have RCC capabilities to perform largely misaligned PiH. We have discussed the development of such a device in Chapter 5, didactics there will be useful in realising the complete system.

A peg may be fixed on the interface as shown in Figure 6.3. The peg is fixed on a mount which encapsulates and fixes the cap in position against the rigid portion of the compliant mechanism The compliant portion will cover the outer rim to transfer gripper load at any roll angle towards the latches. The most important part of the design is the compliant mechanism responsible for transferring the gripper load, which may be anywhere along the rim, to pressing motion at the latches. For this case study we will go ahead with Concept 2, which is relatively simpler and easier to analyse with the familiar remote centre concept.

The most important part of the design is the compliant mechanism responsible for transferring the gripper load to pressing motion at the latches. This task is split into two different mechanisms. First transfer the radial gripper load across the rim. The second transfers the load from the first mechanism into vertical motion. Some trials with topology optimisation for this load transfer mechanism are shown in Figure 6.5. It has been difficult to incorporate the topology optimization results due to the one-node hinges and the circular nature of the rim. From topology optimisation results a 4-bar linkage can be distinguished, this has led to Concept 2 where the 4-bar linkage is realised with notch-type revolute joints. However, these joints often do not perform well since they localise motion and stresses. Also, notice that mechanism one has been switched for the slider cam system. Given the friction between these sliding faces is regulated, replacing flexing components with such rigid body motion will reduce stored (lost) strain energy.
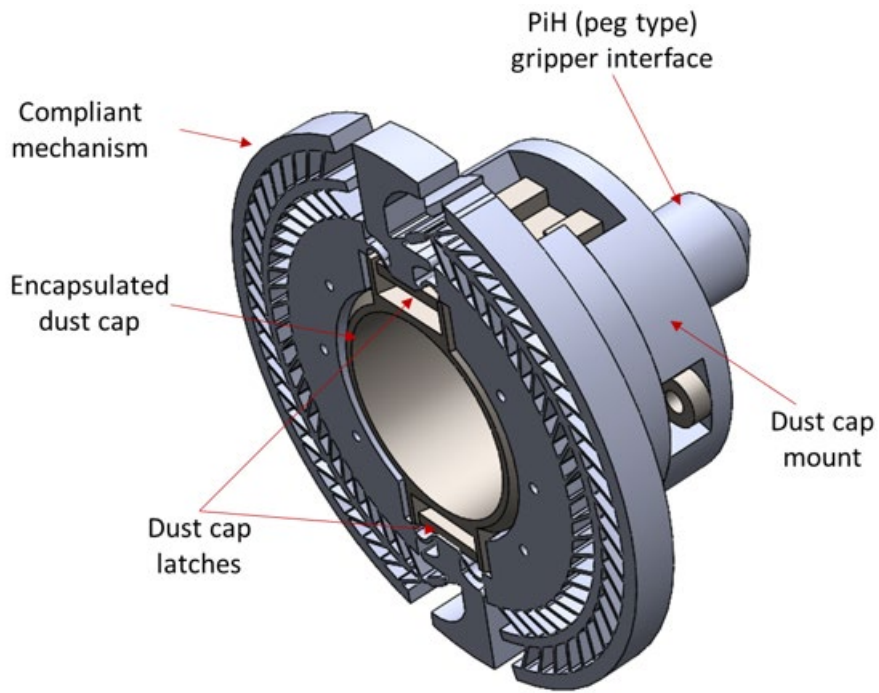
Figure 6.3 Concept 1 parallel jaw interface complete device
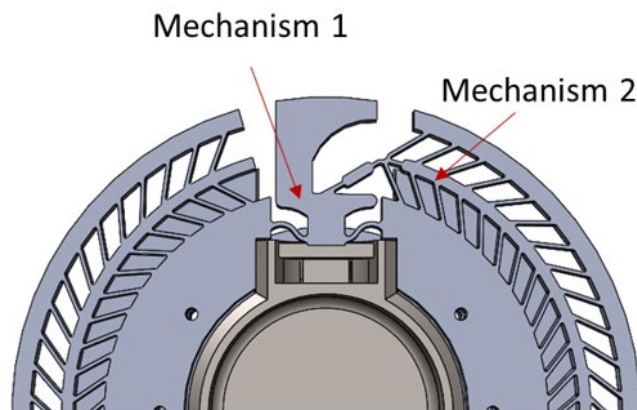
Figure 6.4 Compliant portion of concept 1 showing the two mechanisms
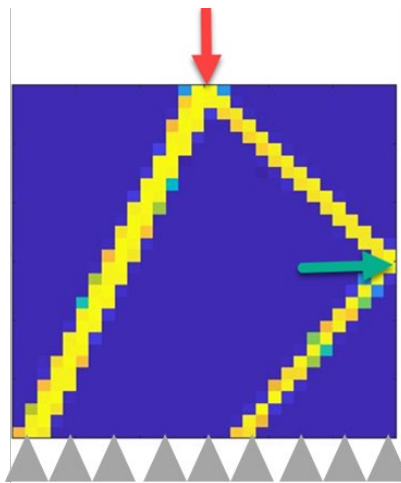
Figure 6.5 Example of topology optimisation for the load transfer mechanism
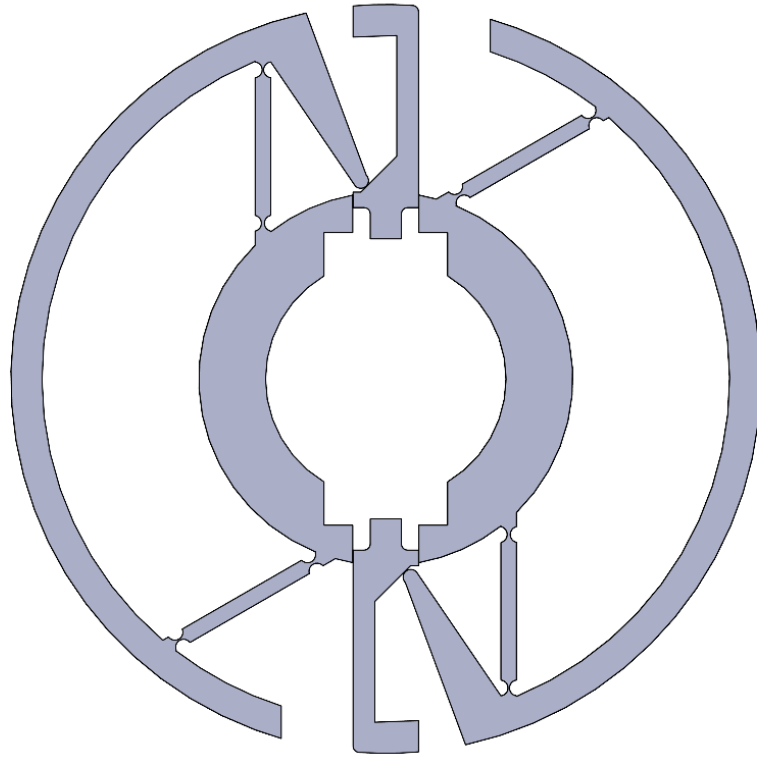
Figure 6.6 Concept 2 compliant mechanism
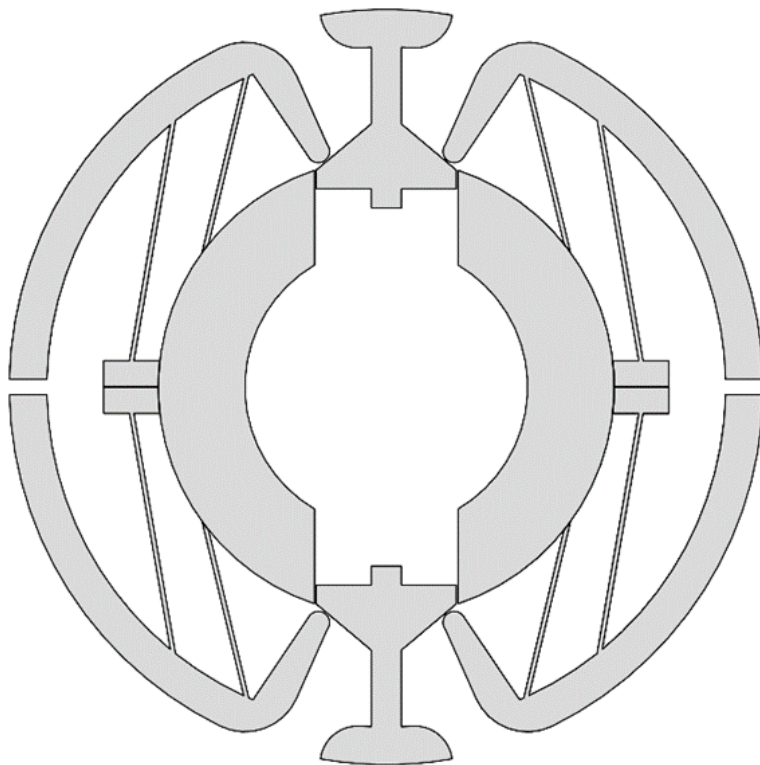
Figure 6.7 Concept 3 parallel jaw interface compliant mechanism portion

For this case study we will go ahead with Concept 3 which is based on intuition and has no notch or small flexures. It is relatively simpler and easier to analyse with the familiar remote centre concept. The cross flexures have a remote centre of rotation point about which Fin generates a moment and rotation (Figure 6.8). This rotation movement slides a cam onto a ramp which generates vertical motion. As Fin moves along the rim the X, and Y components of force vary, however by placing the remote point where moment arms create a resultant in the direction towards the slider, any radial force will cause correct moments. this is true given reaction forces at the other end are also satisfied. Consider replacing the 4-bar RCC linkage with a pin joint pseudo rigid body model. At the instance of gripper contact moments at the RCC point are:

$$F_x d_y + F_y d_x = Kw + Rcos(a)d_{rx} + Rsin(a)d_{ry} - \mu Rsin(a) + \mu Rcos(a) \qquad 6.1$$

We can only vary, K, a, dx, dy and the friction coefficientμ, R will depend on friction from the sliding surface and also the output load. From this analysis, it is clear that we should aim to reduce, M, R and friction coefficient. By reducing friction everywhere, we can reduce R and also the $\mu Rcos(a)$ which has more negative effects than $\mu Rsin(a)$ has a positive effect when a<45deg. We can also see that increasing dy and dx will magnify the effect of R and F which may have both a positive and negative effect. Alpha has a fairly neutral effect if we consider small friction values. However, alpha regulates displacement amplification at the output port. Thus, very low values will result in small displacement at the output port.

If this was a rigid mechanism, we could analytically solve this issue quite easily. However, the compliant mechanism is not exactly a pin joint. By decreasing M, the beam becomes very flexible and reduces the input force required to balance the system for the same output load reflected by R. This in turn means the ratio of forces between F and R which can become an issue, potentially causing buckling and lack of performance. On the other hand, increasing stiffness too much reduces output displacement for the same gripper load.
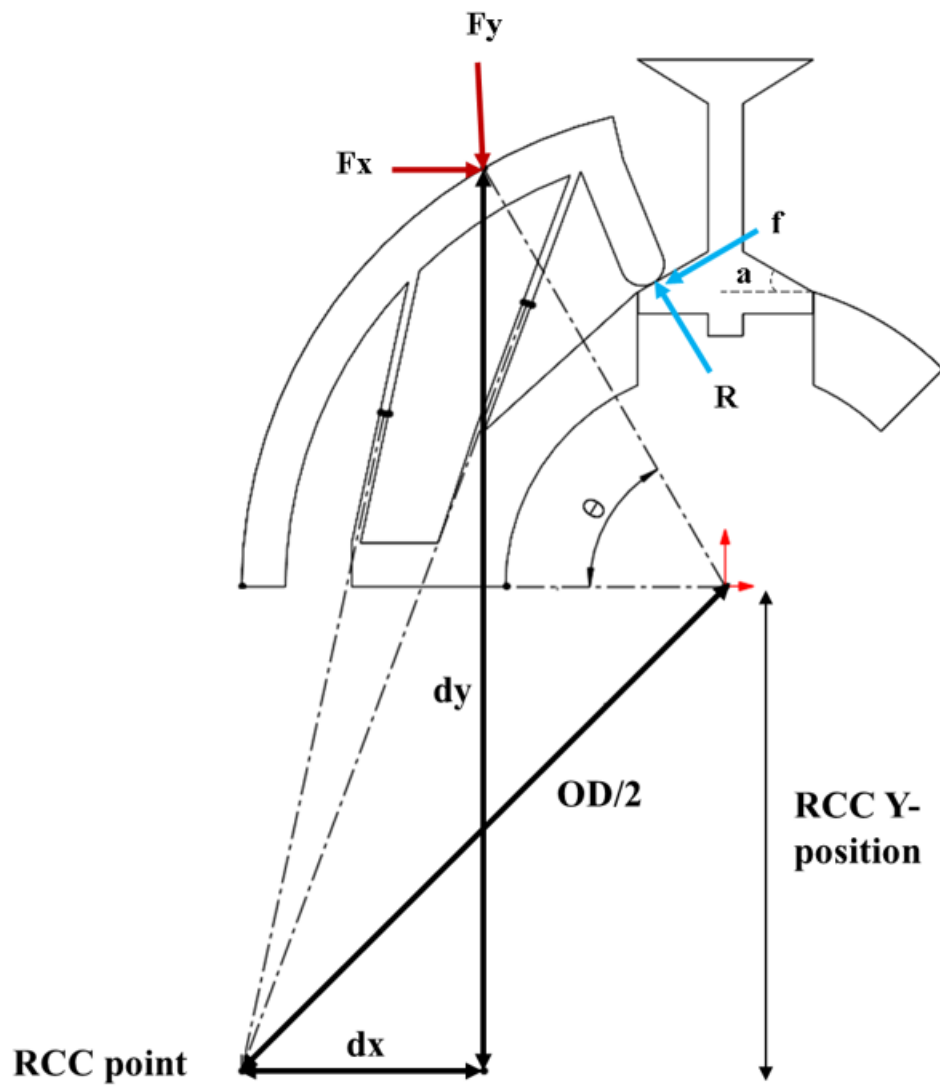
Figure 6.8 Quarter model and quantities of concept 2
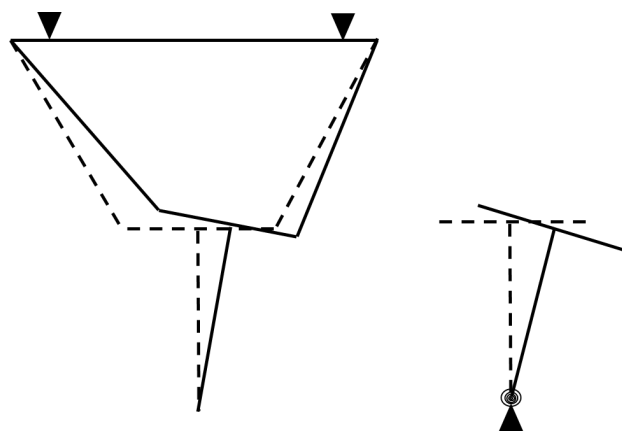
Figure 6.9 Pin-joint model of RCC linkage.

6.2.1 *Material and manufacture*

To reduce friction in contacting faces we can use rolling elements or polymer bearing strips. The latter is a better option considering the cost and assembly of roller bearings. Polymer bearings are lightweight simple with no moving components, it's a self-lubricating material with typical friction coefficients below 0.1. They are very useful for contact-aided compliant mechanisms such as our design here. The idea behind this design makes it easily manufacturable, hence the planar nature which facilitates extruding or EDM with a single material. We have already discussed suitable material for compliant mechanism design, the same applies here. Since we only have access to PLA material for prototyping that is the material selected for this study (E=3Gpa, v=0.33).

6.3 Modelling

Only a portion of the entire design is required for modelling purposes since other portions behave in the same fashion. In this case study we will directly use LS_Dyna Explicit FEA instead of PRBM since simulation run times are feasible (less than an hour per run) on a standard PC. As opposed to the PRBM method this approach also enables stress monitoring, critical for fatigue life estimates.
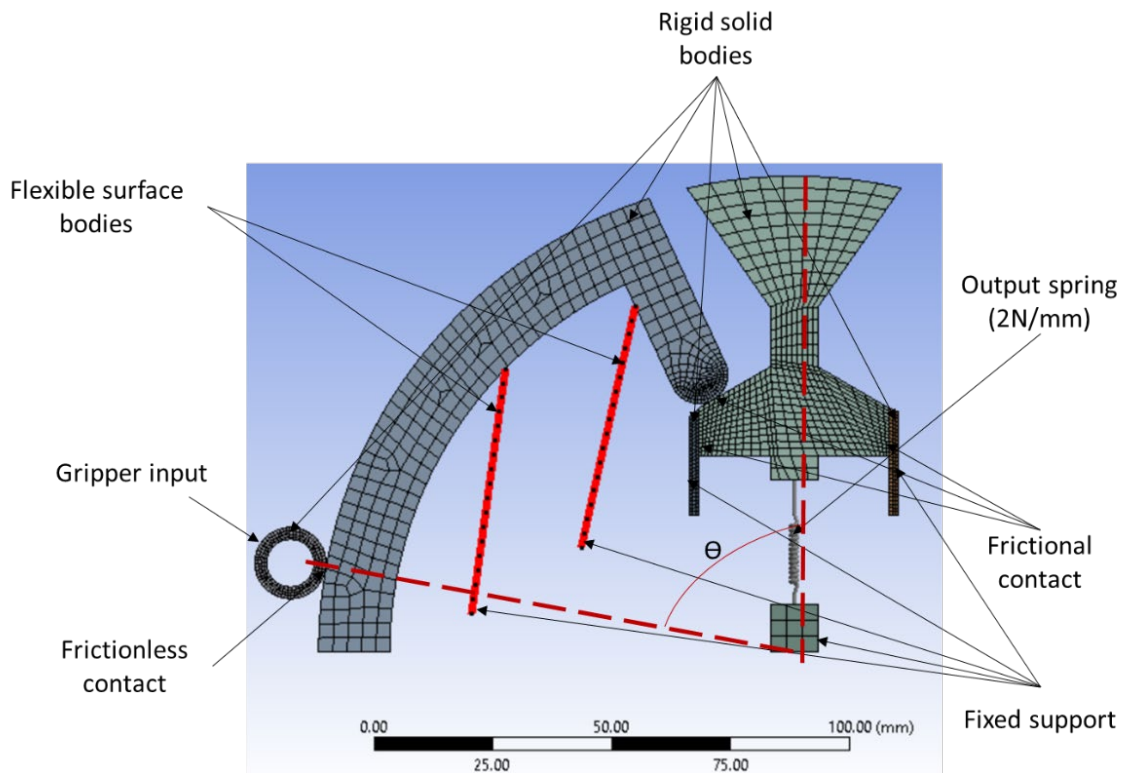
Figure 6.10 LsDyna model of the compliant interface mechanism

Input loads are described as displacement, a constant 7mm in the radial direction across 1 second (constant velocity) representing the parallel jaw of a gripper radially pressing on the rim. The friction coefficient is zero at the gripper contact, assuming roller bearings are incorporated. All other contacts have a constant friction of 0.05 (polymer-bearing material). To represent the stiffness of the dust cap buttons, a linear spring is fixed to the slider along the line of action. The stiffness of the spring is set to 2N/mm to match the return spring of the physical latch. The time step is 7.5×10^{-7}.

The output force is calculated from the displacement of the spring. All thick components have either been removed or replaced with rigid bodies this saves a very significant amount of time in explicit FEA. The flexing beams are modelled with QUAD_4 shell elements. From this simulation setup, we can obtain nodal and elemental stress, strain, reaction force/moment, displacement and more. Unfortunately, it wasn't possible to directly extract reaction forces from rigid bodies. Thus, to estimate the gripper input load, we perform some force translations. Since the friction coefficient is very low, we can reasonably neglect the vertical reaction forces at the side walls of the slider. Summing the vertical reaction force at the fixed end of the beams and the output spring, we have the total vertical reaction force. Knowing the radial input angle, we can estimate the gripper load as follows.

$$Gripper\ input\ force: \frac{total\ vertical\ reaction\ force}{\cos(\theta)} \qquad 6.2$$

Where θ is the radial misalignment angle measured from the vertical.

Since we have no physical test to verify the accuracy of the model, we pay special attention to energy conservation during the simulation. Figure 6.11 shows a typical reading from such a simulation. The energy error is less than 1% indicating sound results. This is monitored across all simulations and we ensure the error is below 5%.
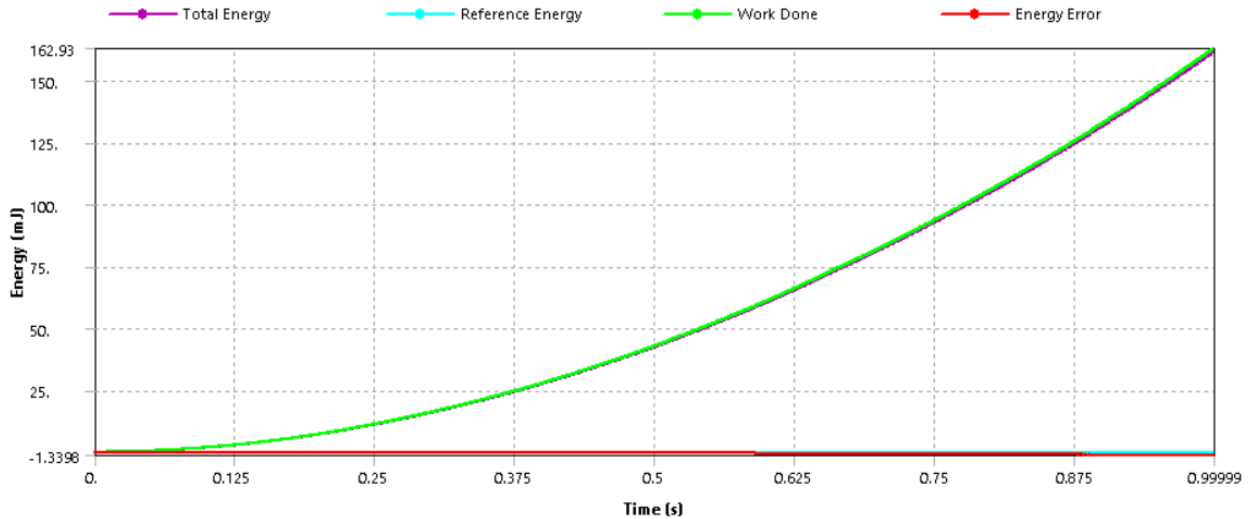
Figure 6.11 Energy conservation plot of a typical simulation with proposed set-up.

6.4 RED plan

Assuming the gripper uses a displacement-regulated drive we will set a constant input radial displacement of 7mm. The mechanism output port must provide sufficient displacement and load to open the latch. Since we have a spring connected at the output port which directly relates displacement to force, we use the output displacement as a performance measure. It is possible to use geometrical advantage as a performance measure but since the input displacement of the gripper is constant, we can directly use the output displacement for more practical results. In this case study we are also interested in maximum von misses stress and estimated maximum gripper force to ensure satisfactory fatigue life and gripper payload.

$$minimise: [-Do; \ max \ stressmax; \ gripper \ force] \qquad 6.3$$

Based on engineering intuition we may also consider a simipfing the above multiobjective optimisation by employing constraints of stress and output displacement. If these are not met we consider the design has failed, either by the latches not opening or material failure.

$$minimise: -Do \qquad 6.4$$
$$Subject \ to: max \ gripper \ force < 100N \ ; \ maxstress < 50MPa$$

Our initial testing has shown that when low beam thickness is used, we get low output displacement and buckling, which results in unreliable stress and force estimates from the regression model. Thus, we approach the RED plan with a slight twist. Here we will perform 2 sets of RED plans. First, we will use a low thickness range and only measure output displacement which will as shown in the results have very good prediction performance. Using this result, we will drive factor ranges to a more stable region of performance which minimises buckling and results in more accurate predictions of stress and force.

A Sphere packing (a type of space-filling design similar to LHS) response surface plan is used to satisfy 2x 18 runs to satisfy second-order models with 1st-order interactions. The design factors are chosen as per the previous analysis, the noise factor is the gripper jaw angle. To maintain the low number of runs (36 instead of 72) we will only use 3 factors for each set of RED plans. The downside of this approach is that we risk not seeing information about interactions between the design factors which are missing between each plan. In this arrangement, we will not see the interaction between the slider angle and RCC-Y position. Nonetheless, we can still make judgement based on their main effects and still guarantee design improvement.

Table 6.1 Response surface plan showing a range of variables for the gripper mechanism

	Experiment variable	Symbol	Range	Units
	Thickness	T	0.5-1.5	mm
Set 1	RCC Y position	Y	1-3	mm
	Angular misalignment	θ	25 to 80	deg
	Thickness	T	1.2-2.6	mm
Set 2	Slider angle	a	20-40	deg
	Angular misalignment	θ	25 to 80	deg

6.5 Results and discussion

Table 6.2 Two sets of response surface plans and results (using the plan for each set)

Set 1	T	Y	θ	Do (mm)	-	-	-
Set 2	T	a	θ	-	Do (mm)	Stress (Mpa)	Force (N)
1	-1.00	-0.99	1.00	0.57	5.30	35.00	68.12
2	-1.00	0.95	-1.00	6.87	10.98	22.61	46.34
3	0.32	-0.90	1.00	5.03	5.86	49.67	81.08
4	-0.97	1.00	0.43	1.28	8.04	33.35	41.91
5	0.17	1.00	0.97	5.45	8.68	50.24	106.30
6	1.00	0.94	0.16	6.49	9.10	50.93	78.96
7	0.95	0.14	1.00	6.65	7.26	57.23	98.22
8	0.89	1.00	-1.00	8.79	11.10	49.95	89.03
9	0.22	-1.00	-0.98	8.92	7.03	41.16	46.26
10	-1.00	-0.85	-1.00	7.23	7.28	24.55	24.86
11	-0.38	-1.00	0.01	4.16	5.88	34.56	27.13
12	-1.00	-0.02	-0.13	1.6	7.34	30.78	25.89
13	1.00	-0.15	-0.84	8.54	8.31	49.03	73.99
14	0.28	-0.05	0.07	6.99	7.36	42.00	48.60
15	-0.55	0.08	0.99	2.28	7.09	41.69	85.36
16	-0.06	1.00	-0.32	6.9	9.76	37.91	53.14
17	1.00	-1.00	0.00	8.68	5.93	47.41	63.51
18	-0.23	0.07	-1.00	8.83	9.01	34.52	44.28

6.5.1 Set 1 results.

Table 6.3 illustrates the coefficients and P-values for each term in the second-order model, which has R^2 =95.8%. This indicates good prediction performance which is also confirmed by looking at model residuals shown in Figure 6.12. From Table 6.3 and the mean effects plot in Figure 6.12, it is easy to notice that thickness is a highly effective design factor in terms of achieving large output displacement. On the contrary RCC y position (Y) is not. Also, the effect

of misalignment is significant along with its thickness interaction. This indicates at various misalignments various thicknesses can improve response. We also see the mean effect of thickness plateaus near the top of the range bound. Indicating further increase in thickness may not improve performance.

Table 6.3 Regression coefficient and P-values for set 1, $R^2 = 95.76\%$

Term	Coeff	P-value
Constant	5.606	0.000
T	2.440	0.000
Y	-0.138	0.598
θ	-2.206	0.000
T*T	-1.008	0.061
Y*Y	0.312	0.505
$\theta*\theta$	1.003	0.057
T*Y	-0.275	0.442
T*θ	1.139	0.013
Y*θ	0.081	0.819
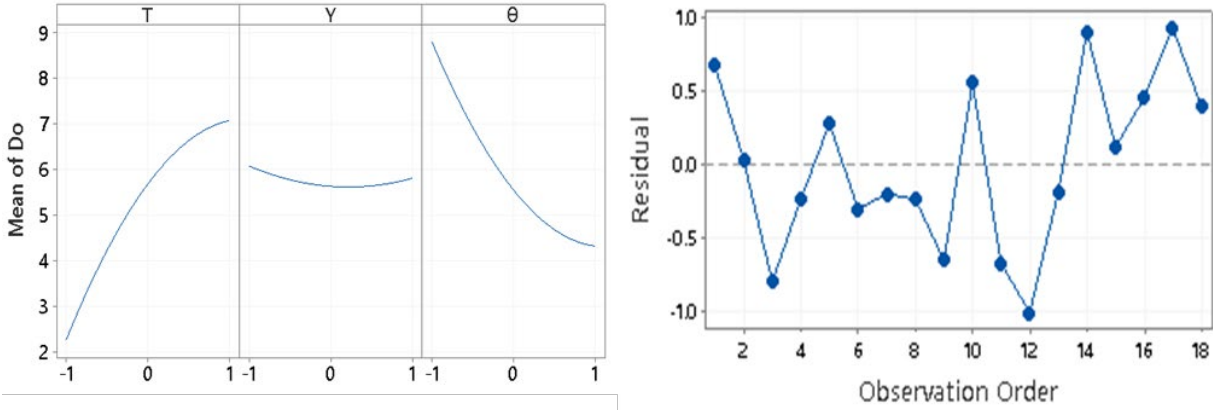
Figure 6.12 Mean effects of factors (left) and residues of the regression model (right)
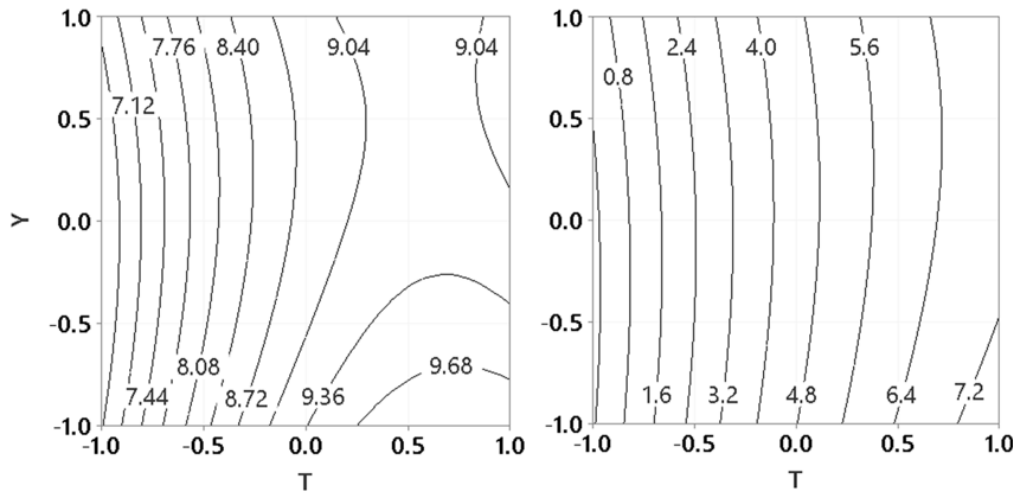
Figure 6.13 Contour plots of predicted Do Vs design factors at low (-1, left) and high (+1, right) noise conditions.

From the predicted contour plots of Figure 6.13, we see the effect of thickness improving response at both high and low noise conditions. With maximum output displacements at the largest misalignment angle (80 deg) around 7.2mm. This is a satisfactory performance since we need at least 6 mm displacement to open the dust cap latches. Figure 6.14 illustrates the overlayed contour plot of the mean response and its standard deviation across the range bound of the misalignment. Increasing thickness increases average performance across the misalignment range. Also reduces the standard deviation of performance indicating a more reliable and robust design.
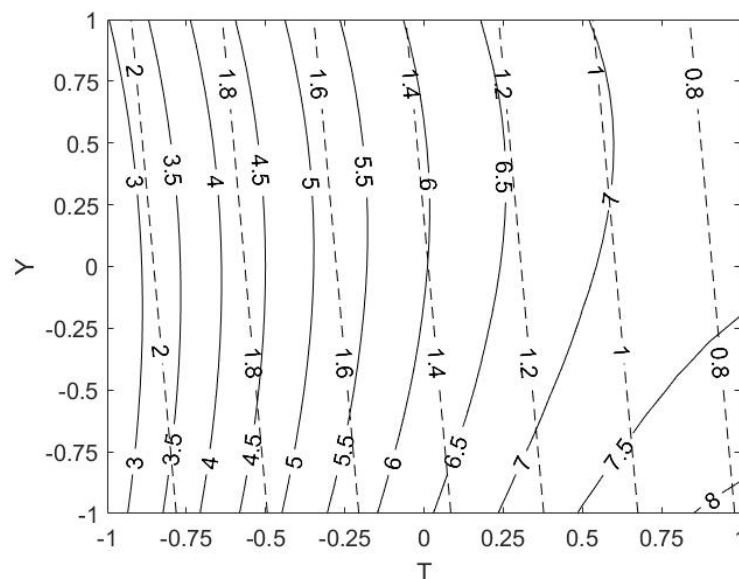
Figure 6.14 Overlaid contour plot of averaged performance and its standard deviation Vs design factor levels.

6.5.2 Set 2 results.

Here we have introduced slider angle as a design factor instead of RCC Y-position which seems to have little effect on performance. we also adjust the thickness range to further study the plateau effect near the top of the range bound. Stress and gripper load are also considered performance measures. The R^2 for Do, stress and force models are 99.5%, 98.6% and 96.9% respectively. We can confirm the prediction capability indicated by R^2 through regression model residuals of Figure 6.15.

Table 6.4 we can once again confirm the significance of thickness across all performance measures. This time around it has less effect on output displacement as apparent from the increased P-value and decreased mean effect (Figure 6.15). We have reached a turning point or optimal region which confirms the plateau hypothesis from set 1 result. Slider angle, a, is significant across output displacement and gripper load, it does not affect stress much. Its effect on output displacement is very large as shown in the mean effects plot. Increasing the slider angle increases gripper load requirements but it also increases the output displacement. Increasing thickness increases gripper load and stress thus we must consider the trade-off between the robustness of output displacement to maintain feasible stress and force limits, this is further discussed by an upcoming analysis.

Table 6.4 Regression model coefficients and P-values for all terms of the 3 responses

Term	Coef (Do)	Coef (Stress)	Coef (Force)	P-Value (Do)	P-Value (Stress)	P-Value (Force)
Constant	7.491	40.09	42.81	0.000	0.000	0.000
T	0.1752	10.822	19.66	0.014	0.000	0.000
a	1.6900	0.929	10.03	0.000	0.108	0.001
θ	-1.0140	4.893	16.84	0.000	0.000	0.000
T*T	-0.1747	-0.509	2.62	0.111	0.605	0.483
a*a	0.1053	-0.671	2.52	0.297	0.484	0.488
θ*θ	0.5359	2.865	26.73	0.001	0.015	0.000
T*a	0.0826	0.488	0.52	0.283	0.502	0.847
T*θ	0.1821	-1.729	-5.01	0.042	0.045	0.106
a*θ	-0.3472	1.066	-0.48	0.001	0.165	0.859
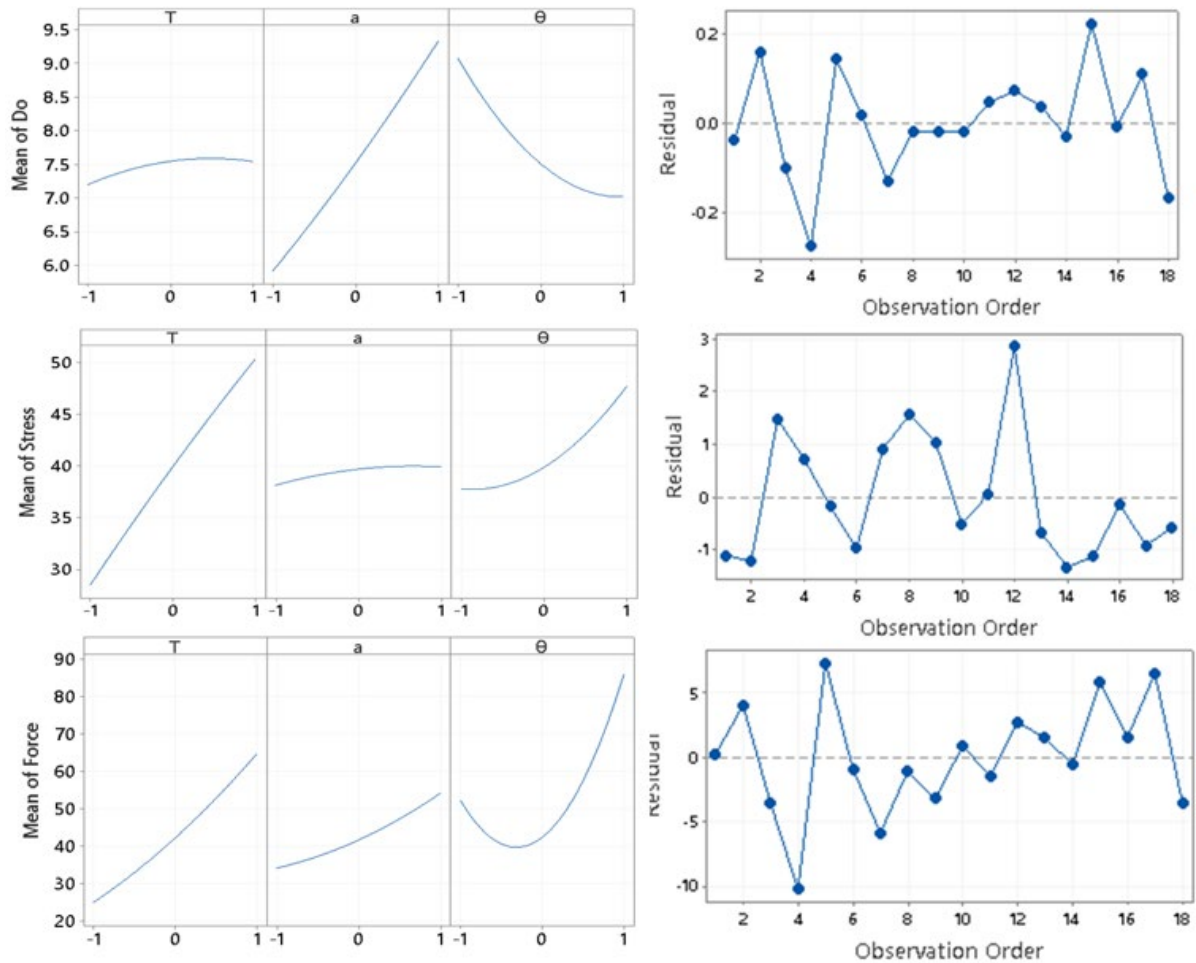
Figure 6.15 Mean effect of factors (left) and residuals of the regression models (right)

Using the results of Figure 6.16 we can identify a suitable design configuration which matches all performance measure requirements. Figure 6.16 A-C shows the averaged performance measure and performance standard deviation across misalignments for all 3 responses. Considerable variation in standard deviation is observed across all performance measures. Also, we can see that increasing the slider angle a, does not affect stress much, but it does increase output displacement and gripper force. Increasing beam thickness increases both stresses and griper load. Figure 6.16 D is the overlayed contour plot of all 3 averaged (across misalignments range) performance measures. We can make a judgment on where we would like the design to operate. Visually [a=1, T=-0.75] seem like desirable points. At this point:

$minimum\ output\ displacement = 9.1 - 3 * 0.91 = 6.37mm$

$maximum\ \max stress = 33 + 3 * 4.6 = 46.8\ Mpa$

$maximum\ \max\ gripper\ force = 50 + 3 * 15.5 = 95\ N$

Multi-objective, genetic algorithm optimisation (see code in Appendix A4) produces virtually similar results [6.1275   44.1770   95.5973] at [a=1, T=-1], when asked to minimise stress and force while maximising displacement.
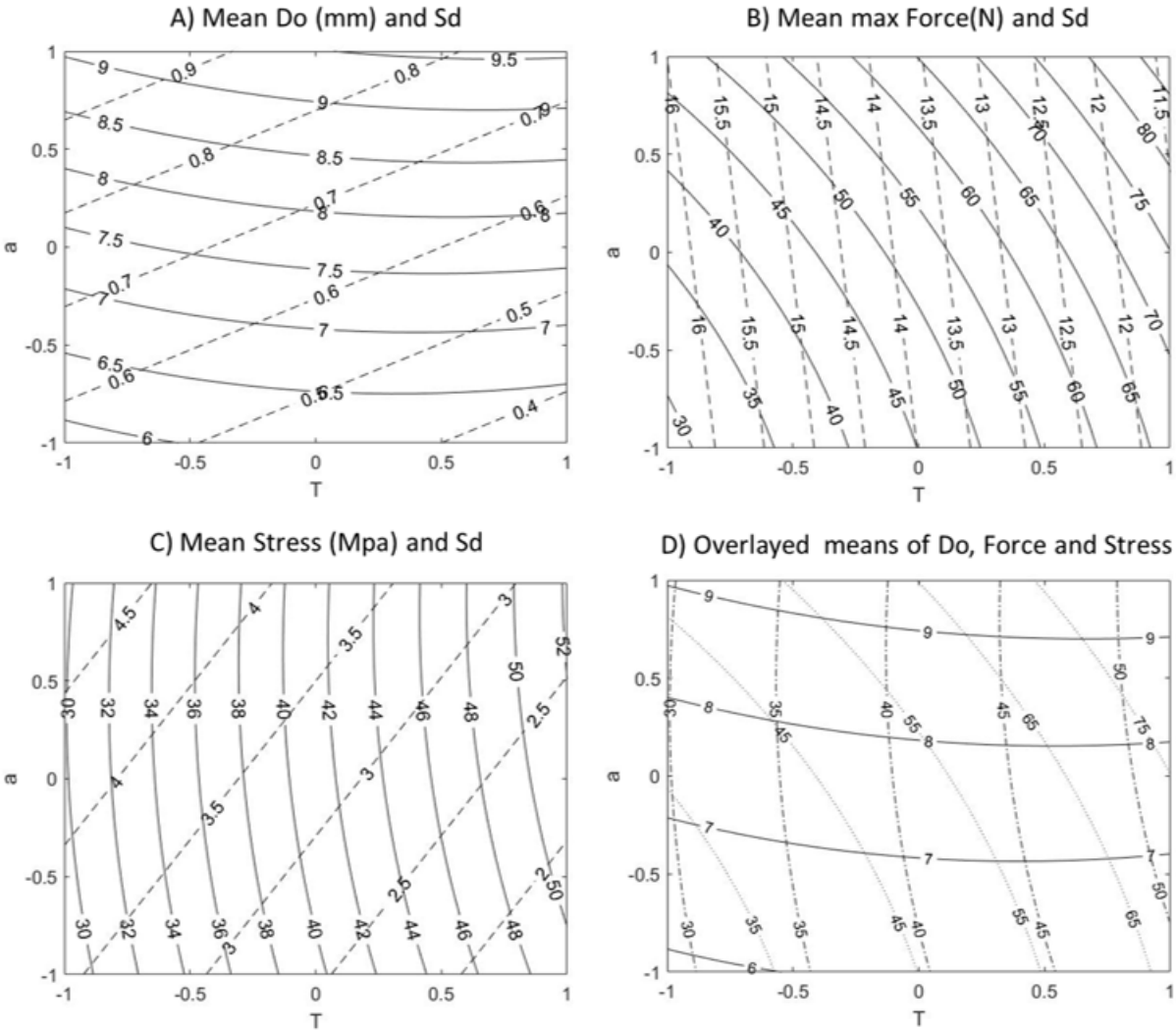
Figure 6.16 Contour plots of averaged performance and performance standard deviation across the misalignment range vs factor levels. For A, B and C, average response (-), Sd (--). For D, Do(-), stress(-.) force (.)

6.6 Summary

In this chapter, we applied the proposed methodology and modelling approach for another class of passive compliance problems faced in fluid servicing. To this end, we demonstrated how to design and evaluate a completely novel type of passive compliance mechanism to enable the manipulation of train fluid port dust caps. This design will find many applications where a standard parallel jaw gripper manipulates an external workpiece whose pose is unknown. For example operating locking latches, without knowing where they exactly are on the workpiece, for removal and replacement of parts in autonomous servicing. The overlayed contour plots of Figure 6.16 provide direct parametric design insight considering practical aspects such as larger deformations and stress. This is certainly one of the unique outputs of the proposed robust design approach, not found in the literature of passive compliance design.

For the case study we used a two-step response surface approach to first drive factor ranges to a near-optimal region, and then to configure the design around that region. In this approach, we did not see the interactions between some design factors. However, we identified that one of these factors (RCC-Y position) does not have a significant effect on output displacement. Hence the removal of that parameter in the second set of analyses was justified. Regardless, we have successfully reached all set goals of this study. We found a range of beam thickness and slider angle which improve output displacement and reduce its variation due to uncertain gripper contact zone. We then explored the design space to identify the most suitable design configuration which satisfies reasonable gripper force and stress in the compliant mechanisms.

The chosen design configuration requires a gripper force of just under 95 N to produce up to 18 N with an output stroke of up to 9.1 mm. This is a good range of performance for a compliant mechanism. We also met the stress constraints of the PLA material. However, in the real application, more heavy-duty material possibly with a higher strength-to-flexibility ratio than PLA. The results obtained directly apply to a 2-inch cam and grove dust cap.

7. FINAL CONCLUSIONS AND FUTURE WORK

7.1 Key remarks

In this work, we demonstrated how passive compliance design can be translated and solved by Robust Engineering Design (RED) methods. A general design methodology was developed and demonstrated in various case studies. We revealed the limitations of existing CyberFluids end-effectors and developed new compliance devices to solve these problems. Using several simulations, we were able to produce new designs more capable of larger misalignments with forces multiple times less than arbitrary compliance devices, or those found in the existing literature (or elsewhere). Furthermore, we conducted parametric analyses and illustrated charts that show end-effector performance vs design characteristics for various operational requirements; these can be used as guidelines in future work.

The proposed methodology considers many practical aspects of design that are overlooked by existing approaches that have more of a focus on modelling than design. These include considerations of design requirements such as material fatigue by stresses which is a critical yet highly overlooked aspect. Furthermore, our approach is distinguished by its generality to account for large deformations of compliant mechanisms and any shape or geometry of interacting components. To this end, we conclude that all aims of the thesis have been achieved, more detailed conclusions, recommendations and future work are discussed in the following.

In a series of physical evaluations, we found that the existing CyberFluids end-effectors result in a large force (around 600N) for little misalignments (5mm). These tests were conducted while the end effector was mounted on the robot. The robot itself has unaccountable compliance (difficult-to-measure mechanical play), if we had considered a rigid robot the forces may have been even higher. This led to the study of Chapter 5 where a new end effector solution with much better force (150N) and misalignment capability (15mm and 5deg) was developed. Here we used the proposed models for performance evaluations, and the robot was considered rigid in both numerical and physical experiments. The performance of the new end effector is many

times better than the existing solution, we demonstrated that in Chapter 5. In Chapter 6 we tackled a completely different problem showing that the proposed approach applies to various robust compliant mechanism problems. This novel design can remove all roll angle misalignment with a gripper payload of 95N. Even though we did meet the stress constraints of the prototype, better material selection is recommended for practical applications.

7.2 Limitations and future work

Chapters 5 and 6 results are based on the proposed modelling approaches, which show good agreement with physical results, they are certainly capable of representing the physical phenomena. However, there are some inaccuracies. We do see error consistency at around 5% for PRBM and 18% for explicit FEA models. In physical experiments there are many imperfections which are hard to control, these include measurements, for example in terms of parallelism, unaccounted or unmeasurable compliances, force sensor error, and variations in friction surfaces. Also, simulations may produce more accurate results by reducing relevant time steps or mesh size. However, this will increase simulation time which is not desirable given that a series of simulations are required to facilitate the proposed methodology. The model inaccuracies are tolerable for our applications as they can easily be offset, for example by upsizing robot actuators in accordance. If necessary, future work on model performance may incorporate precision engineering equipment for physical testing and improvements to models.

A limitation of the RED approach is being able to estimate design factor ranges appropriately. Initial preliminary analysis PRBM (analytical) was found significantly useful as we rapidly identified a suitable range of factors. Then, using a small number of runs with the Taguchi design we significantly improved design robustness and performance. However, when more freely decided on ranges in the response surface approach in Chapter 5, even though results showed zones of improved performance, we did not get substantial results confirming the optimality in terms of performance and robustness. In Chapter 6 we used a different approach with two scaled-down response surfaces, one to drive factor ranges to the optimal region and another to explore that region. This yielded better results since we were able to confirm the optimality as we saw improvement, continued by a plateauing of performance. In general, there are different approaches to enhancing the response surface methods, and perhaps this could have been given more attention. To this end, future work should consider more sequential

approaches to response surface methodology. Another example of such an approach includes the steepest ascent method.

One more aspect which we didn't cover, is the quantitative comparison of design concepts, other designs could have resulted in better performance. This could be a subject for future work. Topology optimisation, FEA and PRBM modelling will contribute to this alongside the development of new designs. We did a very in-depth analysis of topology optimisation in the literature section of this work, only to conclude that the state-of-the-art is not capable of incorporating large load position uncertainty (large misalignment). However, our critical review provides a very good base and opportunity for future work to investigate research contributions in this field.

7.3 Final suggestions

Overall, the rail industry will benefit significantly by incorporating compliant end-effectors in the future design of trains and autonomous systems for maintenance. We have shown how to reduce robot payload and precision requirements which will be much more desirable in economical solutions for mass-scale applications. The end-effector designs can be sized for real applications inside the maintenance depot. However, there are some limitations:

- Commercialisation or appropriate practical implementations of the proposed designs will require further work in terms of materials, manufacturing and developing necessary robot parts such as end-effector/gripper coupling interfaces and RCC-capable grippers. We have discussed this in some detail in chapter 6.

- As we observed by looking at rail classes 168 and 165, not all fluid ports are easily accessible by a 3 DoF cartesian robot (a more economical system). This requires robots with more degrees of freedom, capable of articulation around difficult spots. For example, the engine oil port is underneath the carriage angled at 45 degrees to the vertical. The sand port (sand can behave as fluid during dispensing) is not a coupler but a window where sand is shovelled in. We recommend that sand ports are also switched to the cam and grove couplers. Generally, adapters will be required for existing trains.

Encouraging train manufacturers to incorporate very small design changes in future fleets will reduce maintenance and robot costs. In terms of servicing fluids, this translates to standardised fluid ports which we assumed to be the cam and groove coupling. This is the standard CET port on most if not all modern British rail class. Other recommendations include easily accessible fluid ports and asymmetric interfaces for removable/replacement parts eg, dust caps (or maybe brake pads and show gear), which only latch in particular orientations. Furthermore, we recommend train manufacturers to incorporate compliant devices on replaceable parts for easy unlatching with standard parallel jaw grippers. The mechanism developed in Chapter 6 is a non-costly example of such a device.

The industry should also consider higher-level system design aspects. These may include using the same robot for other tasks, creating flexible robot working stations, and incorporating better condition monitoring with robotic inspections. The final robot design may also change the end-effector requirements. For example, if the robot performs various tasks then the end-effector should be interchangeable in operation. Hence a suitable mechanical interface must be incorporated on the robot side and the end-effector side. Many ideas come to mind for various applications and performance aspects, but these are beyond the scope of this academic endeavour.

REFERENCES

Akpınar, B., 2021. Performance of Different SLAM Algorithms for Indoor and Outdoor Mapping Applications. ASI 4, 101. https://doi.org/10.3390/asi4040101

Alonso, C., Ansola, R., Querin, O.M., 2014. Topology synthesis of Multi-Input–Multi-Output compliant mechanisms. Advances in Engineering Software 76, 125–132. https://doi.org/10.1016/j.advengsoft.2014.05.008

Arvidsson, M., Gremyr, I., 2008. Principles of robust design methodology. Qual. Reliab. Engng. Int. 24, 23–35. https://doi.org/10.1002/qre.864

Asada, H., Kakumoto, Y., 1988. The dynamic RCC hand for high-speed assembly, in: Proceedings. 1988 IEEE International Conference on Robotics and Automation. Presented at the Proceedings. 1988 IEEE International Conference on Robotics and Automation, IEEE Comput. Soc. Press, Philadelphia, PA, USA, pp. 120–125. https://doi.org/10.1109/ROBOT.1988.12035

Atherton, M., Hill, S., Harrison, D., Ajovalasit, M., 2020. Economic and technical feasibility of a robotic autonomous system for train fluid servicing. Proceedings of the Institution of Mechanical Engineers, Part F: Journal of Rail and Rapid Transit 234, 338–350. https://doi.org/10.1177/0954409719830520

Atherton, M.A., Bates, R.A., 2004. Robust optimization of cardiovascular stents: a comparison of methods. Engineering Optimization 36, 207–217. https://doi.org/10.1080/03052150310001639290

Awtar, S., Ustick, J., Sen, S., 2013. An XYZ Parallel-Kinematic Flexure Mechanism With Geometrically Decoupled Degrees of Freedom. Journal of Mechanisms and Robotics 5, 015001. https://doi.org/10.1115/1.4007768

Bendsøe, M.P., Kikuchi, N., 1988. Generating optimal topologies in structural design using a homogenization method. Computer Methods in Applied Mechanics and Engineering 71, 197–224. https://doi.org/10.1016/0045-7825(88)90086-2

Bendsøe, M.P., Sigmund, O., 2004. Topology Optimization. Springer Berlin Heidelberg, Berlin, Heidelberg. https://doi.org/10.1007/978-3-662-05086-6

Bruns, T.E., Tortorelli, D.A., 2001. Topology optimization of non-linear elastic structures and compliant mechanisms. Computer Methods in Applied Mechanics and Engineering 190, 3443–3459. https://doi.org/10.1016/S0045-7825(00)00278-4

Cannon, B.R., Lillian, T.D., Magleby, S.P., Howell, L.L., Linford, M.R., 2005. A compliant end-effector for microscribing. Precision Engineering 29, 86–94. https://doi.org/10.1016/j.precisioneng.2004.05.006

Cao, L., Dolovich, A., Zhang, W.J., 2013. On understanding of design problem formulation for compliant mechanisms through topology optimization. Mech. Sci. 4, 357–369. https://doi.org/10.5194/ms-4-357-2013

Cao, L., Dolovich, A.T., Zhang, W. (Chris), 2015. Hybrid Compliant Mechanism Design Using a Mixed Mesh of Flexure Hinge Elements and Beam Elements Through Topology Optimization. Journal of Mechanical Design 137, 092303. https://doi.org/10.1115/1.4030990

Chen, G., Xiong, B., Huang, X., 2011. Finding the optimal characteristic parameters for 3R pseudo-rigid-body model using an improved particle swarm optimizer. Precision Engineering 35, 505–511. https://doi.org/10.1016/j.precisioneng.2011.02.006

Collins, M.W., Atherton, M.A., Bryant, J.A., 2004. Nature and Design. WIT Press.

Daniel E. Whitney, 2004. Mechanical Assemblies Their Design, Manufacture, and Role in Product Development. OXFORD UNIVERSITY PRESS.

De Cubber, G., Berrabah, S.A., Sahli, H., 2004. Color-based visual servoing under varying illumination conditions. Robotics and Autonomous Systems 47, 225–249. https://doi.org/10.1016/j.robot.2004.03.015

De Leon, D.M., Alexandersen, J., O. Fonseca, J.S., Sigmund, O., 2015. Stress-constrained topology optimization for compliant mechanism design. Struct Multidisc Optim 52, 929–943. https://doi.org/10.1007/s00158-015-1279-z

Deepak, S.R., Dinesh, M., Sahu, D.K., Ananthasuresh, G.K., 2009. A Comparative Study of the Formulations and Benchmark Problems for the Topology Optimization of Compliant Mechanisms. Journal of Mechanisms and Robotics 1, 011003. https://doi.org/10.1115/1.2959094

Delrobaei, M., McIsaac, K.A., 2008. Docking joint for autonomous self-assembly, in: 2008 Canadian Conference on Electrical and Computer Engineering. Presented at the 2008 Canadian Conference on Electrical and Computer Engineering - CCECE, IEEE, Niagara Falls, ON, Canada, pp. 001025–001030. https://doi.org/10.1109/CCECE.2008.4564692

Duckworth, J., 2023. Passenger rail usage.

Dunning, P.D., Kim, H.A., Mullineux, G., 2011. Introducing Loading Uncertainty in Topology Optimization. AIAA Journal 49, 760–768. https://doi.org/10.2514/1.J050670

Eshraghi, K., Jiang, P., Suraci, D., Atherton, M., 2020a. Preliminary Study of End-Effector Compliance for Reducing Insertion Force in Automated Fluid Coupling for Trains. JID 24, 139–161. https://doi.org/10.3233/JID200017

Eshraghi, K., Jiang, P., Suraci, D., Atherton, M., 2020b. PRELIMINARY STUDY ON END-EFFECTOR COMPLIANCE IN AUTOMATED FLUID COUPLING FOR TRAINS.

Estrada, G., Riba, C., Lloveras, J., n.d. AN APPROACH TO AVOID QUALITY ASSEMBLY ISSUES SINCE PRODUCT DESIGN STAGE.

Feng, F., Tang, L., Xu, J., Liu, H., Liu, Y., 2016. A review of the end-effector of large space manipulator with capabilities of misalignment tolerance and soft capture. Sci. China Technol. Sci. 59, 1621–1638. https://doi.org/10.1007/s11431-016-0084-7

Flores-Abad, A., Ma, O., Pham, K., Ulrich, S., 2014. A review of space robotics technologies for on-orbit servicing. Progress in Aerospace Sciences 68, 1–26. https://doi.org/10.1016/j.paerosci.2014.03.002

Frecker, M.I., Ananthasuresh, G.K., Nishiwaki, S., Kikuchi, N., Kota, S., 1997. Topological Synthesis of Compliant Mechanisms Using Multi-Criteria Optimization. Journal of Mechanical Design 119, 238–245. https://doi.org/10.1115/1.2826242

Haskiya, W., Maycock, K., Knight, J.A.G., 1998. A passive compliant wrist for chamferless peg-in-hole assembly operation from vertical and horizontal directions. Proceedings of the Institution of Mechanical Engineers, Part B: Journal of Engineering Manufacture 212, 473–478. https://doi.org/10.1243/0954405981515770

Havlík, Š., 1983. A new elastic structure for a compliant robot wrist. Robotica 1, 95–102. https://doi.org/10.1017/S0263574700001235

Hill, S.A., Atherton, M., Ajovalasit, M., Harrison, D., 2017. Robust automated servicing of passenger trains- fluids.

Hopkins, J.B., Culpepper, M.L., 2011. Synthesis of precision serial flexure systems using freedom and constraint topologies (FACT). Precision Engineering 35, 638–649. https://doi.org/10.1016/j.precisioneng.2011.04.006

Howell, 2001. Compliant mechanisms. Wiley.

Howell, Olsen, Spencer P. Magleby, 2013. Handbook of Compliant Mechanisms. Wiley.

Jiang, J., Bian, C., Ke, Y., 2017. A new method for automatic shaft-hole assembly of aircraft components. AA 37, 64–70. https://doi.org/10.1108/AA-04-2016-032

Kamnik, R., Rodič, G., Mihelj, M., Bajd, T., 2001. Automation of the car battery lid assembly operation. Robotics and Computer-Integrated Manufacturing 17, 435–446. https://doi.org/10.1016/S0736-5845(01)00017-5

Kogiso, N., Ahn, W., Nishiwaki, S., Izui, K., Yoshimura, M., 2008. Robust Topology Optimization for Compliant Mechanisms Considering Uncertainty of Applied Loads. JAMDSM 2, 96–107. https://doi.org/10.1299/jamdsm.2.96

Lobontiu, N., Paine, J.S.N., Garcia, E., Goldfarb, M., 2001. Corner-Filleted Flexure Hinges. Journal of Mechanical Design 123, 346–352. https://doi.org/10.1115/1.1372190

Lyon, S.M., Howell, L.L., 2002. A Simplified Pseudo-Rigid-Body Model for Fixed-Fixed Flexible Segments, in: Volume 5: 27th Biennial Mechanisms and Robotics Conference. Presented at the ASME 2002 International Design Engineering Technical Conferences and Computers and Information in Engineering Conference, American Society of Mechanical Engineers, Montreal, Quebec, Canada, pp. 23–33. https://doi.org/10.1115/DETC2002/MECH-34203

Martin, D., 2007. A Practical Guide to Machine Vision Lighting. Adv Illum2007.

M.Atherton, 2020. Design Lecture notes.

McCallion, H., Johnson, G.R., Pham, D.T., 1979. A compliant device for inserting a peg in a hole. Industrial Robot: An International Journal 6, 81–87. https://doi.org/10.1108/eb004754

Midha, A., Bapat, S.G., Mavanthoor, A., Chinta, V., 2015. Analysis of a Fixed-Guided Compliant Beam With an Inflection Point Using the Pseudo-Rigid-Body Model Concept. Journal of Mechanisms and Robotics 7, 031007. https://doi.org/10.1115/1.4028131

Montgomery, 2012. Design and Analysis of Experiments, *th student version. ed. Wiley.

Moura, J., Mccoll, W., Taykaldiranian, G., Tomiyama, T., Erden, M.S., 2018. Automation of Train Cab Front Cleaning With a Robot Manipulator. IEEE Robot. Autom. Lett. 3, 3058–3065. https://doi.org/10.1109/LRA.2018.2849591

Munk, D.J., Vio, G.A., Steven, G.P., 2015. Topology and shape optimization methods using evolutionary algorithms: a review. Struct Multidisc Optim 52, 613–631. https://doi.org/10.1007/s00158-015-1261-9

Myers, R., Montgomery, D., Anderson-cook, C., 2016. Response surface methodology, 4th ed, Probability and statistics. Wiley.

Parrott, C., Dodd, T.J., Gross, R., 2014. HiGen: A high-speed genderless mechanical connection mechanism with single-sided disconnect for self-reconfigurable modular

robots, in: 2014 IEEE/RSJ International Conference on Intelligent Robots and Systems. Presented at the 2014 IEEE/RSJ International Conference on Intelligent Robots and Systems (IROS 2014), IEEE, Chicago, IL, USA, pp. 3926–3932. https://doi.org/10.1109/IROS.2014.6943114

Parvari Rad, F., Vertechy, R., Berselli, G., Parenti-Castelli, V., 2018. Design and Stiffness Evaluation of a Compliant Joint with Parallel Architecture Realizing an Approximately Spherical Motion. Actuators 7, 20. https://doi.org/10.3390/act7020020

Pedersen, C.B.W., Buhl, T., Sigmund, O., 2001. Topology synthesis of large-displacement compliant mechanisms. Int. J. Numer. Meth. Engng. 50, 2683–2705. https://doi.org/10.1002/nme.148

Pitchandi, N., Subramanian, S.P., Irulappan, M., 2017. Insertion force analysis of compliantly supported peg-in-hole assembly. AA 37, 285–295. https://doi.org/10.1108/AA-12-2016-167

Rahman, T., Ramanathan, R., Seliktar, R., Harwin, W., 1995. A Simple Technique to Passively Gravity-Balance Articulated Mechanisms. Journal of Mechanical Design 117, 655–658. https://doi.org/10.1115/1.2826738

Rail delivery group, 2018. Long Term Passenger Rolling Stock Strategy for the Rail Industry.

Robla-Gomez, S., Becerra, V.M., Llata, J.R., Gonzalez-Sarabia, E., Torre-Ferrero, C., Perez-Oria, J., 2017. Working Together: A Review on Safe Human-Robot Collaboration in Industrial Environments. IEEE Access 5, 26754–26773. https://doi.org/10.1109/ACCESS.2017.2773127

Rommers, J., van der Wijk, V., Herder, J.L., 2021. A new type of spherical flexure joint based on tetrahedron elements. Precision Engineering 71, 130–140. https://doi.org/10.1016/j.precisioneng.2021.03.002

Saab, W., Ben-Tzvi, P., 2016. AGenderless Coupling Mechanism With Six-Degrees-of-Freedom Misalignment Capability for ModularSelf-Reconfigurable Robots. Journal of Mechanisms and Robotics 8, 061014. https://doi.org/10.1115/1.4034014

Saab, W., Racioppo, P., Ben-Tzvi, P., 2019. A review of coupling mechanism designs for modular reconfigurable robots. Robotica 37, 378–403. https://doi.org/10.1017/S0263574718001066

Sathirakul, K., Sturges, R.H., 1998. Jamming conditions for multiple peg-in-hole assemblies. Robotica 16, 329–345. https://doi.org/10.1017/S0263574798000393

Shariatee, M., Akbarzadeh, A., Mousavi, A., Alimardani, S., 2014. Design of an economical SCARA robot for industrial applications, in: 2014 Second RSI/ISM International

Conference on Robotics and Mechatronics (ICRoM). Presented at the 2014 Second RSI/ISM International Conference on Robotics and Mechatronics (ICRoM), IEEE, Tehran, Iran, pp. 534–539. https://doi.org/10.1109/ICRoM.2014.6990957

Sigmund, O., 1997. On the Design of Compliant Mechanisms Using Topology Optimization*. Mechanics of Structures and Machines 25, 493–524. https://doi.org/10.1080/08905459708945415

Sigmund, O., Maute, K., 2013. Topology optimization approaches: A comparative review. Struct Multidisc Optim 48, 1031–1055. https://doi.org/10.1007/s00158-013-0978-6

Southern, W.R., Lyons, C.G., 2002. The study of a passive accommodation device in robotic insertion processes. Journal of Materials Processing Technology 124, 261–266. https://doi.org/10.1016/S0924-0136(01)01131-1

Sturges, R.H., Laowattana, S., 1996. Design of an Orthogonal Compliance for Polygonal Peg Insertion. Journal of Mechanical Design 118, 106–114. https://doi.org/10.1115/1.2826840

Su, H.-J., 2009. A Pseudorigid-Body 3R Model for Determining Large Deflection of Cantilever Beams Subject to Tip Loads. Journal of Mechanisms and Robotics 1, 021008. https://doi.org/10.1115/1.3046148

Thomas, P.R., Bhandari, U., Bullock, S., Richardson, T.S., du Bois, J.L., 2014. Advances in air to air refuelling. Progress in Aerospace Sciences 71, 14–35. https://doi.org/10.1016/j.paerosci.2014.07.001

Tomiyama, T., García, L.R., Kršlin, A., Taykaldiranian, G., 2017. Systems and Conceptual Design of a Train Cab Front Cleaning Robot. Procedia CIRP 59, 61–66. https://doi.org/10.1016/j.procir.2016.09.031

Trease, B.P., Moon, Y.-M., Kota, S., 2005. Design of Large-Displacement Compliant Joints. Journal of Mechanical Design 127, 788–798. https://doi.org/10.1115/1.1900149

Ulrich, Eppinger, 2015. Product design and devolopment, 6th ed. McGraw Hill.

Usubamatov, R., Leong, K.W., 2011. Analyses of peg-hole jamming in automatic assembly machines. Assembly Automation 31, 358–362. https://doi.org/10.1108/01445151111172943

Wang, D., Gao, W., 2019. Robust topology optimization under load position uncertainty. Int J Numer Methods Eng 120, 1249–1272. https://doi.org/10.1002/nme.6180

Wang, Loh, Gu, 1998. Passive compliance versus active compliance in robotbased automated assembly systems. Industrial Robot MCB University Press · ISSN 0143-991X.

Whitney, D.E., 1982. Quasi-Static Assembly of Compliantly Supported Rigid Parts. Journal of Dynamic Systems, Measurement, and Control 104, 65–77. https://doi.org/10.1115/1.3149634

Whitney, D.E., Rourke, J.M., 1986. Mechanical Behavior and Design Equations for Elastomer Shear Pad Remote Center Compliances. Journal of Dynamic Systems, Measurement, and Control 108, 223–232. https://doi.org/10.1115/1.3143771

Wu, J., Gao, J., Luo, Z., Brown, T., 2016. Robust topology optimization for structures under interval uncertainty. Advances in Engineering Software 99, 36–48. https://doi.org/10.1016/j.advengsoft.2016.05.002

Xia, Y., Yin, Y., Chen, Z., 2006. Dynamic analysis for peg-in-hole assembly with contact deformation. Int J Adv Manuf Technol 30, 118–128. https://doi.org/10.1007/s00170-005-0047-4

Xu, J., Hou, Z., Liu, Z., Qiao, H., 2019. Compare Contact Model-based Control and Contact Model-free Learning: A Survey of Robotic Peg-in-hole Assembly Strategies.

Xu, P., Jingjun, Y., Guanghua, Z., Shusheng, B., 2008. The Stiffness Model of Leaf-Type Isosceles-Trapezoidal Flexural Pivots. Journal of Mechanical Design 130, 082303. https://doi.org/10.1115/1.2936902

Yan, X.-T., Brinkmann, W., Palazzetti, R., Melville, C., Li, Y., Bartsch, S., Kirchner, F., 2018. Integrated Mechanical, Thermal, Data, and Power Transfer Interfaces for Future Space Robotics. Front. Robot. AI 5, 64. https://doi.org/10.3389/frobt.2018.00064

Yin, L., Ananthasuresh, G.K., 2003. Design of Distributed Compliant Mechanisms. Mechanics Based Design of Structures and Machines 31, 151–179. https://doi.org/10.1081/SME-120020289

Zhu, B., Zhang, X., Fatikow, S., 2014. A multi-objective method of hinge-free compliant mechanism optimization. Struct Multidisc Optim 49, 431–440. https://doi.org/10.1007/s00158-013-1003-9

Zohoor, H., Shahinpoor, M., n.d. Dynamic Analysis of Peg-In-Hole Insertion for Manufacturing Automation 10.

Zong, G., Pei, X., Yu, J., Bi, S., 2008. Classification and type synthesis of 1-DOF remote center of motion mechanisms. Mechanism and Machine Theory 43, 1585–1595. https://doi.org/10.1016/j.mechmachtheory.2007.12.008

APPENDIX

A1. Example topology optimisation code (MATLAB)
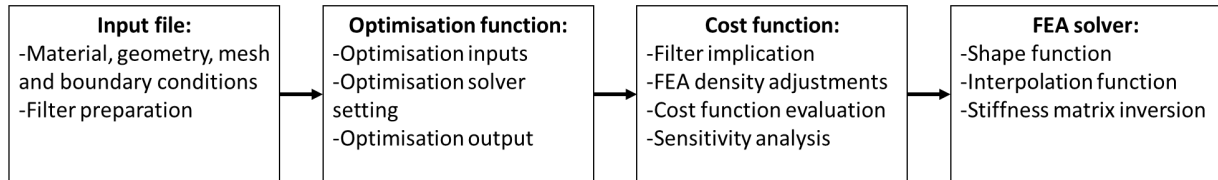
Figure A1.1 Arrangement of topology optimisation code

Example input file

```matlab
%% Input all parameters and go to the next step
%TO parameters
clear all
CM=1; % compliant mechanism yes(1) or no(0), if no, the analysis is
structural
pen=3;                          %penalisation factor for SIMP;
for nu=0.3 pen>=3
fp_r=0.006;                     %filter radius
Vstar=0.25;
P=5000;       %loads
P2=1000;
P3=1000;
P4=1000;
P5=-10000;
P6=-10000;
Pv=-1;           %virtual loads
Pv2=-1;
Pv3=-1;
Uset=0.002;
Kspring=10e7;        %output spring
Kin=[10e2,10e2,10e2,10e2,10e2,10e2]; %input springs
%Material properties
E = 200*10^9;                   % Youngs modulus
nu = 0.25;                      % Poisson's ratio
rho = 8050;                     % Density of the plate
scaleFactor=1.5;
% Mesh/domain properties
thickness = 0.005;                       % Plate thickness
Lx=0.2;                                  %Length of the plate
(along X-axes)
Ly=0.2;                                  %Length of the plate
(along Y-axes
nelx=40;                   %Number of elements along X-axes
nely=40;                   %Number of elements along Y-axes
voids=[0;0;0;0];               %Xcord;Xcord;Ycord;Ycord
location=0.08; %uncertain input, center location
```

```
IntDis=0.04; %uncertain input, interval of location
%% Mesh generation, run the step no inputs reqiured
[nodeCoordinates,elementNodes,ecoord,logicalIndexes,totel]=Mesh_with
_voids(Lx,Ly,nelx,nely,voids);
% determine element coordinates for filtering and voids/solids
% preprocess the rearranging of elements and nodes due to voids or
solids in he domain
nel=size(elementNodes,1);
numberNodes=size(nodeCoordinates,1);
GDof=2*numberNodes;% GDof: global number of degrees of freedom
elements=ones(nel,1);

% PlotMesh(nodeCoordinates,elementNodes); %elements an dnodes
numbering mesh

%% Boundary conditions and loading input required
% fixed nodes
fixedNodeX=[1641:1681]; % fixed in XX
fixedNodeY=[1641:1681]; % fixed in YY
prescribedDof=[fixedNodeX; fixedNodeY+numberNodes];

% force vector
force=zeros(GDof,1); % real force vector for FEA
force2=zeros(GDof,1);
force3=zeros(GDof,1);
force4=zeros(GDof,1);
force5=zeros(GDof,1);
force6=zeros(GDof,1);

Fv=zeros(GDof,1);      %virtual load vector for FEA
Fv2=zeros(GDof,1);     %virtual load vector for FEA
Fv3=zeros(GDof,1);     %virtual load vector for FEA

Fvy=zeros(GDof,1);     %virtual load vector for FEA

%defining load application nodes
node1=((nelx+1)*round((location)*(nely)/Ly,0))-(nelx);
node2=((nelx+1)*round((location+(IntDis/3))*nely/Ly,0))-(nelx);
node3=((nelx+1)*round((location+(2*IntDis/3))*nely/Ly,0))-(nelx);
node4=((nelx+1)*round((location+(IntDis))*nely/Ly,0))-(nelx);
Uinnode=[node1];
Uinnode2=[node2];
Uinnode3=[node3];
Uinnode4=[node4];


Uonode=[861];%define virtual load
Uonode2=[36];%define virtual load
Uonode3=[36];%define virtual load

Uonodey=[Uonode+numberNodes];



Fv(Uonode,1)=Pv;%define virtual load
Fv2(Uonode+numberNodes,1)=Pv2;%define virtual load
```

```matlab
Fv3(Uonode+numberNodes,1)=Pv3;%define virtual load
Fvy(Uonodey,1)=Pv;

force(Uinnode)=P; %define real load
%multiload input
force2(Uinnode2,1)=P2;
force3(Uinnode3,1)=P3;
force4(Uinnode4+numberNodes,1)=P4;


% preparing filter
dist=zeros(nel,nel);
N = cell(nel,1);
Hij=zeros(nel,nel);
for i=1:nel
    for j=1:nel
        dist(i,j)=round(sqrt((ecoord(i,1)-
ecoord(j,1))^2+(ecoord(i,2)-ecoord(j,2))^2),6);
    end
    N{i}=find(dist(i,:)<=fp_r);
    Hij(i,N{i})=fp_r-dist(i,N{i});
end
Ve=zeros(nel,1);
Ve(:,1)=(Lx/nelx)*(Ly/nely)*thickness;
Vt=sum(Ve);
%% Prepare FEA: element stiffness matrix
Ke=zeros(8,8) ;
C=((E)/(1-nu^2))*[1 nu 0;nu 1 0;0 0 (1-nu)/2];
indice = elementNodes(1,:);
 ndof=length(indice);
 [gaussWeights,gaussLocations]=gaussQuadrature('complete');
for q=1:size(gaussWeights,1)
    GaussPoint=gaussLocations(q,:);
    xi=GaussPoint(1);
    eta=GaussPoint(2);
% shape functions and derivatives
    [shapeFunction,naturalDerivatives]=shapeFunctionQ4(xi,eta);

% Jacobian matrix, inverse of Jacobian,
% derivatives w.r.t. x,y
    [Jacob,invJacobian,XYderivatives]=...
        Jacobian(nodeCoordinates(indice,:),naturalDerivatives);

%  B matrix
    B=zeros(3,2*ndof);
    B(1,1:ndof)       = XYderivatives(:,1)';
    B(2,ndof+1:2*ndof)  = XYderivatives(:,2)';
    B(3,1:ndof)       = XYderivatives(:,2)';
    B(3,ndof+1:2*ndof)  = XYderivatives(:,1)';
% stiffness matrix
Ke([1:8],[1:8])=Ke([1:8],[1:8])+B'*C*thickness*B*gaussWeights(q)*det
(Jacob);
end
```

Example optimisation function with Fmincon command

```matlab
lb=1e-3*ones(sum(elements==1),1);
ub=ones(sum(elements==1),1);
x0=0.99*Vstar*ones(sum(elements==1),1);
A=[]; %Stru0ctural (Ve')
b=[]; %Structural(Vt*Vstar)
Aeq=[(Ve')]; %CM (Ve')
beq=[(Vt*Vstar)];%CM (Vt*Vstar)
% nonlcon=[];
@(X)nonlcon4(GDof,Ke,pen,nel,elementNodes,numberNodes,X,prescribedDo
f,force,Uinnode,Uset,Hij,Ve,N,Fv,P,Kspring,Uonode,Pv,Fvy)
counterrrr=0;
% @(X)nonlcon_Robust(GDof,Ke,pen,nel,...
%
elementNodes,numberNodes,X,prescribedDof,force,Fv,Uonode,Kspring,Hij
,N,Ve,force2,force3,Uinnode,Uinnode2,Uinnode3,Kin,Fvy)
options =
optimoptions('fmincon','SpecifyObjectiveGradient',true,'UseParallel'
,true,'Display','iter','MaxIterations',50,'ObjectiveLimit',-
1e+100,'MaxFunctionEvaluations',30000,'OptimalityTolerance',0.01,'St
epTolerance',1.0000e-20);
[X,fval,exitflag,output]=fmincon(@(X)FE4(GDof,Ke,pen,nel,...

elementNodes,numberNodes,X,prescribedDof,force,Fv,Uonode,Kspring,Hij
,N,Ve,CM,P,Pv),x0,A,b,Aeq,beq,lb,ub,@(X)nonlcon4(GDof,Ke,pen,nel,...

elementNodes,numberNodes,X,prescribedDof,force,Uinnode,Uset,Hij,Ve,N
,Fv,P,Kspring,Uonode,Pv,Fvy),options)
% Xmatrix=zeros(nely,nelx);
% for i= 1:nely
%     for j= 1:nelx
%         Xmatrix((nely-i+1),j)=X((nelx*i)-nelx+j);
%     end
% end

%plotting results
XXXX=zeros(nelx*nely,1);
XXXX(totel==1)=X;
Xmatrix=zeros(nelx,nely);
for i= 1:nely
    for j= 1:nelx
        Xmatrix((nely-i+1),j)=XXXX((nelx*i)-nelx+j);
    end
end
%plotting results
figure
patt=ones(100);
K = kron(Xmatrix,patt);
I1=imshow(K);
figure
I2=image(Xmatrix,'CDataMapping','scaled');
colorbar
caxis([0 1])
            xxe = Lx/(2*nelx):Lx/nelx:Lx;
```

```matlab
                yye = Ly/(2*nely):Ly/nely:Ly;
                [XXe,YYe] = meshgrid(yye,xxe);
figure
modifiedImage=0.1<Xmatrix;
I3=imcontour(modifiedImage,10);
modifiedImage3d(:,:,1)=modifiedImage;
modifiedImage3d(:,:,2)=modifiedImage;
figure
zze=zeros(size(xxe));
patch(isocaps(xxe,xxe,[0,1],modifiedImage3d,'zmin'))
% [Q,W] = isocaps(modifiedImage3d,'zmin');
% svlcad('topologygripper2.stl',Q,W)
```

Cost function

```matlab
function
[cost,costgf,stiffness,displacements,SE,MSE]=FE4(GDof,Ke,pen,nel,...

elementNodes,numberNodes,X,prescribedDof,force,Fv,Uonode,Kspring,Hij
,N,Ve,CM,P,Pv);
%intiate matrices
XXX=zeros(nel,1);
stiffness=zeros(GDof);
%Construct Global Stifness matrix
for e=1:nel
%    density filter and element arrangements
XXX(e,1)=(Hij(e,N{e})*Ve(1,1)*X(N{e},1))/sum(Hij(e,N{e})*Ve(1,1));
  indice=elementNodes(e,:);
  elementDof=[ indice indice+numberNodes ];
 %stiffness matrix
  stiffness(elementDof,elementDof)=...
  stiffness(elementDof,elementDof)+(XXX(e,1)^pen)*Ke;
end
%%superimpose external spring stiffness
if CM==1
stiffness(Uonode,Uonode)=stiffness(Uonode,Uonode)+Kspring;
end
%%solve real load case

activeDof=setdiff([1:GDof]', ...
[prescribedDof]);
U=stiffness(activeDof,activeDof)\force(activeDof);
displacements=zeros(GDof,1);
displacements(activeDof)=U;
SE=0.5*(displacements')*stiffness*displacements;

%%Solve virtual load case

Uv=stiffness(activeDof,activeDof)\Fv(activeDof);
uv=zeros(GDof,1);
uv(activeDof)=Uv;
MSE=uv'*stiffness*displacements;
%%Cost function
% cost=-(100000000*MSE*Kspring)/abs(P);
```

```
cost=1000000000*MSE/SE;
costgf=zeros(nel,1);
%
%Gradients

for i=1:nel
  dxixe=zeros(nel,1);
  costg=zeros(nel,1);
      SEg=zeros(nel,1);
  MSEg=zeros(nel,1);
for j=N{i}
indice=elementNodes(j,:);
elementDof=[indice indice+numberNodes];
  Uc(1:8,1)=displacements(elementDof,1);
  Uvv(1:8,1)=uv(elementDof,1);
  MSEg(j,1)=-((Uvv')*(pen*(XXX(j,1)^(pen-1))*Ke)*Uc);
  SEg(j,1)=-0.5*Uc'*(pen*(XXX(j,1)^(pen-1))*Ke)*Uc;
  costg(j,1)=-1000000000*(((MSEg(j,1)*SE)-(MSE*SEg(j,1)))/(SE^2));
dxixe(j,1)=(Hij(j,i)*Ve(j,1))/(Hij(j,:)*Ve(:,1));
end
costgf(i,1)=costg'*dxixe;
end
```

Worst load case robust cost function

```
function
[cost,costgf,stiffness,displacements1,MSE1,MSE2,MSE3]=FEA_robust(GDo
f,Ke,pen,nel,...

elementNodes,numberNodes,X,prescribedDof,force,Fv,Uonode,Kspring,Hij
,N,Ve,CM,P,Pv,force2,force3,force4,force5,force6,Uinnode,Uinnode2,Ui
nnode3,Uinnode4,Uinnode5,Uinnode6,Kin);
%intiate matrices
XXX=zeros(nel,1);
stiffness=zeros(GDof);
%Construct Global Stifness matrix
for e=1:nel
%   density filter and element arrangements
XXX(e,1)=(Hij(e,N{e})*Ve(1,1)*X(N{e},1))/sum(Hij(e,N{e})*Ve(1,1));
  indice=elementNodes(e,:);
  elementDof=[ indice indice+numberNodes ];
 %stiffness matrix
  stiffness(elementDof,elementDof)=...
  stiffness(elementDof,elementDof)+(XXX(e,1)^pen)*Ke;
end
%%superimpose external spring stiffness
stiffness(Uonode,Uonode)=stiffness(Uonode,Uonode)+Kspring;
% stiffness(Uinnode,Uinnode)=stiffness(Uinnode,Uinnode)+Kin(1,1);

% as necessary include other springs shown below

stiffness(Uinnode2,Uinnode2)=stiffness(Uinnode2,Uinnode2)+Kin(1,2);
%
stiffness(Uinnode3,Uinnode3)=stiffness(Uinnode3,Uinnode3)+Kin(1,3);
```

```matlab
%
stiffness(Uinnode4,Uinnode4)=stiffness(Uinnode4,Uinnode4)+Kin(1,4);
%
stiffness(Uinnode5,Uinnode5)=stiffness(Uinnode5,Uinnode5)+Kin(1,5);
%
stiffness(Uinnode6,Uinnode6)=stiffness(Uinnode6,Uinnode6)+Kin(1,6);

%%solve real load case

activeDof=setdiff([1:GDof]', ...
[prescribedDof]);
U=stiffness(activeDof,activeDof)\force(activeDof);
displacements1=zeros(GDof,1);
displacements1(activeDof)=U;

U2=stiffness(activeDof,activeDof)\force2(activeDof);
displacements2=zeros(GDof,1);
displacements2(activeDof)=U2;
%
U3=stiffness(activeDof,activeDof)\force3(activeDof);
displacements3=zeros(GDof,1);
displacements3(activeDof)=U3;

%%Solve virtual load case

Uv=stiffness(activeDof,activeDof)\Fv(activeDof);
uv=zeros(GDof,1);
uv(activeDof)=Uv;

MSE1=uv'*stiffness*displacements1;
MSE2=uv'*stiffness*displacements2;
MSE3=uv'*stiffness*displacements3;
SE1=displacements1'*stiffness*displacements1;
SE2=displacements2'*stiffness*displacements2;
SE3=displacements3'*stiffness*displacements3;

OVec=[(-MSE1/SE1);(-MSE2/SE2);(-MSE3/SE3)];
[OVecW,I]=max(OVec);
%%Cost function
cost=100000000*OVecW;
costgf=zeros(nel,1);
%
%Gradients

for i=1:nel
  dxixe=zeros(nel,1);
    SEg=zeros(nel,1);
  MSEg=zeros(nel,1);
  costg=zeros(nel,1);
for j=N{i}
indice=elementNodes(j,:);
elementDof=[indice indice+numberNodes];
  Uc(1:8,1)=displacements1(elementDof,1);
  Uc2(1:8,1)=displacements2(elementDof,1);
  Uc3(1:8,1)=displacements3(elementDof,1);
  Uvv(1:8,1)=uv(elementDof,1);
```

```matlab
    if I(1,1)==1
        UcW=Uc;
        MSEw=MSE1;
        SEw=SE1;
    elseif I(1,1)==2
        UcW=Uc2;
        MSEw=MSE2;
        SEw=SE2;
    elseif I(1,1)==3
        UcW=Uc3;
        MSEw=MSE3;
        SEw=SE3;
    end

    MSEg(j,1)=-((Uvv')*(pen*(XXX(j,1)^(pen-1))*Ke)*UcW);
    SEg(j,1)=-0.5*UcW'*(pen*(XXX(j,1)^(pen-1))*Ke)*UcW;
    costg(j,1)=-100000000*(((MSEg(j,1)*SEw)-(MSEw*SEg(j,1)))/(SEw^2));

dxixe(j,1)=(Hij(j,i)*Ve(j,1))/(Hij(j,:)*Ve(:,1));
end
costgf(i,1)=costg'*dxixe;
end
```

A2. Planar endeffector design

Item #	Description	Material	Quantity
1	Guide funnel	AL6082	1
2	Dixon Ez-link 200	AL1xxx	1
3	Clamp part	AL6082	2
4	RCC mechanism	PLA (FDM)	1
5	Structure	AL6082	1

Part name   RCC mechanism
Dimentions are in   mm
Linear tolernace   +/-0.05
Angular tolernace   +/- 0.05 deg
Scale   Do not scale
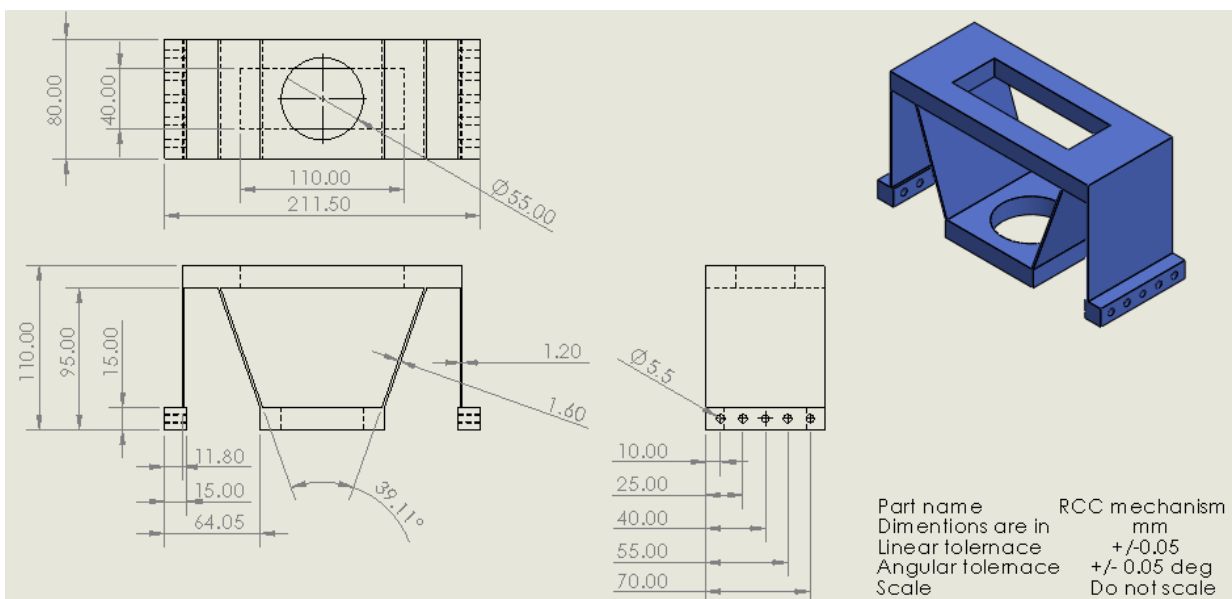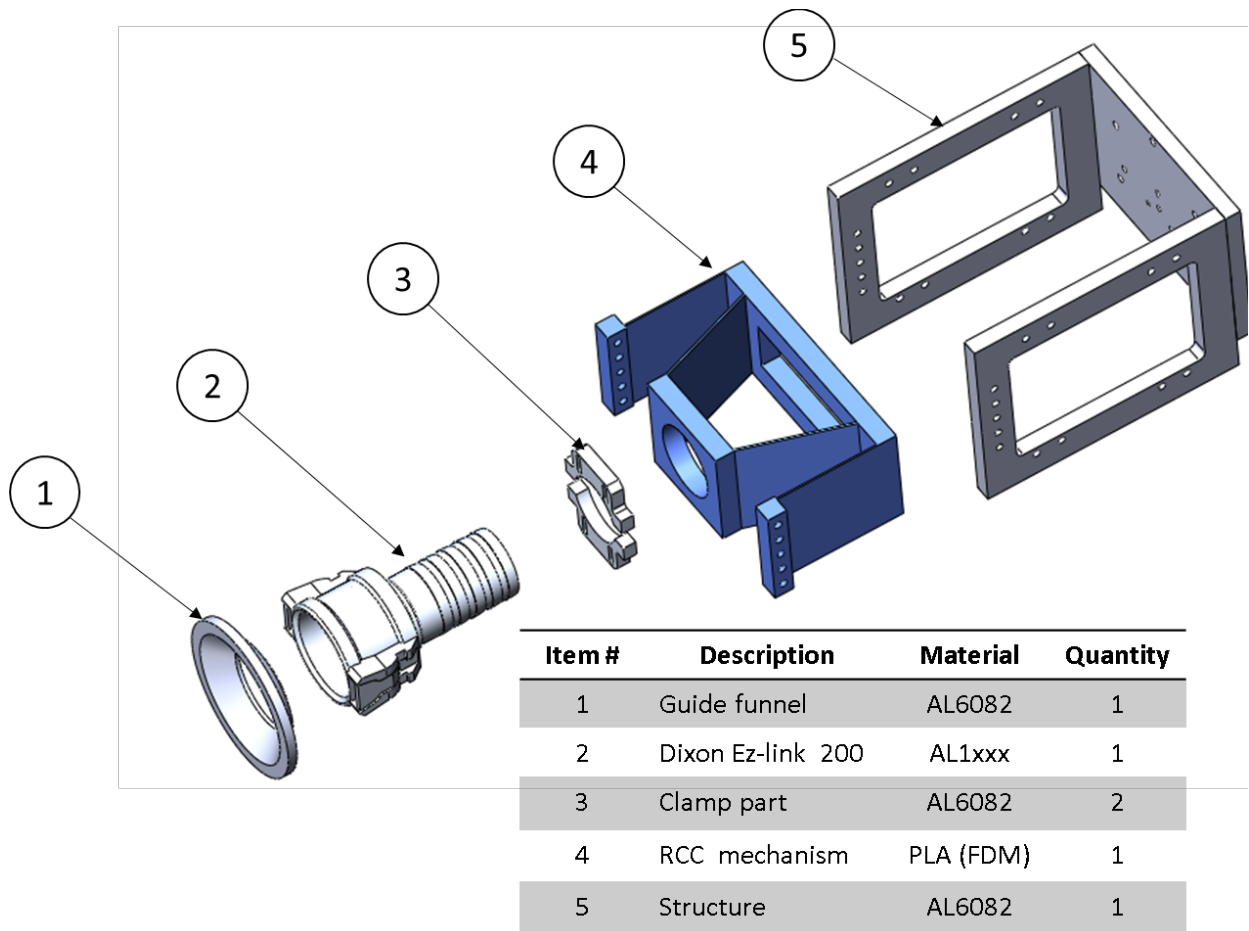
A3. Response surface CCD plan for Chapter 5

Table A2.1 Response surface CCD plan for Chapter 5

Run #	I2/I1 L	L P/d	e_0	Θ	C/D	F	I2/I1 L	P/W L	e_0	Θ	C/D	F
1	-1	-1	-1	-1	-1	-1	150	10	-0.015	-5	0.006	0.15
2	1	-1	-1	-1	-1	-1	300	10	-0.015	-5	0.006	0.15
3	-1	1	-1	-1	-1	-1	150	15	-0.015	-5	0.006	0.15
4	1	1	-1	-1	-1	-1	300	15	-0.015	-5	0.006	0.15
5	-1	-1	1	-1	-1	-1	150	10	0.015	-5	0.006	0.15
6	1	-1	1	-1	-1	-1	300	10	0.015	-5	0.006	0.15
7	-1	1	1	-1	-1	-1	150	15	0.015	-5	0.006	0.15
8	1	1	1	-1	-1	-1	300	15	0.015	-5	0.006	0.15
9	-1	-1	-1	1	-1	-1	150	10	-0.015	5	0.006	0.15
10	1	-1	-1	1	-1	-1	300	10	-0.015	5	0.006	0.15
11	-1	1	-1	1	-1	-1	150	15	-0.015	5	0.006	0.15
12	1	1	-1	1	-1	-1	300	15	-0.015	5	0.006	0.15
13	-1	-1	1	1	-1	-1	150	10	0.015	5	0.006	0.15
14	1	-1	1	1	-1	-1	300	10	0.015	5	0.006	0.15
15	-1	1	1	1	-1	-1	150	15	0.015	5	0.006	0.15
16	1	1	1	1	-1	-1	300	15	0.015	5	0.006	0.15
17	-1	-1	-1	-1	1	-1	150	10	-0.015	-5	0.008	0.15
18	1	-1	-1	-1	1	-1	300	10	-0.015	-5	0.008	0.15
19	-1	1	-1	-1	1	-1	150	15	-0.015	-5	0.008	0.15
20	1	1	-1	-1	1	-1	300	15	-0.015	-5	0.008	0.15
21	-1	-1	1	-1	1	-1	150	10	0.015	-5	0.008	0.15
22	1	-1	1	-1	1	-1	300	10	0.015	-5	0.008	0.15
23	-1	1	1	-1	1	-1	150	15	0.015	-5	0.008	0.15
24	1	1	1	-1	1	-1	300	15	0.015	-5	0.008	0.15
25	-1	-1	-1	1	1	-1	150	10	-0.015	5	0.008	0.15
26	1	-1	-1	1	1	-1	300	10	-0.015	5	0.008	0.15
27	-1	1	-1	1	1	-1	150	15	-0.015	5	0.008	0.15
28	1	1	-1	1	1	-1	300	15	-0.015	5	0.008	0.15
29	-1	-1	1	1	1	-1	150	10	0.015	5	0.008	0.15
30	1	-1	1	1	1	-1	300	10	0.015	5	0.008	0.15
31	-1	1	1	1	1	-1	150	15	0.015	5	0.008	0.15
32	1	1	1	1	1	-1	300	15	0.015	5	0.008	0.15
33	-1	-1	-1	-1	-1	1	150	10	-0.015	-5	0.006	0.3
34	1	-1	-1	-1	-1	1	300	10	-0.015	-5	0.006	0.3
35	-1	1	-1	-1	-1	1	150	15	-0.015	-5	0.006	0.3
36	1	1	-1	-1	-1	1	300	15	-0.015	-5	0.006	0.3
37	-1	-1	1	-1	-1	1	150	10	0.015	-5	0.006	0.3
38	1	-1	1	-1	-1	1	300	10	0.015	-5	0.006	0.3
39	-1	1	1	-1	-1	1	150	15	0.015	-5	0.006	0.3
40	1	1	1	-1	-1	1	300	15	0.015	-5	0.006	0.3

#												
41	-1	-1	-1	1	-1	1	150	10	-0.015	5	0.006	0.3
42	1	-1	-1	1	-1	1	300	10	-0.015	5	0.006	0.3
43	-1	1	-1	1	-1	1	150	15	-0.015	5	0.006	0.3
44	1	1	-1	1	-1	1	300	15	-0.015	5	0.006	0.3
45	-1	-1	1	1	-1	1	150	10	0.015	5	0.006	0.3
46	1	-1	1	1	-1	1	300	10	0.015	5	0.006	0.3
47	-1	1	1	1	-1	1	150	15	0.015	5	0.006	0.3
48	1	1	1	1	-1	1	300	15	0.015	5	0.006	0.3
49	-1	-1	-1	-1	1	1	150	10	-0.015	-5	0.008	0.3
50	1	-1	-1	-1	1	1	300	10	-0.015	-5	0.008	0.3
51	-1	1	-1	-1	1	1	150	15	-0.015	-5	0.008	0.3
52	1	1	-1	-1	1	1	300	15	-0.015	-5	0.008	0.3
53	-1	-1	1	-1	1	1	150	10	0.015	-5	0.008	0.3
54	1	-1	1	-1	1	1	300	10	0.015	-5	0.008	0.3
55	-1	1	1	-1	1	1	150	15	0.015	-5	0.008	0.3
56	1	1	1	-1	1	1	300	15	0.015	-5	0.008	0.3
57	-1	-1	-1	1	1	1	150	10	-0.015	5	0.008	0.3
58	1	-1	-1	1	1	1	300	10	-0.015	5	0.008	0.3
59	-1	1	-1	1	1	1	150	15	-0.015	5	0.008	0.3
60	1	1	-1	1	1	1	300	15	-0.015	5	0.008	0.3
61	-1	-1	1	1	1	1	150	10	0.015	5	0.008	0.3
62	1	-1	1	1	1	1	300	10	0.015	5	0.008	0.3
63	-1	1	1	1	1	1	150	15	0.015	5	0.008	0.3
64	1	1	1	1	1	1	300	15	0.015	5	0.008	0.3
65	-2.82843	0	0	0	0	0	12.86797	12.5	0	0	0.007	0.225
66	2.828427	0	0	0	0	0	437.132	12.5	0	0	0.007	0.225
67	0	-2.82843	0	0	0	0	225	5.428932	0	0	0.007	0.225
68	0	2.828427	0	0	0	0	225	19.57107	0	0	0.007	0.225
69	0	0	-2.82843	0	0	0	225	12.5	-0.04243	0	0.007	0.225
70	0	0	2.828427	0	0	0	225	12.5	0.042426	0	0.007	0.225
71	0	0	0	-2.82843	0	0	225	12.5	0	-14.1421	0.007	0.225
72	0	0	0	2.828427	0	0	225	12.5	0	14.14214	0.007	0.225
73	0	0	0	0	-2.82843	0	225	12.5	0	0	0.004172	0.225
74	0	0	0	0	2.828427	0	225	12.5	0	0	0.009828	0.225
75	0	0	0	0	0	-2.82843	225	12.5	0	0	0.007	0.012868
76	0	0	0	0	0	2.828427	225	12.5	0	0	0.007	0.437132
77	0	0	0	0	0	0	225	12.5	0	0	0.007	0.225
78	0	0	0	0	0	0	225	12.5	0	0	0.007	0.225
79	0	0	0	0	0	0	225	12.5	0	0	0.007	0.225
80	0	0	0	0	0	0	225	12.5	0	0	0.007	0.225

81	0	0	0	0	0	0	225	12.5	0	0	0.007	0.225
82	0	0	0	0	0	0	225	12.5	0	0	0.007	0.225
83	0	0	0	0	0	0	225	12.5	0	0	0.007	0.225
84	0	0	0	0	0	0	225	12.5	0	0	0.007	0.225
85	0	0	0	0	0	0	225	12.5	0	0	0.007	0.225
86	0	0	0	0	0	0	225	12.5	0	0	0.007	0.225
87	0	0	0	0	0	0	225	12.5	0	0	0.007	0.225
88	0	0	0	0	0	0	225	12.5	0	0	0.007	0.225
89	0	0	0	0	0	0	225	12.5	0	0	0.007	0.225
90	0	0	0	0	0	0	225	12.5	0	0	0.007	0.225

A4. Multi-objective genetic algorithm for Chapter 6 (MATLAB)

```matlab
lb=[-1 1]
ub=[-1 1]
[x,v] = gamultiobj(@fit,2,[],[],[],[],lb,ub)

function [C]=fit(x)
counter0=0

for X3=-1:0.1:1
    counter0 = 1+counter0;

D(counter0,1)=  7.491 + 0.1752*x(1) + 1.6900*x(2) - 1.0140*X3 -
0.1747*x(1)*x(1) + 0.1053*x(2)*x(2) + 0.5359*X3*X3...
+ 0.0826*x(1)*x(2) + 0.1821*x(1)*X3 - 0.3472*x(2)*X3;

S(counter0,1)=  40.09 + 10.822*x(1) + 0.929*x(2) +4.893*X3 -
0.509*x(1)*x(1) - 0.671*x(2)*x(2) + 2.865*X3*X3...
+ 0.488*x(1)*x(2) - 1.729*x(1)*X3 + 1.066*x(2)*X3;

F(counter0,1)=  42.81 + 19.66*x(1) + 10.03*x(2) + 16.84*X3 + 2.62*x(1)*x(1)
+ 2.52*x(2)*x(2) + 26.73*X3*X3...
+ 0.52*x(1)*x(2) - 5.01*x(1)*X3 - 0.48*x(2)*X3;
end

AverageD=mean(D,'all');
standandD=std(D,0,'all');
AverageS=mean(S,'all');
standandS=std(S,0,'all');
AverageF=mean(F,'all');
standandF=std(F,0,'all');

C(1,1)=-(AverageD-3*standandD);
C(2,1)=AverageF+3*standandF;
C(3,1)=AverageS+3*standandS;
end
```

A5. Stationary and mobile CyberFluids for in-field testing

Having secured funding from EPSRC (IAA) 2023 with the collaboration of Chiltern Railway, the author designed and built CyberFluids+. A prototype used for in-field testing of autonomous train fluid servicing systems with stationary and mobile robotic configurations. It aims to showcase and drive our clever end effector technology which reduces payloads and sensing requirements in turn results in a faster and more economical solution. you will notice the end effector is the same design as described in Chapter 5 and illustrated in Figure 5.7

CyberFluids+ (2023) is an extension to CyberFliuds (2019) which is our almost full-scale lab-based system that was developed with the help of RSSB and UKRI (innovateUK).